



# Application of NMR/MRI and gamma-ray attenuation analysis to the repair of old concrete: investigation of moisture transport, impact on hydration of repair mortar and durability of repaired concrete

Biyun Wang

## ► To cite this version:

Biyun Wang. Application of NMR/MRI and gamma-ray attenuation analysis to the repair of old concrete: investigation of moisture transport, impact on hydration of repair mortar and durability of repaired concrete. Other. Université Paris-Est, 2015. English. NNT : 2015PESC1159 . tel-01379585

**HAL Id: tel-01379585**

**<https://theses.hal.science/tel-01379585>**

Submitted on 11 Oct 2016

**HAL** is a multi-disciplinary open access archive for the deposit and dissemination of scientific research documents, whether they are published or not. The documents may come from teaching and research institutions in France or abroad, or from public or private research centers.

L'archive ouverte pluridisciplinaire **HAL**, est destinée au dépôt et à la diffusion de documents scientifiques de niveau recherche, publiés ou non, émanant des établissements d'enseignement et de recherche français ou étrangers, des laboratoires publics ou privés.

# Application of NMR/MRI and gamma-ray attenuation analysis to the repair of old concrete

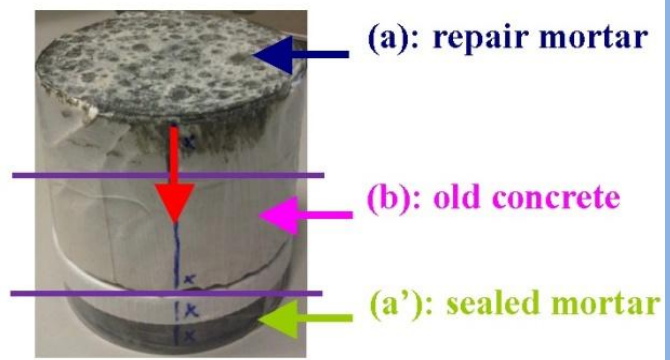
- Investigation of moisture transport, impact on hydration of repair mortar and durability of repaired concrete



Normandy bridge



Concrete degradation



Biyun WANG

IFSTTAR

22/09/2015



## THÈSE

Présentée pour obtenir le grade de

**DOCTEUR DE L'UNIVERSITÉ PARIS-EST**

Domaine: Structures et Matériaux

Présentée par: **Biyun WANG**

**Le 22 Septembre 2015**

Sujet de la thèse:

**Application des analyses par RMN/IRM et gamma-densimétrie à la réparation**

**du béton âgé** - Étude des transferts hydriques, de l'impact sur l'hydratation du mortier de réparation et sur la durabilité du béton réparé

**Application of NMR/MRI and gamma-ray attenuation analysis to the repair of**

**old concrete** - Investigation of moisture transport, impact on hydration of repair mortar and durability of repaired concrete

### Jurys:

Prof. Jean-Louis Gallias (L2MGC - U. Cergy-Pontoise) Rapporteur

Prof. Abdelhafid Khelidj (GeM - U. Nantes) Rapporteur

Prof. Carmen Andrade (IETcc, Espagne) Examinatrice / Présidente du jury

Dr. Didier Stemmelen (LEMTA – U. Lorraine) Examineur

Dr. Pamela Faure (Navier - IFSTTAR) Examinatrice / Conseillère d'études

Dr. Mickaël Thiery (STAC/DGAC) Invité / Conseiller d'études

Dr. HDR. Véronique Baroghel-Bouny (FM2D - IFSTTAR) Directrice de thèse



## Résumé

La zone d'enrobage des aciers des structures en béton armé est soumise au cours de la vie de l'ouvrage à l'action de divers agents agressifs (ions chlorure, dioxyde de carbone, etc.) qui sont susceptibles d'entraîner la corrosion des armatures. Dans le cadre de la maintenance de l'ouvrage, une réparation du béton dégradé est généralement imposée afin d'assurer l'intégrité et la sécurité de la structure, et d'en allonger la pérennité.

Cette étude s'attache à explorer les transferts hydriques qui limitent l'efficacité de la réparation au cours de l'hydratation du mortier de réparation. L'évolution microstructurale et les profils hydriques sont obtenus par des techniques non-destructives comme l'imagerie par résonance magnétique (IRM) et la gamma-densimétrie (GD) depuis le très jeune âge jusqu'à 28 jours. La durabilité du béton réparé est concernée.



Figure 0.1: Le schéma représentatif de la dégradation et de la réparation

L'effet du séchage est évité dans cette étude. Le mortier isolé d'une même formulation est préparé pour la comparaison du comportement d'hydratation avec le mortier de réparation. Sur les Figures 0.2, le système réparé que nous étudions est représenté à gauche; diverses techniques classiques aident à compléter les résultats obtenus par IRM et GD sont à droite.

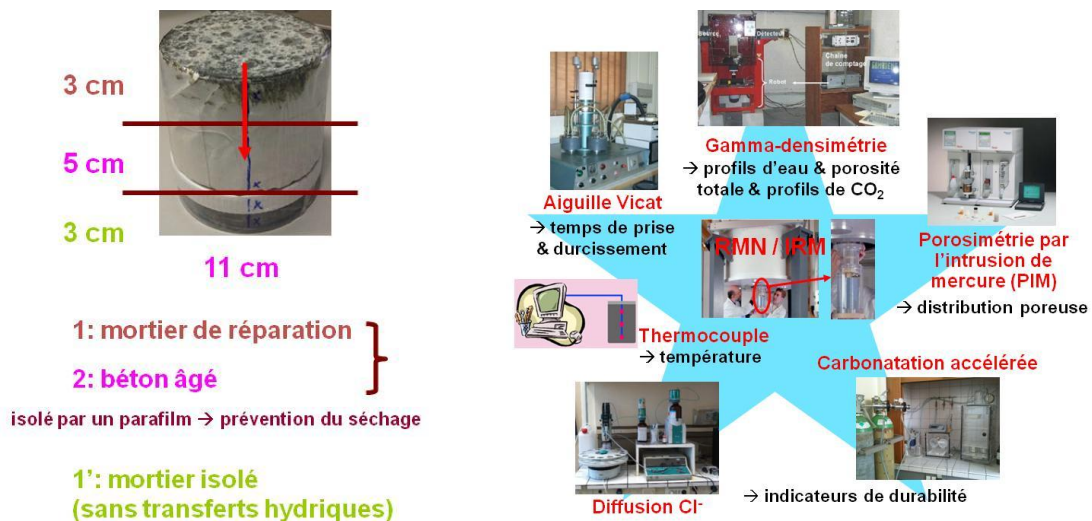


**Figure 0.2: Le système réparé et les techniques d'exploration de la réparation**

Les transferts hydriques à l'interface sont visualisés pendant la réparation (0 - 28 jours), afin de permettre une exploration en profondeur des mécanismes de couplages physico-chimiques. On cherche à rendre plus efficace la réparation par cette méthodologie, en étudiant divers matériaux de réparation, divers états du substrat (saturé ou séché) et diverses conditions environnementales, etc.

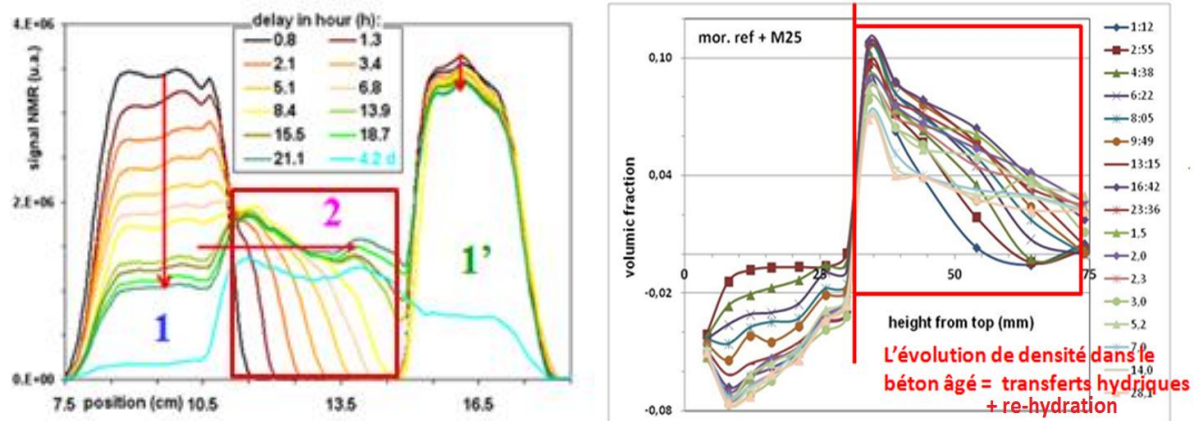


**Figure 0.3: Les transferts hydriques visualisés à l'interface du mortier vers le béton (Profils SPI (IRM) et de densité (GD))**

De plus, après la réparation (1 - 2 mois), la porosité totale est mesurée par GD ou la porosimétrie par l'intrusion de mercure (PIM). La distribution poreuse est aussi examinée par PIM selon la hauteur du système de réparation.

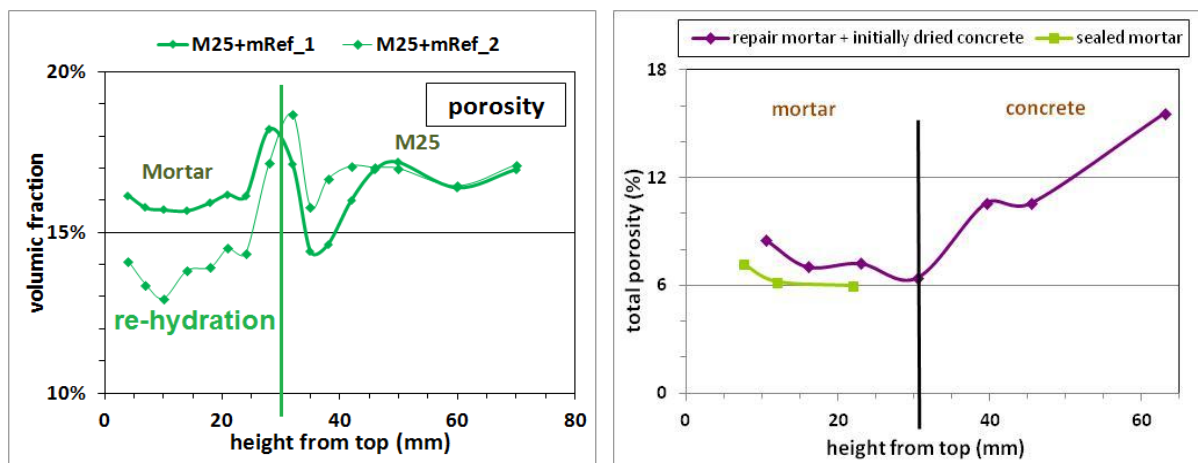


**Figure 0.4: La porosité totale après la réparation détectée par GD et par PIM**

Les indicateurs de durabilité ( $Cl^-$  et  $CO_2$ ) après la réparation (> 2 mois) montrent le blocage de la pénétration des ions chlorures et un effet non-évident pour la pénétration du dioxyde de



carbone. L'évolution est suivie au fur et à mesure pendant la pénétration, afin d'explorer l'efficacité de la réparation en vue d'une vie de service prolongée.

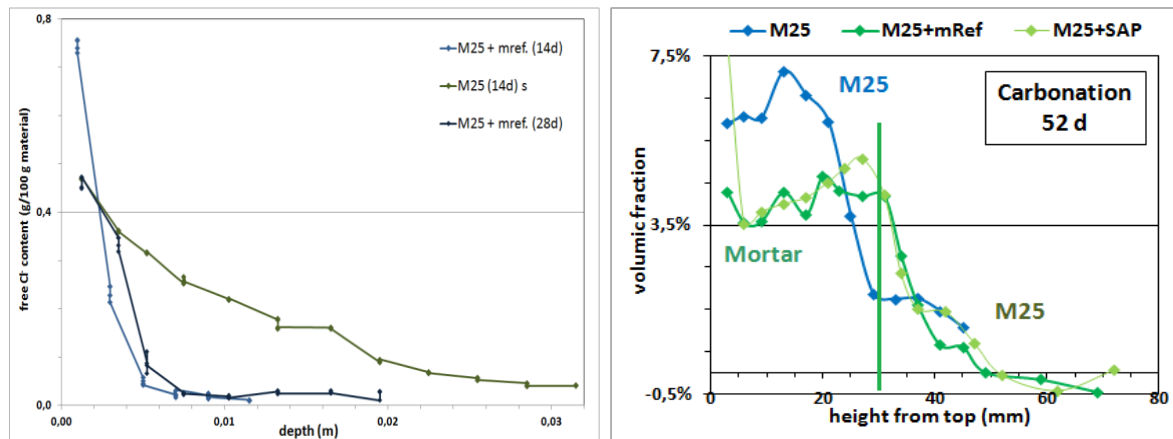


**Figure 0.5: L'effet après la procédure de réparation à la diffusion des ions chlorures et à la carbonatation**

Cette méthodologie pourra être appliquée aussi sur d'autres systèmes, où il existe des transferts hydriques: par exemple, une couche de protection en Béton Fibré à Ultra-haute Performance (BFUHP) sur le béton ordinaire.

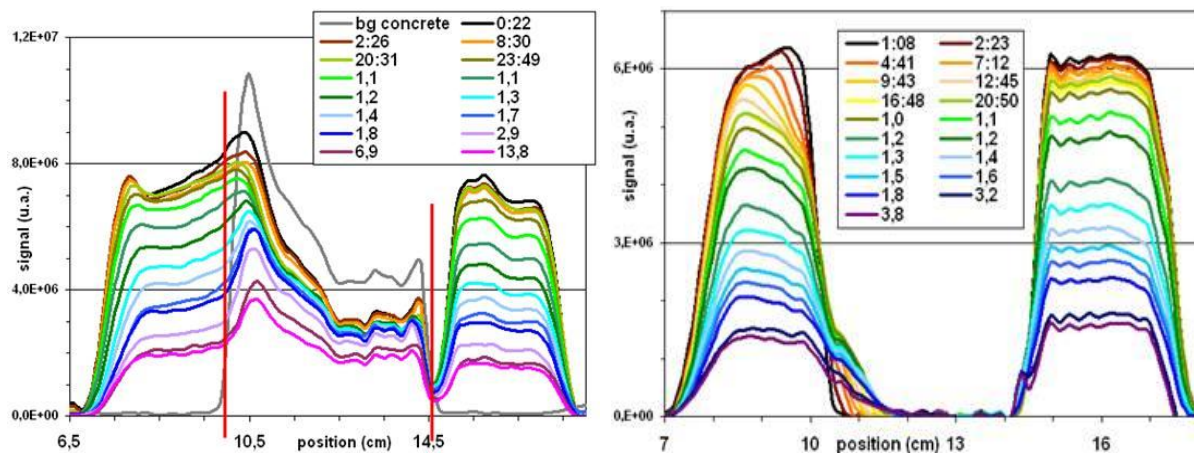


**Figure 0.6: Transferts hydriques pour BFUHP frais + béton M25 frais, BFUHP frais + béton M25 âgé**

En conclusion, cette méthodologie qui combine des techniques non-destructives et destructives, est un outil pour étudier le système de réparation par un moyen systématique et quantitatif. L'efficacité de la réparation est étudiée, à partir de tests comparatifs, afin d'améliorer la durabilité à long-terme.



## Abstract

The coating area of steel reinforced concrete structures is subjected during service lifetime to various aggressive agents (carbon dioxide, chloride ions, etc.), which causes corrosion of steel rebars. Concerning the maintenance, repair works of degraded concrete cover are generally imposed to ensure its integrity and structural safety, to prolong service lifetime and to extend long-term durability.

This thesis aims in exploring moisture transfer which limits the efficiency of repair works during mortar hydration. Water profiles and density evolution are obtained by non-destructive techniques such as Magnetic Resonance Imaging (MRI) and Gamma-Ray Attenuation (GRA) since casting until 28 days. The configuration of repair systems is designed. The effect of drying is avoided in this thesis. Sealed mortar of the same formula is prepared to compare its hydration performance with the repair mortar. Various conventional techniques (Vicat needle, Thermocouple) help to complement the results obtained by MRI and GRA.

Moisture transfer at the interface between the repair mortar and the old concrete is investigated during the repair procedure, which allows exploring the mechanisms of physico-chemical couplings. Efficient repair works can be determined with various repair materials (reference and SAP-modified mortars) and substrates (initially-dried and initially-saturated M25 concretes), and under various environmental conditions, etc.

Furthermore, total porosity is measured by GRA and Mercury Intrusion Porosimetry (MIP) after the repair procedure (1 - 2 months). Pore size distribution (PSD) is also investigated by MIP at different heights within the repair systems.

Durability indicators (1D CO<sub>2</sub> and Cl<sup>-</sup>) after the repair procedure (> 2 months) present a non-evident influence on penetration depth of accelerated carbonation, and an obvious prevention of chloride diffusion. The penetration process is followed during penetration time, and the durability of repaired concrete is concerned.

This methodology could also be applied on various systems where exist moisture transfer. For example, a protective layer of Ultra-High Performance Fiber-Reinforced Concrete (UHPFRC) on conventional concrete, which is comparable to investigated repair systems in this thesis, with both dimensional and technical similarities.

In conclusion, this methodology is an efficient tool to investigate the repair systems in a systematic and quantitative way, by combining non-destructive and destructive techniques. It is interesting to compare aforementioned systems. Repair efficiency under aggressive conditions is followed in order to ensure a long-term durability.

## Acknowledgements and Special thanks

Firstly, I want to thank their abundant contributions to my thesis: Prof. Jean-Louis Gallias from University of Cergy-Pontoise (France), Prof. Abdelhafid Khelidj from University of Nantes (France) as my reporters, and Prof. Carmen Andrade from Instituto de Ciencias de la Construcción Eduardo Torroja (IETcc, Spain), Dr. Didier Stemmelen from LEMTA - University of Lorraine (France) as my examiners. They provided numerous instructions on my thesis report and during my thesis defense.

Special thanks to supervisor of my thesis: Dr. Véronique Baroghel-Bouny, who has given me courage and abundant instructions to perform this thesis. Like a beacon, she showed me the way in domain of cement-based materials, with spirits and methods to continue my pursuits in research and development.

Many thanks to my study advisers: Dr. Mickaël Thiery and Dr. Paméla Faure, who have given me countless helps with a lot of instructions to progress little by little this thesis. Specially to mention the “corrections” made by Dr. Mickaël Thiery. Thanks to his instructions not only in writing articles and this thesis report, but also in possessing a positive attitude on research works. Dr. Paméla Faure contributed enormously in NMR/MRI part, and also set me an example as excellent female researcher who perfectly balances family life and career, which is always a quite difficult topic to be solved.

In IFSTTAR (Institut Français des Sciences et Technologies des Transports, de l'Aménagement et des Réseaux (Fr), i.e., French institute of science and technology for transport, spatial planning, development and networks), this thesis was contributed by many technicians and researchers in “Formulation, microstructure, modélisation et durabilité des matériaux de construction” (FM2D) and Navier groups. Thanks to Mr. Jean-François Bouteloup (technician, FM2D) for the preparation of carbonation container, instructions on saturation test and cutting specimens. Thanks to Mr. Alexandre Deman (ex-technician, FM2D) for the training courses of GRA and MIP techniques, instructions on chloride diffusion test and concentration measurement. Thanks to Dr. Hieu-Thao Huynh (researcher, FM2D) for his instructions on special admixtures such as super-plasticizer, superabsorbent polymer, aramid fibers and metakaolin. Thanks to Mr. Jean-Daniel Simitambe (technician, FM2D) and his technical group for manufacturing concrete and instructions on Vicat needle test. Thanks to Dr. Stéphane Rodts (researcher, Navier) and Dr. François Bertrand (engineer, Navier) for setting NMR/MRI sequences and machine maintenance. Thanks to Dr. Teddy

Fen-chong (researcher, FM2D) for the utilization of thermocouples to monitor temperature within cement matrix during hydration.

This experimental protocol has also been applied in studying the interactions between UHPFRC materials and conventional concrete. This thesis was developed by a PhD exchange project with Laboratory of Maintenance Construction and Safety for Civil Structures (MCS) at École Polytechnique Fédérale de Lausanne (EPFL). Thanks to Dr. Hadi Kazemi-Kaymab for his kindness to encourage me in personal life and professional works, his diligence and devotion to research will also influence me in the future. Thanks to his supervisor, Dr. Denarie Emmanuel (professor), for providing mix design of UHPFRC materials and his instructions in cooperated investigations with very high scientific level.

Thanks to my colleagues and at the same time my friends: Dr. Xiaomeng Wang, Dr. Mickaël Saillio, Dr. Jiyun Shen, Dr. Antoine Morandea and Dr. Zhidong Zhang, for all the helps and discussions frequently during very rough research works. I also want to give my special thanks to three Chinese, as in ancient Chinese proverb: “There must be a mentor for me among any three travelers”, I indeed learned many experiences from them.

Thanks to my supervisors of master internship: Dr. André Nonat and Dr. Sylvie Pourchet, who contributed instructions to an innocent young woman in the domain of cement-based materials and opened a door to continue my long journey.

Thanks to all my friends and PhD students in Paris, in other places of Europe, in USA and in China, etc., who I met during several conferences and seminars, for your supports and mind exchanges on my thesis and other aspects in relevant fields.

I also want thanks my parents and other family members. It has been more than 8 years since my departure from my home town Hefei in China, when I decided to continue my pursuits in Europe. I cannot finish this thesis without their supports especially those of my dear mother.

Special thanks to my husband Mr. Yantao Qu, who always supports the way I have chosen. He has also shared family responsibility especially during charged years of my thesis. Even when this destination seemed as impossible to be achieved, he was always at my side.

Kiss to my little Yvan Qu, a little angel but also a terrible demon at the same time, who has changed the track and attitude of my life. The first steps were always the hardest. After miserable years since his premature birth, I will be much stronger to face other difficulties, and more insistent to believe in love and aspiration, in research and personal development.

# List of abbreviations and notations

## **Cement-based Materials and admixtures**

AFm: calcium aluminate monosulfate ( $\text{Al}_2\text{O}_3\text{-Fe}_2\text{O}_3\text{-mono}$ )  
Aft: Ettringite, calcium sulfoaluminate hydrates ( $\text{Al}_2\text{O}_3\text{-Fe}_2\text{O}_3\text{-tri}$ )  
 $\text{C}_3\text{S}$ : tricalcium silicate (alite)       $\text{C}_2\text{S}$ : dicalcium silicate (belite)       $\text{C}_3\text{A}$ : tricalcium aluminate (celite)       $\text{C}_4\text{AF}$ : tetracalcium aluminoferrite (ferrite)  
CH: portlandite  
C-S-H: calcium silicate hydrate, so called C-S-H gel  
Notations in cement industry: C = CaO, S =  $\text{SiO}_2$ , H =  $\text{H}_2\text{O}$ , A =  $\text{Al}_2\text{O}_3$ , F =  $\text{Fe}_2\text{O}_3$   
OPC: Ordinary Portland Cement  
 $P_c$ : capillary pressure  
PSD: Pore Size Distribution  
s/c: sand to cement ratio in mass  
SAP: Super-Absorbent Polymer  
SAP/c: superabsorbent polymer to cement ratio in mass  
SF: Silica Fume  
SP: Super-Plasticizer  
SP/c: super-plasticizer to cement ratio in mass  
 $S_w$ : degree of saturation  
UHPFRC: Ultra-High Performance Fiber-Reinforced Concrete  
w/c: water to cement ratio in mass  
 $\alpha$ : degree of cement hydration

## **Nuclear Magnetic Resonance / Magnetic Resonance Imaging techniques**

$a_t$ : Acquisition Time, parameter of FID sequence  
a.u.: arbitrary unit  
CONTIN: program developed by Provencher to obtain a distribution of relaxation time by Laplace inversion  
FID: Free Induction Decay, free precession signal  
FoV: Field of View, parameter of SPI sequence  
FWHM: Full Width at Half Maximum, peak parameter  
 $I_{\text{FID}}$ : Intensity of Free Induction Decay  
IR: Inversion-Recovery sequence, used for longitudinal relaxation time  $T_1$  measurement

MRI: Magnetic Resonance Imaging

NMR: Nuclear Magnetic Resonance

RF: Radio Frequency

Rg: Receiver Gain, parameter of SPI sequence

S/N: ratio signal to noise

SN: Scan Number, parameter of SPI sequence

SPI: Single Point Imaging, MRI sequence

SPRITE: Single Point Ramped Imaging T<sub>1</sub> Enhancement, MRI sequence

T<sub>1</sub>: longitudinal relaxation time, spin-lattice

T<sub>2</sub>: transverse relaxation time, spin-spin

TE: Echo Time, parameter of IR and SPI sequence

t<sub>i</sub>: Inversion Time, parameter of IR sequence

TR: Repetition Time, parameter of IR and SPI sequence

t<sub>p</sub>: Phase encoding Time, parameter of SPI sequence

### **Conventional Techniques**

BET: Method of calculating specific surface area of a material from an isothermal adsorption of water or nitrogen (named by its authors Brunauer, Emmett and Teller)

GRA: Gamma-Ray Attenuation

MIP: Mercury Intrusion Porosimetry

P<sub>Hg</sub>: mercury pressure

r<sub>p</sub>: pore radius

### **Others**

RH: Relative Humidity (%)

# Table of Contents

<b>R ésumé.....</b>	<b>5</b>
<b>Abstract .....</b>	<b>8</b>
<b>Acknowledgements and Special thanks .....</b>	<b>9</b>
<b>List of abbreviations and notations.....</b>	<b>11</b>
<b>Cement-based Materials and admixtures .....</b>	<b>11</b>
<b>Nuclear Magnetic Resonance / Magnetic Resonance Imaging techniques.....</b>	<b>11</b>
<b>Conventional Techniques.....</b>	<b>12</b>
<b>Others .....</b>	<b>12</b>
<b>Table of Contents.....</b>	<b>13</b>
<b>List of Figures .....</b>	<b>17</b>
<b>List of Tables.....</b>	<b>21</b>
<b>General introduction.....</b>	<b>23</b>
<b>1. Chapter 1: Degradation mechanisms of old concrete and repair techniques, hydration process and long-term durability of repair systems.....</b>	<b>27</b>
<b>1.1 Degradation mechanisms of old concrete and conventional repair techniques.....</b>	<b>30</b>
1.1.1 Degradation process.....	30
1.1.2 Classification of degradation mechanisms .....	31
1.1.3 Conventional repair techniques .....	32
<b>1.2 Moisture properties during hydration process of repair mortar.....</b>	<b>34</b>
1.2.1 Moisture properties during different stages of hydration .....	34
1.2.1.1 Within cement matrix at early age .....	34
1.2.1.2 During the repair procedure.....	35
1.2.2 Hydration process and constituents of hydrated cement matrix .....	35
<b>1.3 Long-term durability of repair systems .....</b>	<b>38</b>
1.3.1 Carbonation.....	39
1.3.2 Chloride penetration .....	40
<b>1.4 Global overview .....</b>	<b>41</b>
<b>2. Chapter 2: Materials, techniques, feasibility .....</b>	<b>45</b>
<b>2.1 Design of repair systems .....</b>	<b>47</b>
<b>2.2 Materials.....</b>	<b>48</b>
2.2.1 Cement.....	49
2.2.2 Concrete substrates .....	50

2.2.3 Cement pastes and mortars for the investigation of setting process .....	50
2.2.4 Repair mortars .....	53
2.2.5 UHPFRC matrix and with aramid fibers .....	54
2.2.6 Technical details of casting procedure .....	55
<b>2.3 Selected techniques during different stages of hydration .....</b>	<b>56</b>
2.3.1 For the investigation of only cement pastes and mortars .....	56
2.3.1.1 NMR relaxometry.....	56
2.3.1.2 Conventional techniques .....	62
2.3.1.3 Numerical simulations .....	63
2.3.2 For the investigation of repair systems .....	64
2.3.2.1 At early age (since casting until 28 days).....	64
MRI - SPI sequence (moisture profiles) .....	64
GRA (density profiles).....	66
2.3.2.2 At middle age (since 2 months).....	68
GRA (total porosity) .....	68
MIP (total porosity & PSD) .....	69
2.3.2.3 After repair procedure (since 2 months until long term).....	71
Water immersion.....	71
Carbonation.....	71
Attack by chloride ions .....	72
<b>2.4 Global overview .....</b>	<b>73</b>
<b>3. Chapter 3: Monitoring of setting process at early age of hydration.....</b>	<b>77</b>
<b>3.1 Definition of mechanical and chemical setting times .....</b>	<b>79</b>
<b>3.2 Monitoring of <math>T_1</math> / <math>I_{FID}</math> to monitor water mobility and free water content - NMR relaxometry as a probe for setting process and water depletion.....</b>	<b>81</b>
3.2.1 Compared with results obtained by thermocouple (temperature), Vicat needle (setting time) and numerical modeling (water depletion).....	81
3.2.1.1 Mechanical setting time related to the percolation of solid network....	81
3.2.1.2 Chemical setting time related to hydration reactions and temperature evolution.....	86
3.2.1.3 Comparison of mechanical and chemical setting times.....	87
3.2.1.4 Effect of FID data treatment methods.....	89
Selection of capillary peak for FID acquisition .....	89
Deletion of different points of FID acquisition.....	92



3.2.2 Numerical simulation as a probe for free water depletion.....	94
<b>3.3 NMR results for various cement pastes / mortars .....</b>	<b>95</b>
3.3.1 Cement pastes made of gray and white OPC.....	95
3.3.2 Effect of the addition of standard sand (cement paste vs. mortar) .....	97
3.3.3 Effect of the addition of super-plasticizer .....	99
3.3.4 Effects of the replacement of cement by silica fume.....	103
<b>3.4 Global overview .....</b>	<b>106</b>
<b>4. Chapter 4: Investigation of moisture transfer and its impact on hydration and microstructure of repair systems, during and after a repair procedure .....</b>	<b>111</b>
<b>4.1 During early ages of repair procedure (0 - 28 days).....</b>	<b>114</b>
4.1.1 Investigation of moisture profiles by SPI sequence .....	114
4.1.1.1 Reference repair mortar on initially-dried M25 .....	116
4.1.1.2 Reference repair mortar on initially-saturated M25 .....	118
4.1.1.3 Repair mortar with SAP on initially-dried M25 .....	121
4.1.1.4 Conclusion .....	124
4.1.2 Application of characterized methodology on UHPFRC materials .....	124
4.1.2.1 UHPFRC matrix and with fibers on initially-dried M25 .....	125
4.1.2.2 UHPFRC matrix and with fibers on initially-saturated M25 .....	129
4.1.2.3 Fresh UHPFRC matrix ( $w/c = 0.16$ ) on fresh concrete M25 ( $w/c = 0.84$ ).....	132
4.1.3 Relations between SPI integration and FID - global free water content and chemical setting times.....	134
4.1.4 Investigation of moisture transfer within old concrete by density profiles .....	137
4.1.4.1 Reference repair mortar on initially-dried M25 .....	137
4.1.4.2 Comparison with SPI profiles .....	138
<b>4.2 After 90-day repair procedure .....</b>	<b>140</b>
4.2.1 Total porosity determined by GRA .....	140
4.2.2 Total porosity and porous distribution determined by MIP .....	143
4.2.3 Repair efficiency and preview of durability .....	147
4.2.3.1 Profiles of water immersion by GRA (wetting properties) .....	147
Reference repair mortar and with SAP on initially-dried M25.....	147
Reference repair mortar on initially-saturated M25.....	149
4.2.3.2 Carbonation profiles and penetration depth.....	150
4.2.3.3 Accelerated $Cl^-$ diffusion profiles.....	152

<b>4.3 Global overview .....</b>	<b>153</b>
<b>5.     <i>Conclusions and perspectives</i> .....</b>	<b>157</b>
<b><i>Bibliography</i>.....</b>	<b>161</b>

# List of Figures

Figure 0.1: Le schéma représentatif de la dégradation et de la réparation .....	5
Figure 0.2: Le système réparé et les techniques d'exploration de la réparation.....	6
Figure 0.3: Les transferts hydriques visualisés à l'interface du mortier vers le béton (Profils SPI (IRM) et de densité(GD)) .....	6
Figure 0.4: La porosité totale après la réparation détectée par GD et par PIM .....	6
Figure 0.5: L'effet après la procédure de réparation à la diffusion des ions chlorures et à la carbonatation .....	7
Figure 0.6: Transferts hydriques pour BFUHP frais + béton M25 frais, BFUHP frais + béton M25 âgé.....	7
Figure 1.1: (a) Diagram of corrosion mechanism under general condition [5]; (b) Degradation procedure of reinforced concrete cover [6]. .....	31
Figure 1.2: Representative schema of cement matrix during hydration process. ....	36
Figure 1.3: (a) Representative schema of hydrated cement phase; (b) Illustration of water distribution in C-S-H by model Feldman and Sereda (1970) .....	36
Figure 1.4: Detectable water by NMR/MRI in different states during cement hydration.....	38
Figure 1.5: Carbonation mechanism of Portlandite in cement matrix. ....	39
Figure 1.6: Penetration mechanism of attack by chloride ions. ....	40
Figure 2.1: Summary of investigated systems .....	47
Figure 2.2: Schema of repair systems for (a) techniques in which metallic compounds are forbidden; (b) other traditional techniques. ....	47
Figure 2.3: Formula of applied aramid fibers.....	52
Figure 2.4: (a) Photo of SAP gel; (b) Formula of SAP powders (Luquasorb 1161 <sup>®</sup> and Aldrich <sup>®</sup> ).....	52
Figure 2.5: Application of UHPFRC materials on conventional concrete .....	54
Figure 2.6: Polarization: (a) by magnetic field <b>B0</b> , energy levels of spin $\pm \frac{1}{2}$ ; (b) Precession of magnetic moment with angular velocity around <b>B0</b> ; Resonance: (c) phenomenon of double precession. ....	58
Figure 2.7: T <sub>1</sub> relaxation: (a) Regrowth of magnetization in longitudinal plane; (b) Characterization. ....	58
Figure 2.8: T <sub>2</sub> relaxation: (a) Phase shift of spins in transverse plane; (b) Characterization. ..	59
Figure 2.9: Inversion recovery sequence and the conversion by inverse Laplace transform. ..	61
Figure 2.10: FID acquisition sequence and acquired signal with exponential envelope. ....	61

Figure 2.11: (a) Schematic diagram of thermocouple; (b) Photo of Vicat needle equipment. .	63
Figure 2.12: Schematic of imaging gradients: $x = \text{GSS}$ , $y = \text{GPE}$ , $z = \text{GR}$ . .....	65
Figure 2.13: One-dimensional SPI sequence. ....	66
Figure 2.14: (a) GRA equipment at IFSTTAR; (b) Gamma-ray absorption principle .....	67
Figure 2.15: Determination of water porosity by GRA: (a) Drying at 45 °C in vacuum oven; (b) Saturating in vacuum by distilled water; (c) Principle of calculating the total porosity. ...	68
Figure 2.16: Sample preparation before MIP tests: (a) Cut to different layers; (b) Freeze-drying.....	69
Figure 2.17: Mercury porosimetry equipment of “Pascal 140” and “Pascal 440”. .....	70
Figure 2.18: Protocol of water immersion test .....	71
Figure 2.19: Equipment of accelerated carbonation.....	72
Figure 2.20: Container of chloride ions diffusion .....	73
Figure 2.21: Dosage of chloride ions concentration.....	73
Figure 3.1: Cement paste made of gray OPC at $w/c = 0.35$ (C35): (a) continuous $T_1$ distribution during hydration and identification of optimum $T_1$ value; (b) monitoring of optimum $T_1$ value and of NMR signal amplitude $I_{\text{FID}}$ since $t = 0$ until 66 h. ....	80
Figure 3.2: Cement paste made of gray OPC of $w/c = 0.35$ (C35):(a) evolution of optimum $T_1$ value compared to the penetration depth of Vicat needle; (b) evolution of $1/T_1$ compared to penetration depth; (c) $T_1$ derivative ( $dT_1/dt$ ) compared to penetration depth derivative ( $dp/dt$ ). .....	82
Figure 3.3: Cement paste made of white OPC of $w/c = 0.386$ (WC38): (a) evolution of optimum $T_1$ value compared to the penetration depth of Vicat needle; (b) evolution of $1/T_1$ compared to penetration depth; (c) $T_1$ derivative ( $dT_1/dt$ ) compared to penetration depth derivative ( $dp/dt$ ). .....	84
Figure 3.4: Time derivative of NMR signal amplitude $dI_{\text{FID}}/dt$ and temperature evolution: (a) for $w/c = 0.35$ gray OPC cement paste (C35); (b) for $w/c = 0.386$ white OPC cement paste (WC38). ....	86
Figure 3.5: Time derivative of optimum $T_1$ value $dT_1/dt$ and NMR signal amplitude $dI_{\text{FID}}/dt$ for cement pastes made of gray OPC of $w/c =$ (a) 0.35 (C35) and (b) 0.45 (C45). ....	88
Figure 3.6: Cement paste made of gray OPC of $w/c = 0.45$ : (a) Distribution of FID intensity (b) FID diagrams according to the range of $T_1$ accumulation by the distinguish of capillary / physically-bound water (c) Time derivative of $I_{\text{FID}}$ according of the range of $T_1$ accumulation. ....	90

Figure 3.7: UHPFRC without fibers: (a) FID diagrams according to the range of $T_1$ accumulation by the distinguish of capillary / physically-bound water (b) Time derivative of $I_{FID}$ according of the range of $T_1$ accumulation. ....	92
Figure 3.8: Cement paste made of gray OPC of w/c = 0.45: (a) Effect of deleted points of FID acquisition; (b) Derivation of $I_{FID}$ in different conditions of deleted points .....	93
Figure 3.9: Monitoring of $I_{FID}$ , simulated kinetics of water depletion, and indirect assessment of the time evolution of the water consumption from data provided in [48]. Case for cement pastes made of gray OPC of w/c = (a) 0.35 (C35) and (b) 0.45 (C45). ....	95
Figure 3.10: Time derivative of optimum $T_1$ value $dT_1/dt$ and NMR signal amplitude $dI_{FID}/dt$ for cement pastes made of white OPC of w/c = (a) 0.35 (WC35); (b) 0.40 (WC40); (c) 0.50 (WC50). ....	97
Figure 3.11: Time derivative of optimum $T_1$ value $dT_1/dt$ and NMR signal amplitude $dI_{FID}/dt$ for the w/c = 0.35 cement paste (C35) and the w/c = 0.42 mortar of s/c = 2.0 (M42). ....	98
Figure 3.12: Effect of the addition of super-plasticizer: (a) $dT_1/dt$ and (b) $dI_{FID}/dt$ for C35 and C30SP; (c) $dT_1/dt$ and (d) $dI_{FID}/dt$ for M42 and M38SP. ....	101
Figure 3.13: Time derivative of optimum $T_1$ value $dT_1/dt$ and NMR signal amplitude $dI_{FID}/dt$ for (a) UHPFRC and (b) UHPFRC + fibers. ....	103
Figure 3.14: Time derivative of (a) optimum $T_1$ value $dT_1/dt$ and (b) NMR signal amplitude $dI_{FID}/dt$ for C35 and C35SF; Time derivative of (c) optimum $T_1$ value $dT_1/dt$ and (d) NMR signal amplitude $dI_{FID}/dt$ for C45 and C45SF. ....	105
Figure 3.15: Analysis of the relation (a) between <i>mechanical</i> (MS) and <i>chemical</i> (CS) setting times for various mix designs; (b) zoom in cement pastes and mortars without super-plasticizer; (c) analysis of the relation between the full width at half maximum of MS and CS. ....	108
Figure 4.1: Configuration of repair system and SPI profiles.....	114
Figure 4.2: Reference mortar on initially-dried concrete: (a) SPI profiles; (b) Integration of accumulated intensities.....	117
Figure 4.3: Reference mortar on initially-saturated concrete: (a) SPI Profiles (b) Integration of accumulated intensities and bleeding at top surface of repair mortar. ....	119
Figure 4.4: Repair mortar containing SAP on initially-dried concrete (a) SPI Profiles (b) Integration of accumulated intensities. ....	122
Figure 4.5: UHPFRC matrix and with fibers on initially-dried concretes (a) Configuration of composite system; (b) (b') SPI Profiles; (c) (c') Integration of accumulated intensities; (d) PSD within UHPFRC materials by MIP after 3 days of hydration. ....	127

Figure 4.6: UHPFRC materials on initially-saturated concretes: (a) (a') SPI profiles; (b) (b') Immediate moisture transfer after placing; (c) (c') Integration of accumulated intensities. ..	131
Figure 4.7: Fresh UHPFRC without fibers on fresh concrete M25 (a) SPI profiles (b) Immediate moisture transfer after placing (bg concrete = background, initial profile of concrete) .....	133
Figure 4.8: For sealed UHPFRC without fibers: (a) Evolution of SPI accumulation & FID intensity; (b) Derivative of SPI accumulation & FID intensity corresponding to <i>chemical</i> setting. For sealed UHPFRC with fibers: (a') Evolution of SPI accumulation & FID intensity; (b') Derivative of SPI accumulation & FID intensity corresponding to <i>chemical</i> setting. ....	136
Figure 4.9: Density profiles (0 - 28 days) of “repair mortar ref. + initially-dried M25” by comparing to initial state before casting in M25, to (a) 1.2h after casting (b) 28 days in repair mortar. ....	138
Figure 4.10: SPI profiles by MRI and density profiles by GRA (0 - 28 days) of “repair mortar ref. + initially-dried M25”: (a) within concrete both by comparing to initial state (b) within repair mortar by comparing to initial state by SPI and to stable state by GRA. ....	139
Figure 4.11: Total porosity determined by GRA in repair mortar and sealed mortar for: reference mortar on (a) initially-dried M25; (b) initially-saturated M25; (c) SAP mortar on initially-dried M25 .....	142
Figure 4.12: Total porosity by MIP for: sealed mortars + reference repair mortars on (a) initially-dried M25, (b) initially-saturated M25. ....	144
Figure 4.13: Porous distribution for: (a) repair mortar, (b) M25, in “ref. mor. + ini. dried M25”; (a') repair mortar, (b') M25, in “ref. mor. + ini. sat. M25”; (c) repair and sealed mortars in both systems .....	146
Figure 4.14: Water immersion properties and total porosity after repair procedure for: reference mortar on (a) initially-dried M25 at 100 days (since casting) (b) initially-saturated M25 at 70 days. ....	148
Figure 4.15: Water immersion properties and total porosity after repair procedure for reference repair mortar on initially-saturated M25 at 70 days since casting .....	149
Figure 4.16: Density profiles by GRA to investigate carbonation profiles for (a) reference mortar + M25; (b) mortar with SAP + M25; (c) only M25 concrete. ....	151
Figure 4.17: (a) Free chloride ions content in M25 and repair system at 14 and 28 days; (b) Free and total chloride ions content for only M25 at different ages. ....	153

## List of Tables

Table 2-1: Chemical and potential mineral compositions of gray and white OPCs. ....	50
Table 2-2: Mix design of concrete M25 in which aggregates are considered as in dry state... ..	50
Table 2-3: Cement pastes for monitoring relaxation times .....	51
Table 2-4: Mix design and abbreviations for the investigation of setting process. ....	53
Table 2-5: Composition of UHPFRC with aramid fibers .....	55
Table 3-1: <i>Mechanical</i> and <i>chemical</i> setting times and full width at half maximum ( $\Delta MS$ , $\Delta CS$ ) determined on $dT_1/dt$ and $dI_{FID}/dt$ diagrams (pre-peak durations: $\Delta MS^-$ , $\Delta CS^-$ , post-peak durations: $\Delta MS^+$ , $\Delta CS^+$ ) for cement pastes made of gray OPC of $w/c = 0.35$ (C35) and $0.45$ (C45). ....	88
Tableau 3-2: <i>Mechanical</i> and <i>chemical</i> setting times and full width at half maximum ( $\Delta MS$ , $\Delta CS$ ) determined on the $dT_1/dt$ and $dI_{FID}/dt$ diagrams (pre-peak durations: $\Delta MS^-$ , $\Delta CS^-$ , post-peak durations: $\Delta MS^+$ , $\Delta CS^+$ ) for the cement pastes made of white cement WC35 ( $w/c = 0.35$ ), WC40 ( $w/c = 0.40$ ) and WC50 ( $w/c = 0.50$ ). ....	97
Tableau 3-3: <i>Mechanical</i> and <i>chemical</i> setting times and full width at half maximum ( $\Delta MS$ , $\Delta CS$ ) determined on the $dT_1/dt$ and $dI_{FID}/dt$ diagrams (pre-peak durations: $\Delta MS^-$ , $\Delta CS^-$ , post-peak durations: $\Delta MS^+$ , $\Delta CS^+$ ) for C35 and M42 (mortar). ....	99
Table 3-4: <i>Mechanical</i> and <i>chemical</i> setting times and the full width at half maximum ( $\Delta MS$ , $\Delta CS$ ) determined on the $dT_1/dt$ and $dI_{FID}/dt$ diagrams (pre-peak durations: $\Delta MS^-$ , $\Delta CS^-$ , post-peak durations: $\Delta MS^+$ , $\Delta CS^+$ ) for C35, C30SP, M42 and M38SP. ....	101
Table 3-5: <i>Mechanical</i> and <i>chemical</i> setting times and full width at half maximum ( $\Delta MS$ , $\Delta CS$ ) determined on the $dT_1/dt$ and $dI_{FID}/dt$ diagrams (pre-peak durations: $\Delta MS^-$ , $\Delta CS^-$ , post-peak durations: $\Delta MS^+$ , $\Delta CS^+$ ) for UHPFRC, UHPFRC + fibers. ....	103
Table 3-6: <i>Mechanical</i> and <i>chemical</i> setting times and full width at half maximum ( $\Delta MS$ , $\Delta CS$ ) determined on the $dT_1/dt$ and $dI_{FID}/dt$ diagrams (pre-peak durations: $\Delta MS^-$ , $\Delta CS^-$ , post-peak durations: $\Delta MS^+$ , $\Delta CS^+$ ) for C35, C35SF, C45 and C45SF. ....	106
Table 4-1: Effect of drying during hydration process of repair system by integrated intensities of SPI profiles and mass verification.....	118
Table 4-2: Estimated saturation rate for optimized repair efficiency .....	120
Table 4-3: Effect of drying during hydration process of repair system by integrated intensities of SPI profiles and mass verification.....	121





## General introduction

The degradation of reinforced concrete structures due to corrosion of steel rebars reduces their mechanical performance and service lifetime. In order to prevent further deterioration of various degradation mechanisms, it is generally recommended to repair and to rebuild the concrete cover. The interactions, not only between the microstructural evolution and the hydration process of repair mortar, but also between moisture transfer and water depletion due to hydration reactions, are important to be firstly understood.

The long-term durability of a repair system depends on many parameters. Moisture transfer hinders the hydration process of repair mortar and the performance of the whole system. It occurs especially at the interfaces: between the fresh repair mortar and the old concrete, between the repair system and surrounding environment. In this thesis, moisture transfer at the mortar - concrete interface is focused on, while drying effect is avoided by coating. However, aforementioned phenomena are not yet completely investigated in existing repair techniques, as they are generally based on empiricism. It lacks predictive and methodological approach to follow *in-situ* evolution during repair procedure.

This thesis was performed in FM2D and Navier groups in IFSTTAR, situated in Champs-sur-Marne in France. It is principally based on non-destructive techniques, such as: Nuclear Magnetic Resonance (NMR relaxometry) / Magnetic Resonance Imaging (MRI), and Gamma-Ray Attenuation (GRA).

In term of characterization, it is firstly aimed at investigating the setting times of repair mortars. The detection of available water content for an efficient hydration is also important to be monitored during complete repair procedure, and especially around setting.

For various cement pastes and mortars, global water content was monitored by the investigation of Free Induction Decay (FID) signal obtained through a simple “pulse-acquisition” sequence. The evolution of water mobility was monitored by the investigation of relaxation time  $T_1$  obtained through an “Inversion Recovery” (IR) sequence and Laplace inversion for analysis. The NMR results were complemented by conventional techniques (Vicat needle test, temperature monitoring), which were performed immediately after casting until 3 days. Moreover these results were completed by a numerical modeling which evaluates water depletion due to hydration reactions until 100 days.

For various repair systems with selected mortars on old concretes M25 (low grade concrete is selected in order to enhance transfer properties), moisture transfer was continuously

visualized with a “Single Point Imaging” (SPI) sequence. Reference repair mortars and Super-Absorbent Polymer (SAP) modified mortars were prepared to investigate water retention properties. Moisture transfer within repair systems was also investigated by monitoring density evolution by GRA. These results were acquired immediately after placing, since early age until 28 days, and compared with SPI profiles.

GRA and Mercury Intrusion Porosimetry (MIP) techniques were used in repair systems after two months, to investigate the microstructural evolution after a repair procedure (within both mortar and concrete). Furthermore, accelerated carbonation and chloride penetration tests were performed on the repair systems after two months, in order to investigate the capacity of resistance to aggressive agents after repair procedure.

The experimental protocols were also applied to study the interactions between Ultra High Performance Fiber Reinforced Concrete (UHPFRC) used as a repair material (with and without fibers) on the same concrete M25. This thesis was developed through a PhD exchange project with laboratory of Maintenance Construction and Safety for Civil Structures (MCS) at École Polytechnique Fédérale de Lausanne (EPFL) in Switzerland.

In this thesis report, a general overview on commonly encountered degradation mechanisms and repair techniques which are frequently used in civil engineering are presented in “Chapter 1: Degradation mechanisms of old concrete and repair techniques, hydration process and long-term durability of repair systems”. Cement hydration process and constituents of hydrated products, a description of moisture properties during repair works, especially the moisture transfer at the interface, and related parameters which influence long-term durability of repaired systems, etc., are detailed.

The designed configuration of repair systems, the formula of selected materials (cement pastes, mortars, concrete substrates, UHPFRCs, etc.), the descriptions of non-destructive (NMR/MRI, GRA, etc.) and other conventional techniques (Vicat needle, Thermocouple, MIP, etc.) for characterization are presented in “Chapter 2: Materials, techniques, feasibility”. The experimental protocols, data treatment and analytic methods are detailed for each technique at different ages during and after a repair procedure.

“Chapter 3: Monitoring of setting process at early age of hydration” provides information on hydration process related to chemical reactions by monitoring the longitudinal relaxation time

$T_1$  (NMR relaxometry). By comparing the results with those obtained by Vicat needle test and temperature monitoring, the evolution of the main  $T_1$  peak or of the FID signal are observed to identify the different ages of hydration. Different definitions of the *mechanical* and *chemical* setting times are thus described in section 3.1 before analysis. NMR data have been complemented thanks to the results obtained by conventional techniques and the numerical simulation from general points of view.

“Chapter 4: Investigation of moisture transfer and its impact on hydration and microstructure of repair system, during and after a repair procedure” firstly presents the assessment of moisture profiles by SPI sequence. Concerning moisture transfer at the interface, its impacts on hydration of the repair mortar and on repair efficiency of the complete systems were investigated. Moisture transfer profiles within concrete are also monitored by GRA technique. A good agreement with results obtained by MRI techniques is deserved. Porosity and pore size distribution (PSD) of the repair systems after repair procedure are quantified by MIP. Moreover, water immersion tests illustrate the resistance to liquid penetration of the repair systems. Their long-term durability is also assessed by further investigation of accelerated carbonation and chloride penetration. The comparison of concentrations and penetration depths at various penetration durations reveals the positive performance of repair mortars in function of preventing aggressive agents.

Finally, conclusions and perspectives of this thesis are summarized. The application of this complete methodology to investigate repair works will be interesting in the future. Due to obtained experimental results, further developments of analysis and numerical simulations will be predicted.



# ***1. Chapter 1: Degradation mechanisms of old concrete and repair techniques, hydration process and long-term durability of repair systems***

## **Summary**

---

<b><u>1.1 Degradation mechanisms of old concrete and conventional repair techniques.....</u></b>	<b>30</b>
<u>1.1.1 Degradation process.....</u>	30
<u>1.1.2 Classification of degradation mechanisms .....</u>	31
<u>1.1.3 Conventional repair techniques .....</u>	32
<b><u>1.2 Moisture properties during hydration process of repair mortar.....</u></b>	<b>34</b>
<u>1.2.1 Moisture properties during different stages of hydration .....</u>	34
<u>1.2.1.1 Within cement matrix at early age.....</u>	34
<u>1.2.1.2 During the repair procedure.....</u>	35
<u>1.2.2 Hydration process and constituents of hydrated cement matrix .....</u>	35
<b><u>1.3 Long-term durability of repair systems .....</u></b>	<b>38</b>
<u>1.3.1 Carbonation.....</u>	39
<u>1.3.2 Chloride penetration .....</u>	40
<b><u>1.4 Global overview .....</u></b>	<b>41</b>

---

**Degradation process** of old concrete structures needs to be previously understood before repair works. Its **mechanisms** are classified according to external (environmental) and internal (interactions) conditions. Current commercial **repair techniques** are carried out and based on empiricism. Their protocols are detailed step by step according to technical guide books.

During the repair procedure, the impacts of “**moisture properties**” on hydration process of the repair mortar are focused on. “**Water**” performance is always a key parameter to be investigated, concerning its effects on hydration reactions, microstructural evolution, and moisture transfer, etc.

The evolutions of repair systems at **micro** (moisture and ions transfers, PSD, etc.) and **macro scales** (crackings, shrinkage, etc.) are related to various couplings and the efficiency during repair procedure. By using **appropriate materials** and **techniques**, improved performance is thus verified.

The indicators of long-term **durability** after the repair procedure are investigated, especially on the resistance of repair systems to **aggressive agents** such as carbon dioxide and chloride ions.

Degradation process of reinforced concrete is presented and its mechanisms are classified, conventional repair techniques are described step by step in section 1.1. Moisture properties during different ages of hydration process of the repair mortar (at early ages and in long term) are presented in section 1.2. Durability indicators which will influence service lifetime of repair systems are detailed in section 1.3.



The service lifetime of reinforced concrete structures is subject to the action of various aggressive agents (ex: oxygen, sulfate, carbon dioxide, chloride ions from deicing salts, sea water or chlorinated setting accelerators which are initially presented in concrete, etc.). Due to porous microstructure of concrete cover, oxygen can easily diffuse and be dissolved in pore solution, through concrete cover and then onto the surface of steel rebars. The corrosion products with expansive properties result in the appearance of crackings and spallings, and create the passage for aggressive agents from environment to steel rebars [1]. The defects appear within concrete cover and reduce severely its mechanical performance by reducing the effective area of reinforcement structures. This phenomenon causes dangerous consequence in terms of users' safety.

The cost of repair works is expensive and has increased considerably over the last twenty years. It becomes an economic problem especially for post-war constructions in Europe. They were not built in strict compliance, were constructed by poor technique and absence in research experiences of durability. Concrete cover with weak or uncertain thickness is usually vulnerable to face pathologies, and its variable quality associated to defects during installation make the structures particularly unstable [2].

To prevent the deterioration of degradation, to ensure the integrity and future safety of concrete structures, and to extend their service lifetime, it is recommended to repair and to rebuild the concrete structures. Repair works are usually carried out by removing the degraded concrete cover (sand blasting, chip-off hand tools, etc.), cleaning and applying a primer on the steel rebars and finally casting a layer of repair mortar on degraded concrete [3]. Existing repair techniques are generally based on empiricism, their developments are mainly based on feedback from the profession, but abundant methods were considered unsuccessful. Various degradations impose difficulty to perform an effective repair work. Few data have been published to clarify the mechanisms governing repair procedure. Manufacturers typically keep the principle action of commercial repair products as secret. During the mortar repair procedure (except repair methods with epoxy, painting, etc.), it lacks an experimental and theoretical approach to predict the complex physico-chemical interactions among moisture transfer, microstructural evolution, porosity and PSD, etc. of repair systems.

In this thesis, "moisture properties" serves as a key parameter: such as water depletion during hydration process of the repair mortar, and moisture transfer at the interface between the fresh repair mortar and the old concrete since early age until hardening. Water evaporation from the repair systems to environment is prevented to simplify the investigation; only the internal

interactions are considered. The effect of drying within the composite system made of new and old cement paste was already investigated by SPI sequence by Faure *et al.* [4]. This parameter is worth considering during repair procedure, but in this thesis, the water depletion due to hydration reactions coupled with moisture transfer are focused on, drying process is thus too complex to be combined. It is also quite difficult to distinguish the influences created by the application of various materials.

The interactions between the formation of hydrated microstructure and water depletion (intrinsic relation between hydrated compounds and chemical reactions) are also simulated by numeric modeling. By comparing theoretical and experimental results, it makes possible to investigate the hydration mechanisms in both ways.

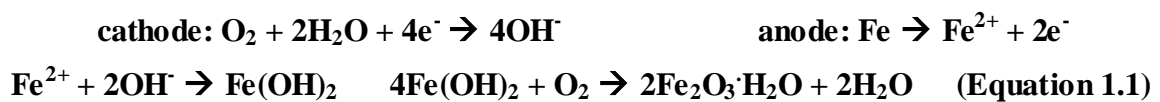
The durability of repair systems can be followed by conventional indicators thus as accelerated carbonation and chloride penetration, in order to predict the reinforced resistance to aggressive agents during prolonged service lifetime after the repair procedure.

## **1.1 Degradation mechanisms of old concrete and conventional repair techniques**

To achieve a successful repair work, the inspection and diagnosis of degradation causes are necessary to ensure repair efficiency. The understandings of degradation procedures under various conditions are useful to select appropriate repair materials.

### **1.1.1 Degradation process**

The armature of steel rebars coated with reinforced concrete is often considered as a porous and semi-permeable structure. Degradation will be caused when the structure is subject to the action of various aggressive agents during predictive service lifetime. The damage due to corrosion of steel rebars presents 80% of observed pathologies and creates the crackings on concrete cover. Electrochemical reactions are shown in Equation 1.1 and Figure 1.1 (a), which are related to simplified conditions (without complex and combined reactions with other hydrated compounds) [5]. According to ionic reactions, iron (II) hydroxide is thus precipitated and quickly oxidized.



Generally, degradation process of reinforced concrete has two successive periods, the mechanisms of degrading procedure are shown in Figure 1.1 (b) [6]:

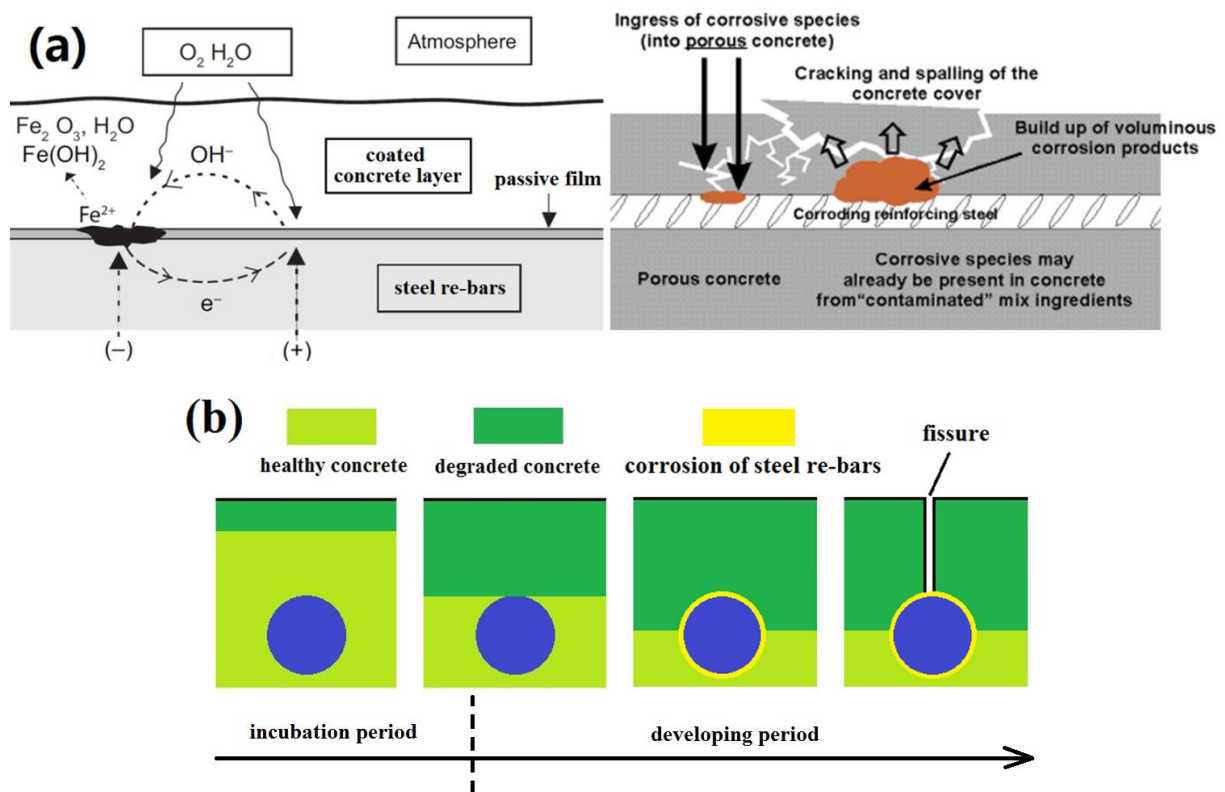


**Figure 1.1: (a) Diagram of corrosion mechanism under general condition [5]; (b) Degradation procedure of reinforced concrete cover [6].**

- An incubation period corresponds to slow alteration of concrete; the degradation of structures was not yet visible.

It ends when the formed corrosion products by internal reactions of cement hydration reach a "critical mass" and cause harmful expansion of concrete; or when the concrete cover no longer protects the steel rebars against corrosion (for example, if carbonated).

- A developing period (i.e., growth period) corresponds to the deterioration of existed degradation.

It begins when the damage is already visible and the corrosion of steel rebars evolves. At this age, repair works become difficult and costly to be achieved. It is thus suggested to perform repair works during incubation period.

### 1.1.2 Classification of degradation mechanisms

Actually, degradation is often caused by physico-chemical exchanges between surrounding environment and hydrated cement matrix. The concrete structures suffer the attacks as time evolves. This procedure involves various types of mass transfer, and performs in different ways depending on various conditions. For example, the quality of concrete structure is

affected severely in both hot and dry climates (such as constructions near equator area), or under both wet and chloride penetration conditions (such as piers of cross-sea bridge under and close to salty sea water).

Different causes and mechanisms of degradation are detailed and classified as detailed in technical guidebook of IFSTTAR [6]:

*Physical (Mechanical):*

- 1) Surface degradation: abrasion / erosion / cavitation / external cracking and spalling.
- 2) Internal cracking: gradients in humidity or temperature / freezing or thawing / crystallization pressure / structural loading / exposure to extreme high temperature (fire) / shrinkage / sensitive expansion or contraction of aggregates / bad thermal compatibility between aggregates and cement matrix.

*Chemical:*

Attack by fresh water, salty sea water or chloride solution (brine) / attacked by acid or sulfates (ground water or due to local environment) / oxidation of sulfides in aggregates / formation of secondary thaumasite and ettringite / alkali-silica reaction / alkali-carbonate reaction.

*Physico-chemical:*

Corrosion of steel rebars / degradation due to electrolytic action / spalling due to melting salt / alkali-aggregate reaction.

Generally, factors which affect the degradation are related to characteristics of concrete composition, internal micro-climate, external environment, conception of design work, installation and maintenance of the structure, etc. The mechanisms of concrete degradation are principally related to major damage causes, such as carbonation, attack by chloride ions, sulphate or acid attack, freeze-thaw cycles, drying-wetting cycles, alkali reactions, etc., corrosion of steel rebars are thus induced. Due to extreme environmental conditions, degradation rates will be accelerated.

### **1.1.3 Conventional repair techniques**

To extend the service lifetime of old concrete and to protect newly constructed structures by the prevention of aggressive agents, it is recommended to apply repair materials on concrete cover which enables to hinder aging and to reduce the deterioration of degradation.

Before a repair work, several questions need to be configured: “Why the degradation is caused?” “How to repair this concrete structure?” “How much will it cost?” “How long the protection will last after the repair procedure?” Aforementioned questions need to be

answered in an economical and durable way, in order to design a systematic approach with sufficient information of its evolution during repair procedure.

To ensure an efficient work, the selections of convenient repair products and techniques are essential. Surface preparation procedure of degraded concrete is also important. The characterization of microstructural evolution and moisture properties under different environmental conditions (temperature, RH, etc.) controls repair procedure as well.

All these objectives cannot always be achieved at the same time. Concerning each repair work, the satisfaction to aforementioned aspects depends on choices' hierarchy and the requirement of durability.

The following six steps of repair procedure are presented, which has been developed, used, and evaluated over an extended period of service lifetime. This methodology is suitable to repair newly constructed concrete with defects, as well as old concrete structures which have been damaged with long duration of exposure caused by strict conditions [3]:

- Step 1: Detection of the degradation causes (damages or defects);
- Step 2: Auscultation - diagnosis (identification of pathologies and assessment of the extent of degraded area);
- Step 3: Preparation of purposed repair system. Harmful elements need to be eliminated or cleaned (dirts and superficial deposits, such as dust, oil and grease, paraffin wax, curing compounds, efflorescence of calcite, etc.). Incompact concrete structures must be removed, joints and cracks should be patched with mortar;
- Step 4: Application of repair products (site condition, respect to curing specification);
- Step 5: Investigation of repair efficiency (expected performances: reinforced mechanical properties of repaired concrete, extended service lifetime, etc.);
- Step 6: Surveillance and monitoring (during the first years after repair work).

Moreover, other problems concerning the efficiency and sustainability of repair work also need to be considered, for both the repair materials and degraded concrete. It should be taken into account that, precautions have to be respected as follows [3]:

1. Thermal (expansion coefficient) and mechanical compatibilities (elastic modulus, adhesion, compressive and tensile strength) especially at the interface between the repair products and degraded concretes to maximally avoid the formation of crackings.

2. Limitation of immediate moisture transfer from repair products towards environment and the degraded concrete. Rapid-setting mortars with water retention properties are prior applied to reduce harmful effects on mortar hydration, in order to minimize the risk of drying shrinkage, to promote maturation of repair products and to avoid poor durability properties. The influences caused by moisture transfer on formation of hydrated compounds and microstructural evolution are confined. Appropriate curing conditions and pre-treatments, such as: spraying to humidify the degraded surface, etc. are also suggested.

## **1.2 Moisture properties during hydration process of repair mortar**

Concrete and mortar are composite materials consisting of aggregates in various sizes (formed by inert grains agglomerated with hydraulic binder). In concurrent applied composition, aggregates are sands, grains of stone, and gravels for concrete, and standard sands for mortar; the hydraulic binder is usually Portland cement. Cement paste is presented of 25% to 40% in the volume of concrete, and 35% to 50% in the volume of mortar. The corresponding physical and chemical properties of concrete and mortar are directly related to the characteristics of hydrated cement phase.

In general, cement-based materials are porous solids with pores filled with various liquids and gaseous phases at micro scales. To explain the moisture properties, it is necessary to firstly understand different stages of hydration process. The classification of different water molecules after hardening period is related to various techniques of characterization.

### **1.2.1 Moisture properties during different stages of hydration**

The understanding of moisture properties helps us to better view the physico-chemical interactions during a repair procedure, where moisture transfer exists during mortar hydration process since early age until hardening. The evolution of water content within the fresh mortar and the old concrete strongly influences the final performance.

#### **1.2.1.1 Within cement matrix at early age**

Water is a reactant for hydration reactions (about half of the mixing water is consumed at the end of deceleration period [7]). The residual water remains within cement matrix and evolves over time: it exists in created pores after autogenous deformation, the evaporation to environment results in shrinkage. The moisture gradient between bulk (almost saturated at sufficient w/c ratio) and surface (degree of saturation ( $S_w$ ) varies due to external condition) causes transfer from inside to outside, thus the pores are partially-filled with air. During this

procedure, the refinement of capillary pores plays the most important role. The distribution of water is also related to microstructure (PSD) and sorption property after stabilization.

The degree of surface protection is based on its composition (w/c ratio, mineral additives such as limestone filler, metakaolin, silica fume, fly ash, slag, etc.) and curing techniques in place. By reducing w/c ratio, cement grains get closer to each other, the space to be filled is confined. There exists less possibility to form a big gap, thus capillary porosity is reduced. Total pore volume (cumulative porosity) decreases while the average diameter of largest pores decrease simultaneously. Theoretically sufficient w/c ratio is around 0.42 for complete hydration [8]. But in practice, hydration is never complete. There always exists some capillary porosity even though for very low w/c ratio around 0.25. Since the volume of formed hydrates is smaller than the volume of initial constitutions (present anhydrous grains), that will create spaces not filled with water (self-desiccation or endogenous shrinkage). Mineral additions can significantly modify concrete performance to environmental conditions.

#### **1.2.1.2 During the repair procedure**

Moisture properties in repair systems are complex, which involve different fluids (such as: pore solution, liquid or vapor water, air bubbles, etc.) since casting until hardening. There exist both passages from mortar to concrete and to environment, which lead to the evolution in relative humidity (RH), capillary pressure ( $p_c$ ) and  $S_w$  in pores, and cause shrinkage.

Furthermore, hydration reactions were not completed and there exist non-hydrated compounds in old concrete if w/c ratio is not sufficient. Water diffuses from repair mortar into old concrete and leads to a re-hydration phenomena, while water shortage within repair mortar also results in microstructural defects. These two opposite aspects need to be balanced to obtain an optimized condition to confirm effective repair works.

#### **1.2.2 Hydration process and constituents of hydrated cement matrix**

During hydration process, five periods can be distinguished as shown in Figure 1.2 [7]:

- 1. Dissolution of cement grains and release of ions in solution;
- 2. Dormant or induction period;
- 3. Setting period or acceleration of hydration;
- 4. Hardening period or deceleration of hydration;
- 5. Cure and hydration of residual anhydrates.



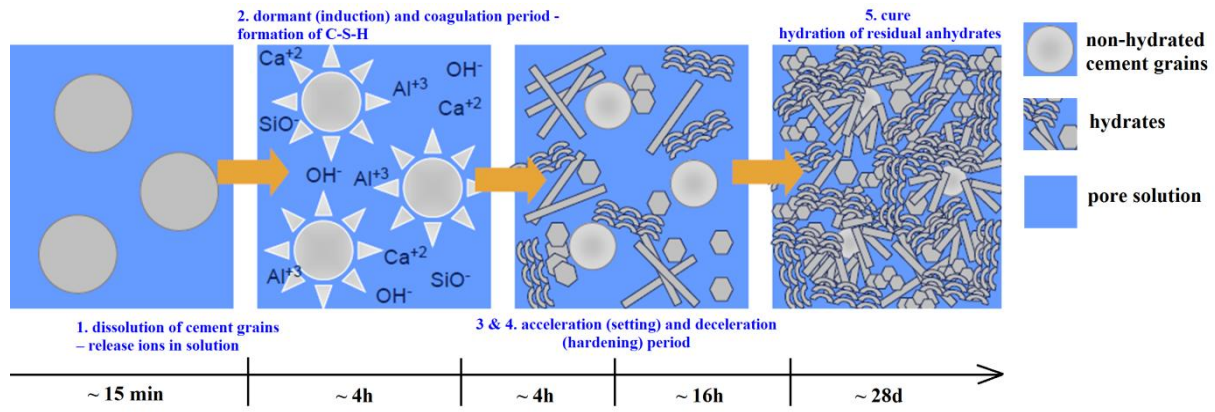


**Figure 1.2: Representative schema of cement matrix during hydration process.**

Although cement matrix is macroscopically homogeneous (the order of magnitude is  $10^{-2}$  m), its chemical composition, crystal structure and morphology are completely heterogeneous. These parameters are also sensitive to environmental conditions during casting.

The hydrated cement paste is generally constituted by hydration products (hydrates: Calcium Silicate Hydrate (C-S-H), hydrated lime (portlandite)  $\text{Ca}(\text{OH})_2$ , sulfoaluminate AFt and AFm phases, etc.), non-hydrated cement grains, capillary porosity and air bubbles, etc., as shown in Figure 1.3 (a) [9]. The water distribution in C-S-H layer is schematically illustrated by a classical model Feldman and Sereda as shown in Figure 1.3 (b).

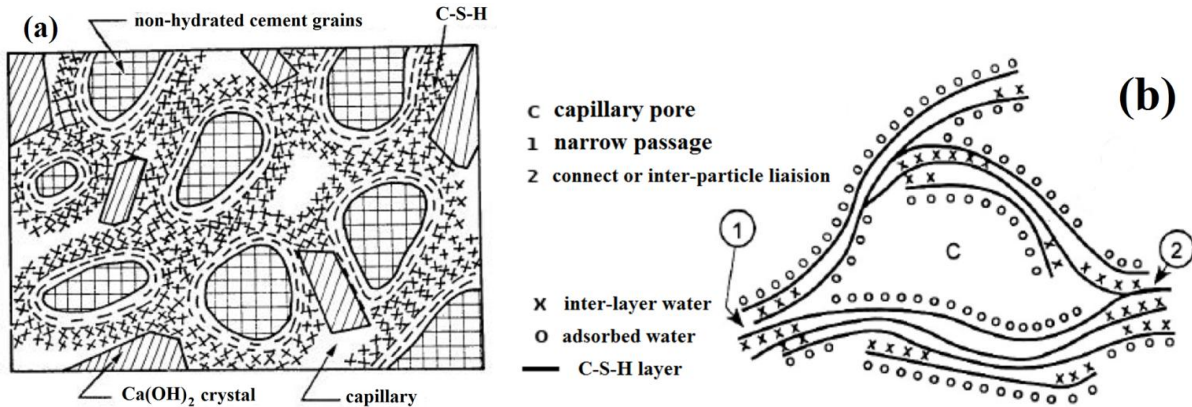


**Figure 1.3: (a) Representative schema of hydrated cement phase; (b) Illustration of water distribution in C-S-H by model Feldman and Sereda (1970)**

Within the hydrated cement phase after hardening period, there exist various water molecules with different properties of mobility (related to  $^1\text{H}$ -NMR measurements). This part of water is corresponding to hydrated microstructure and also related to long-term durability. Depending on the distribution and physico-chemical state of water molecules, the classification is detailed as follows (adhesive strength:  $A > B > C > D$  less free  $>$  D more free) [10]:

A) **Chemically-bound** water (density ~ 1.2)

This part of water is related to integral part of C-S-H gel (about 23% by weight of reacted cement). It is very stable and cannot evaporate except during the decomposition of C-S-H at very high temperature.

B) Zeolitic water (**inter-layer C-S-H**) (density ~ 1.0)

This part of water is not chemically bound, but remains between C-S-H layers by hydrogen bonding. The humidity should be decreased below 30% for evaporation, which will cause a very important shrinkage of cement phase.

C) Adsorbed water (**physically-bound** water) (density ~ 1.0)

This part of water is physically bound onto solid surface (especially within pores of gel). A layer of about six sphere-packing water molecules (thickness ~ 1.2 nm due to 1 water molecule = 0.343 nm) is retained by hydrogen bonds. Most of the adsorbed water may be evaporated if the humidity is below 50%. This water loss is largely responsible for shrinkage.

D) Free water (**capillary** water) (density ~ 1.0)

This part of water corresponds to excess water when cement grains are totally consumed. Depending on the size of capillary porosity, the water may be more or less free because of the importance of surface forces (thickness ~ 4.3 nm).

More free: contained in largest capillary porosity ( $> 0.05 \mu\text{m}$ ), does not cause important shrinkage of cement phase.

Less free: contained in smallest capillary porosity ( $0.005 \mu\text{m}$  to  $0.05 \mu\text{m}$ ) and held by capillary tension. The humidity should be decreased below 90% to begin its evaporation, which has an important influence on the shrinkage of cement phase.

The specific volume of physically weakly bound water is about  $0.99 \text{ cm}^3/\text{g}$ , which is very close to that of free water in salt solution equal to  $1.04 \text{ cm}^3/\text{g}$  at room condition (temperature =  $20^\circ\text{C}$ , pressure = 1 atm) [11]. They can evaporate through drying at  $105^\circ\text{C}$  and are denoted as evaporable water. Meanwhile the specific volume of hydrate water is only  $0.75 \text{ cm}^3/\text{g}$ . Therefore chemically-bound water, C-S-H inter-layer water and physically strongly bound water are all considered as non-evaporable, which has great disadvantages during conventional drying process of being quite long. It may take several weeks and this amount of loss water corresponds only 0.2% to 0.3% by comparing to evaporable water content [10].

Through NMR/MRI techniques, not only is evaporable water (in macro pores) possible to be detected, but also C-S-H inter-layer water and physically strongly bound water (in mesopores). These aforementioned states and related porosities within cement matrix are

shown in Figure 1.4 [12] and important for further investigations. This point of view bases on water classification and is essential for this thesis. The technical and analytical details will be described in sections 2.3 and 3.2.

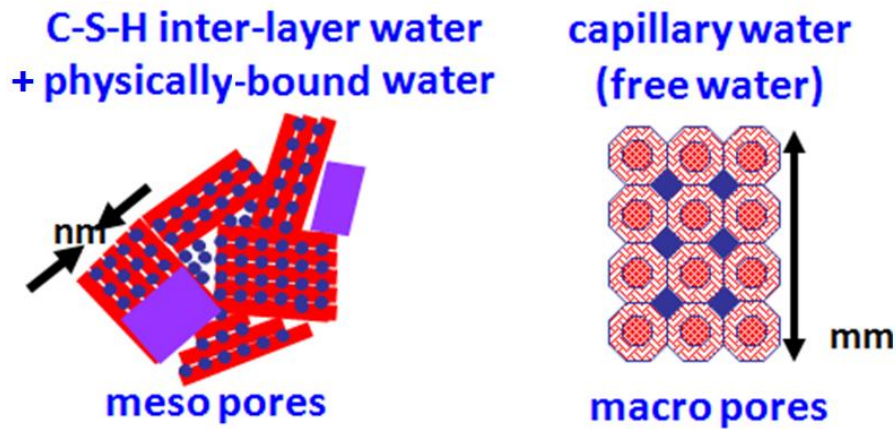


Figure 1.4: Detectable water by NMR/MRI in different states during cement hydration

### **1.3 Long-term durability of repair systems**

Performance of repair system is often determined by its microstructure. Excellent durability is corresponding to excellent mechanical properties (compressive or tensile strength, expansion type, construction joints, endogenous deformation, etc.) and to low permeability (capillary pores network,  $S_w$ , porosity, tortuosity or connectivity, etc.). Inadequate resistance of construction (designed structures, crackings caused by shrinkage or due to service loads, joint problems, etc.) and low resistances of concrete lead to a poor durability [13]. The effects of mineral additions are based on type and dosage and also increase or decrease concrete durability. Slightly porous concretes are generally more durable. Because their low permeability hinder the penetration of liquid (water, solution), gas (water vapor, carbon dioxide) and other aggressive agents (sulfate,  $Cl^-$ , etc.). Due to the shortage of preferential passages in three dimensions of specimens, their resistances to degradation are ensured.

The two most common causes to degradation of old concrete are presented as follows [14]:

- 1. Global breakdown of passivity by neutralization of concrete, predominantly by reaction with carbon dioxide;
- 2. Local breakdown of passive film on steel rebars by chloride ions.

Water is involved in both causes while shrinkage-cracking caused by drying effect is not investigated. During carbonation procedure, it is both a medium (optimal RH accelerated kinetics) and a product of carbonation reaction ( $CO_2 + Ca(OH)_2 \rightarrow CaCO_3 + H_2O$ ). The pH

value (from 13 in non-carbonated areas to less than 9 in degraded areas) is reduced and chemical equilibrium between the hydrates within cement matrix and pore solution is changed. Chloride diffusion is related to environmental RH as it is always accelerated by immersion into salty solution. The penetration of  $\text{Cl}^-$  ions is prevented in dried condition or slowed down in low RH condition, but intensified during drying-wetting cycles. At high RH at about 95%, dissolution of hydrates (fissures, defects, etc.) is initiated. When the penetration zone reaches steel rebars, corrosion is promoted by the formation of expansive products.

It is also worth mentioning that, introduced water during degradation also leads to re-hydration while there exist non-hydrated compounds within both repair mortar and old concrete. However as detailed previously, excess water deteriorates microstructure and the long-term durability is not assured, the disadvantages take precedence over the advantages. Both aspects need to be simultaneously considered.

### 1.3.1 Carbonation

Carbon dioxide in gaseous form usually comes from external environment. It dissolves in pore solution within cement matrix and reacts with certain hydrated compounds to form calcium carbonate or hydrated siliceous material (silica gel) and water. RH is also an important parameter for penetration as it dissolves carbon dioxide from gas to weak acid solution. Predominant mechanisms in carbonation of portlandite  $\text{Ca}(\text{OH})_2$  and calcium silicate hydrates  $\text{C}_x\text{S}_y\text{H}_z$  are shown in Figure 1.5, Equations 1.2 and 1.3. They are both formed by hydration reactions of  $\text{C}_3\text{S}$  (alite) and  $\text{C}_2\text{S}$  (belite) clinker phases. The latter reaction is considered as topochemical (without material transport or dissolution-precipitation) between heterogeneous phases [15].

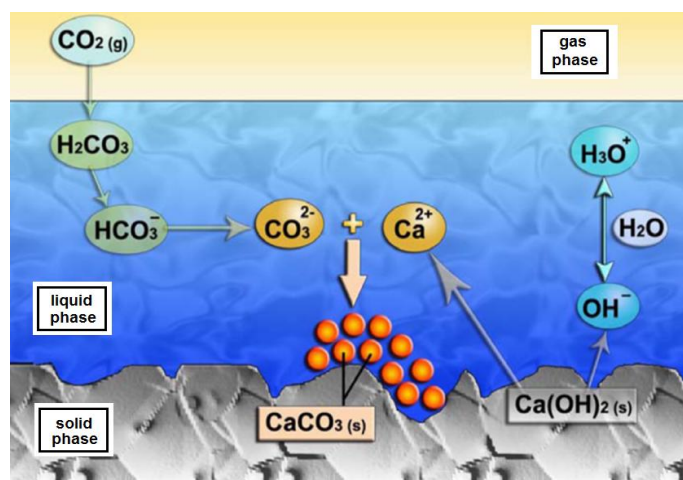
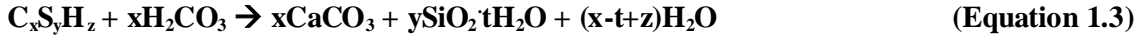


Figure 1.5: Carbonation mechanism of Portlandite in cement matrix.



The pore solution of concrete is an alkaline solution with a pH close to 13, for structures exposed to air and under health conditions. Steel rebars are passivated in such environment. The penetration of carbon dioxide reduces the pH of pore solution until 9, and the structure becomes corrosive because the electrical potential of steel rebars goes into corrosion area according to Pourbaix diagram of Fe-H<sub>2</sub>O. It leads to the dissolution of structure and the formation of defects (such as pores, crackings, etc.). And the degradation also allows the passage of aggressive agents which deteriorate the structure.

### 1.3.2 Chloride penetration

The source of chloride ions always comes from external environment such as sea water or salts commonly used for road deicing in winter, but also possible originates within composition of cement-based materials such as aggregates, additions, and setting accelerators Calcium Chloride 37. Chloride ions penetrate by diffusion during immersion or by capillary action during drying process and freeze-thaw cycles. They cause premature corrosion of steel rebars and spallings of concrete cover. When the concentration of chloride ions is sufficiently high, passivated film which protects steel rebars is destroyed.

Penetration mechanisms of chloride ions are shown schematically in Figure 1.6 [16].

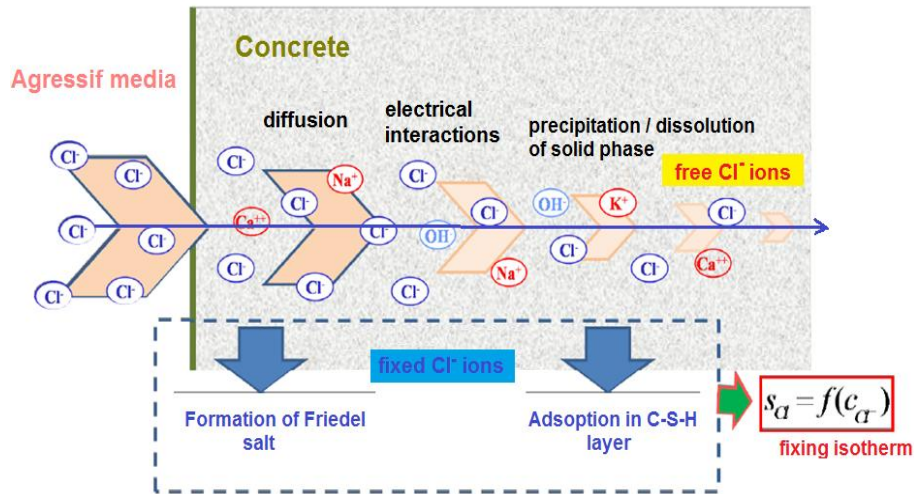


**Figure 1.6: Penetration mechanism of attack by chloride ions .**

Chloride ions appear with different states in concrete structure [17]:

- Chemically-bound ions (for example, Friedel's salt) and physically-bound ions by adsorption onto C-S-H gel (ionic exchange between OH<sup>-</sup> and Cl<sup>-</sup> ions).
- Free ions of ionic form in pore solution and do not react with cement matrix.

Ions transfers are not only affected by their concentration, but also depend on interactions between chloride ions and cement matrix, as well as chloride fixation capacity on constituents of cement phase. This procedure thus depends on environmental chloride load and concrete properties. The latter is primarily described by the permeability and chloride binding capacity which is influenced by w/c ratio, cement type, construction quality, curing condition, polymer admixtures and mineral additions.

Generally, this procedure in saturated medium is simply monitored by diffusion of chloride ions and mathematically described by Fick's second law of diffusion, caused by gradient of chloride concentration between the surface exposed to chloride solution and the non-polluted inside of concrete structures [18]. Physico-chemical reactions between chloride ions and solid phase hinder ions transport and thus decrease the amount of free chloride ions in solution. As chloride moves through the concrete, part of it is removed from solution by chemical and physical binding, a phenomenon sometimes referred to as filter effect. Given a high chloride binding capacity, this might substantially slow down the increase of chloride concentration in the pore solution of the internal concrete.

Indeed, the most common case is non-saturated condition (tidal zone [19], a test method was developed and applied in this thesis). The total quantity of chloride ions ( $C_{Cl,tot}$  in mol m<sup>-3</sup> concrete) is expressed as in equation 1.4:

$$C_{Cl,tot} = S_{Cl} + \emptyset * C_{Cl} \quad \text{(Equation 1.4)}$$

$S_{Cl}$  (in mol m<sup>-3</sup> concrete) is the accumulated amount of bound chloride ions in solid phase, and  $C_{Cl}$  (in mol m<sup>-3</sup> solution) is the amount of free chlorides in pore solution,  $\emptyset$  is the porosity of materials, corresponding to the evaporable water content.

## **1.4 Global overview**

Moisture properties are essentially important to be focused on in this thesis. Water is involved during cement hydration and repair procedure, and also influences long-term durability. Detectable water by NMR/MRI includes not only evaporable water but also some non-evaporable water, which is quite difficult to be investigated by conventional techniques. After

bibliographical research in various aspects related to repair works, appropriate materials and techniques need to be selected, in order to establish a complete methodology of investigation. The selection of repair materials is related to their intrinsic properties, such as initial w/c ratio, rapidity of setting process, water permeability, accessible porosity, etc., which will influence immediate moisture transfer at the interface between the repair mortar and the old concrete. This point will be developed in section 2.2.

By combining different techniques, such as non-destructive techniques NMR/MRI and GRA, and other conventional techniques, repair procedure is followed since casting until hardening during hydration process. This point will be developed in section 2.3.

Mechanical resistances are not evaluated in this thesis to reduce the experimental difficulties and to simplify the investigations. Because the expansion of repair products is minimized, the compressive and traction strength of old concrete is considered as constant, the effects of these aspects are not evident in moisture properties.



In conclusion, in order to investigate the effect of **immediate moisture transfer** at early age and the **durability** of repair system in long term, and to distinguish the effect of different formulas, **moisture properties** are focused on.

Different repair mortars with appropriate proprieties were applied on the same substrate. Especially during **setting process**, non-destructive and conventional techniques were used to monitor the **water depletion** (setting indicator) within repair mortar and to investigate the moisture transfer from mortar to concrete.

Repair mortar with **weak shrinkage** at early age is applied, and the mechanical proprieties are ignored to simplify and to concentrate on the main objectives.

Generally, the key word is “**water**” during hydration in this thesis. Two different scales are focused on: setting (chemically and physically bound water) and moisture transfer (free capillary water). Various materials and corresponding techniques will be detailed in chapter 2.





## 2. Chapter 2: Materials, techniques, feasibility

### Summary

---

<b><u>2.1 Design of repair systems</u></b> .....	<b>47</b>
<b><u>2.2 Materials</u></b> .....	<b>48</b>
<u>2.2.1 Cement</u> .....	49
<u>2.2.2 Concrete substrates</u> .....	50
<u>2.2.3 Cement pastes and mortars for the investigation of setting process</u> .....	50
<u>2.2.4 Repair mortars</u> .....	53
<u>2.2.5 UHPFRC matrix and with aramid fibers</u> .....	54
<u>2.2.6 Technical details of casting procedure</u> .....	55
<b><u>2.3 Selected techniques during different stages of hydration</u></b> .....	<b>56</b>
<u>2.3.1 For the investigation of only cement pastes and mortars</u> .....	56
<u>2.3.1.1 NMR relaxometry</u> .....	56
<u>2.3.1.2 Conventional techniques</u> .....	62
<u>2.3.1.3 Numerical simulations</u> .....	63
<u>2.3.2 For the investigation of repair systems</u> .....	64
<u>2.3.2.1 At early age (since casting until 28 days)</u> .....	64
<u>MRI - SPI sequence (moisture profiles)</u> .....	64
<u>GRA (density profiles)</u> .....	66
<u>2.3.2.2 At middle age (since 2 months)</u> .....	68
<u>GRA (total porosity)</u> .....	68
<u>MIP (total porosity &amp; PSD)</u> .....	69
<u>2.3.2.3 After repair procedure (since 2 months until long term)</u> .....	71
<u>Water immersion</u> .....	71
<u>Carbonation</u> .....	71
<u>Attack by chloride ions</u> .....	72
<b><u>2.4 Global overview</u></b> .....	<b>73</b>

---

**Rapid-setting** repair mortars with **low w/c ratio** and various admixtures are chosen to be applied on an old concrete specimen, in order to satisfy

aforementioned requirements of a repair work. Sealed mortars are prepared simultaneously as repair mortars for parallel comparison of hydration kinetics during and after repair procedure. In this thesis, moisture properties are mainly related to free water, and frequently to physically-bound water. Drying effect (i.e., evaporation to environment) is avoided in order to simplify the case.

At different ages of hydration, appropriate **techniques of characterization** related to **moisture properties** are also chosen to study different repair systems. Key parameters such as **setting times**, **temperature evolution**, and **free water depletion** within mortars themselves, **moisture transfer** at the interface, **microstructural evolution** of different parts within the whole systems (mortars, old concretes, and the mortar - concrete interface), and **durability indicators** after the repair procedure, etc., are investigated. Theoretical principles and experimental equipments are detailed in this chapter.

The diffusion of aggressive agents is assumed to investigate long-term durability. Primarily, these properties are based on experimental results from water immersion, accelerated carbonation, and chloride penetration tests.

By using various techniques on different composite systems, the **methodology** of characterization for a theoretical study of the complete procedure is proposed. It is worth mentioning that, this methodology can be applied in many systems, where exist both moisture transfer and water depletion.

The performances of repair materials and repair systems are equally important. Their properties during and after a repair procedure are both interesting to be considered.

In order to investigate aforementioned aspects, three different configurations have been designed in this thesis, as shown in Figure 2.1:

- Only repair mortars;
- Repair systems (fresh mortar + concrete) isolated from environment;
- Repair systems (hardened mortar + concrete) subjected to aggressive agents after a repair procedure.

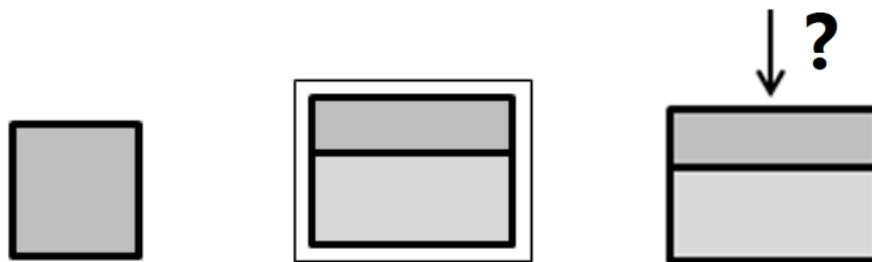


**Figure 2.1: Summary of investigated systems**

Based on these systems, the selection of repair materials, substrates and appropriate techniques of characterization will be detailed in following sections. The materials with relevant properties have been used to investigate hydration process, moisture transfer, etc., during and after repair procedure. It is prior important to find a convenient methodology of characterization, rather than to declare the global application under complex site conditions.

## **2.1 Design of repair systems**

As previously explained, the repair systems are fixed as illustrated in Figures 2.2 (a) and (b), to distinguish internal water depletion from moisture transfer at the interface, as well as its impacts on hydration of the repair mortar.



**Figure 2.2: Schema of repair systems for (a) techniques in which metallic compounds are forbidden; (b) other traditional techniques.**

The main objectives to prepare these systems are described as follows:

- \* To quantify moisture transfer at the interface between the fresh repair mortar (1) and the old concrete (2);
- \* To compare the hydration process of the fresh repair mortar (1) in contact with the old concrete and that of the sealed mortar with the same formula (1');
- \* To facilitate the investigation of the long-term durability of the repair system.

In this thesis, water evaporation to environment is avoided since the (1) + (2) and (1') configurations are respectively sealed (global isolation of the whole system). These two parts are prepared simultaneously and placed separately. Part (1) + (2) is sealed by a parafilm (thin polymer layer) and part (1') is isolated in a plastic mold for techniques such as NMR/MRI. Metallic compound is forbidden because of harmful effects on the homogeneity of magnetic field. Part (1) + (2) and (1') are coated by self-adhesive aluminum paper for other traditional techniques such as GRA, MIP and durability indicators, etc. It is worth mentioning that, the effects of coating materials were counted out during data treatment, by comparing the obtained signals to background measurement before the casting of repair and sealed mortars.

These systems are prepared with a diameter of 11 cm, and a height of 3 cm for the repair and sealed mortars, as well as 5 cm for the old concretes. Plastic circular molds were used to maintain the form of fresh repair mortar as shown in Figures 2.2. Silicone with neglect quantity is applied between the mold and the concrete. Thus gaps and slight crackings are filled, in order to prevent rapid liquid flowing by lateral side from the fresh repair mortar to the old concrete since placing. Moisture transfer is thus monitored in only one dimension.

It is worth mentioning that, the configuration of this system is related to both classical size of cement-based materials (diameter of 11cm) and homogenous range of magnetic field within MRI apparatus (height of  $3 + 5 + 3 = 11$  cm). According to inherent properties of magnetic core, the height of whole system is limited within appropriate area, in order to avoid boundary effects and inaccurate profiles within inhomogeneous magnetic field.

## **2.2 Materials**

According to conventional repair methods [3] and appropriate techniques, the materials corresponding to different parts within the repair systems are presented as follows. Degraded

concrete substrates are fixed in only one type, and reference repair products (mortars with low w/c and s/c) were selected. Repair mortars with relevant properties instead of commercial repair products were used in this thesis, the goal of investigation is to establish an efficient methodology of characterization during and after the complete repair procedure.

### 2.2.1 Cement

In this thesis, all cement-based materials were prepared either with gray or white Ordinary Portland Cement (OPC), the compositions are detailed as follows and shown in Table 2-1:

\* The same type of gray OPC was used to prepare both concrete substrates and mortars (to ensure their mechanical and physical compatibilities): CPA-CEM I 52.5 R PM ES CP2:  $C_3S = 64.2\%$ ,  $C_2S = 11.68\%$ ,  $C_3A = 2.6\%$ ,  $C_4AF = 13.1\%$ , gypsum = 3 % (chemical composition: CaO 65.38 %, SiO<sub>2</sub> 20.54 %, Al<sub>2</sub>O<sub>3</sub> 3.59 %, Fe<sub>2</sub>O<sub>3</sub> 4.13 %) from Saint-Vigor (Le Havre Lafarge). It is called cement instead of gray OPC as frequently used in this thesis.

\* A white OPC: CEM I 52.5:  $C_3S = 71.9\%$ ,  $C_2S = 9.6\%$ ,  $C_3A = 10.8\%$ ,  $C_4AF = 0.9\%$ , gypsum = 5.5 % (constituent proportions are calculated by Bogue's equations and according to chemical composition: CaO 66.30 %, SiO<sub>2</sub> 22.24 %, Al<sub>2</sub>O<sub>3</sub> 4.25 %, Fe<sub>2</sub>O<sub>3</sub> 0.29 %) was used to prepare four cement pastes of w/c ranging from 0.35 to 0.50. This white OPC is widely used in NMR analysis since it contains very low iron content.

Constituents		Gray cement CEM I (%)
Calcium oxide	CaO	65.38
Soluble silica	SiO <sub>2</sub>	20.54
Ferric oxide	Fe <sub>2</sub> O <sub>3</sub>	4.13
Aluminum oxide	Al <sub>2</sub> O <sub>3</sub>	3.59
<i>Titanium oxide</i>	<i>TiO<sub>2</sub></i>	<i>0.19</i>
<i>Magnesium oxide</i>	<i>MgO</i>	<i>0.86</i>
<i>Sodium oxide</i>	<i>Na<sub>2</sub>O</i>	<i>0.18</i>
<i>Potassium oxide</i>	<i>K<sub>2</sub>O</i>	<i>0.29</i>
<i>Manganese oxide</i>	<i>MnO</i>	<i>0.07</i>
<i>Sulfur trioxide</i>	<i>SO<sub>3</sub></i>	<i>2.67</i>
<i>Insoluble residual</i>		<i>0.84</i>
<i>Loss at 1150 °C</i>		<i>1.24 (H<sub>2</sub>O: 0.36 + CO<sub>2</sub>: 0.88)</i>

Total analyzed elements		99.98
-------------------------	--	-------

Constituents		White cement CEM I (%)
Calcium oxide	CaO	66.30
Soluble silica	SiO <sub>2</sub>	22.24
Ferric oxide	Fe <sub>2</sub> O <sub>3</sub>	0.29
Aluminum oxide	Al <sub>2</sub> O <sub>3</sub>	4.25
<i>Titanium oxide</i>	<i>TiO<sub>2</sub></i>	<i>0.17</i>
<i>Magnesium oxide</i>	<i>MgO</i>	<i>0.50</i>
<i>Sodium oxide</i>	<i>Na<sub>2</sub>O</i>	<i>0.01</i>
<i>Potassium oxide</i>	<i>K<sub>2</sub>O</i>	<i>0.09</i>
<i>Manganese oxide</i>	<i>MnO</i>	<i>0.00</i>
<i>Sulfur trioxide</i>	<i>SO<sub>3</sub></i>	<i>2.86</i>
	<i>P<sub>2</sub>O<sub>5</sub></i>	<i>0.05</i>

<i>Insoluble residual</i>	<b>0.62</b>	Total analyzed elements	<b>99.63</b>
<i>Loss at 1150 °C</i>	2.87		

**Table 2-1: Chemical and potential mineral compositions of gray and white OPCs.**

### 2.2.2 Concrete substrates

The degraded concretes are chosen as M25 in this thesis, because its high porosity and permeability make the phenomena of moisture transfer more evident [20], in order to validate a methodology of characterization in a simplified way. The formula corresponds to a low-grade building concrete with a high w/c ratio of 0.84. Its compressive strength is 25 MPa, while its mechanical strength is low and durability is poor. The composition is shown in Table 2-2, various aggregates and sands with different granularities are used:

Gravel boulonnais 12.5/20 kg/m <sup>3</sup>	Gravel boulonnais 5/12.5 kg/m <sup>3</sup>	Boulonn ais sand 0/5 kg/m <sup>3</sup>	Seine sand 0/4 kg/m <sup>3</sup>	Cement CEM I 52.5R kg/m <sup>3</sup>	Added water kg/m <sup>3</sup>	Total w/c	Aggre gates/ C	Occlud ed air (%)	Slump Abrams cone (cm)	$R_{28j}^{moy}$ (MPa) measured at 28 days
<b>619</b>	<b>388</b>	<b>453</b>	<b>446</b>	<b>230</b>	<b>193</b>	<b>0.84</b>	<b>8.29</b>	<b>1.1</b>	<b>20</b>	<b>24.0±3.6</b>

**Table 2-2: Mix design of concrete M25 in which aggregates are considered as in dry state.**

Specimens with cylindrical form are stored under water for 10 months after casting (d = 11 cm, h = 22 cm). Initial states of concrete substrates are supposed to be similar (same age, hydration state, preparation procedure, etc.). The specimens are then cut into desired size (d = 11 cm, h = 5 cm), by using a machine fitted with an abrasive disk working under flowing water which determines a quality work in order of millimeters. This method makes it possible to obtain a relatively flat and regular surface. But sometimes it involves small crackings and defects, and it is also difficult to control position and thickness with precision.

Before repair works, these specimens need to be firstly pretreated in order to stop hydration process and to maintain the same age before experiments. They are dried in oven for 1 month with constant temperature controlled at 45 °C to avoid thermal dehydration. Due to unique chosen substrate, the influences with various repair products are focused on during and after the repair procedure.

### 2.2.3 Cement pastes and mortars for the investigation of setting process

The cement pastes with various admixtures for monitoring relaxation times and feasibility are summarized in Table 2-3. T<sub>1</sub> and T<sub>2</sub> are respectively longitudinal and transverse relaxation

times in NMR relaxometry techniques, which will be described in section 2.3.1.1. Initial  $T_1$  value is related to longitudinal relaxation time by the first measurement since casting. It corresponds to free water content, i.e., w/c ratio of each specimen. Both relaxation times are investigated in order to well understand the setting process.

Type	Admixtures	w/c or w/binder	Measurements
Cement paste		<b>0.325, 0.352, 0.375, 0.401, 0.425</b>	Monitoring of $T_1$ , $T_2$ & w/c in relation to initial $T_1$
Cement paste + 2% super-plasticizer (SP)	CHRYSO <sup>®</sup> Fluid Optima <sup>®</sup> 175	<b>0.300</b>	Monitoring of $T_1$ , $T_2$
Cement paste + mineral additions	Limestone filler 30% (/binder)	<b>0.325, 0.350, 0.375, 0.400, 0.425, 0.500</b>	w/c in relation to initial $T_1$
	Metakaolin 10% (/binder)	<b>0.35</b>	Monitoring of $T_1$ , $T_2$
Cement paste + fibers Technora <sup>®</sup>	2% (volume) L = 2 cm Ø = 0.8 mm	<b>0.399</b>	Measure of initial $T_1$
Cement paste + SAP polymer	BASF Luquasorb 1161 <sup>®</sup>	<b>0.300</b>	Monitoring of $T_1$ , $T_2$
	Aldrich 435325 <sup>®</sup>		Measure of initial $T_1$

**Table 2-3: Cement pastes for monitoring relaxation times**

Fly ash and slag are widely-used admixtures in conventional cement pastes and mortars. But their applications are not suitable in this thesis, as they contain very high iron content. NMR signals of only cement pastes with fly ash or slag perform weakly according to feasibility tests. The mineral additions such as limestone filler and metakaolin are thus selected.

Aramid fibers (2 - 3 cm in length) absorb and maintain water within cement matrix. The molecular formula of these fibers is shown in Figure 2.3 (Teijin Aramid - Technora<sup>®</sup>: copoly (p-phenylene/3, 4'- diphenyl ether terephthalamid) [21]. They correspond to para-aramid fibers with hydrolytic aging properties which influence moisture transfer, sensitivities in RH and temperature, etc., during hydration. Concerning the durability after 1.5 years, only slight chain degradation at the surface was revealed under alkaline conditions. These evolutions do not affect the mechanical properties significantly, residual tensile strength is higher than 95% and tensile modulus remains constant throughout the aging duration. High stability of Technora<sup>®</sup> assures its reinforcement properties within cement-based materials [22].

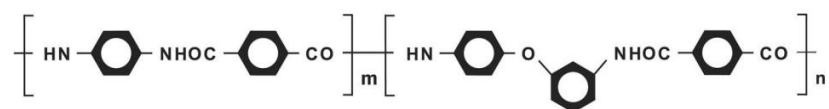




**Figure 2.3: Formula of applied aramid fibers**

Super-absorbent polymers (SAP) have the ability to absorb a significant amount of liquid from the surroundings and to retain the liquid within structure without dissolving, i.e., water retention properties. They were mostly used as a urine absorber in disposable diapers, and are innovatively applied for internal post curing of cement-based materials during recent years. SAPs can be produced with water absorption of up to 5000 times their own weight. However, in dilute saline solution as within cement matrix, the absorbency of commercially produced SAPs is around 50 g / g. From a chemical point of view, all the water inside a SAP can essentially be considered as bulk water [23, 24].

To better investigate moisture properties of repair systems, two SAP powders with different capacities of water absorption and desorption properties are selected. Luquasorb 1161<sup>®</sup> from BASF is a sodium polyacrylate (absorption coefficient: 51 g of 0.9% saline solution / g), while 435325 Aldrich<sup>®</sup> from Sigma-Aldrich is a poly-(acrylic acid) partial potassium salt (27 g of 1% saline solution / g). Their properties are based on technical documents and molecular formulas are respectively shown in Figure 2.4 (b), their granularity is both about 0.4 to 0.5 mm (parallel as standard sand) at dry condition.

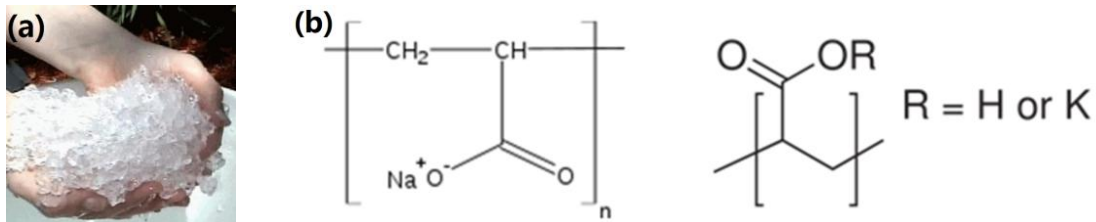


**Figure 2.4: (a) Photo of SAP gel; (b) Formula of SAP powders (Luquasorb 1161<sup>®</sup> and Aldrich<sup>®</sup>)**

According to experimental results of feasibility tests, the mix designs made of gray OPC with relatively low w/c ratio from 0.3 to 0.4 and low content of super-plasticizer (less than 0.5 % /c in mass) are selected. Optimal workability is observed and bleeding effect due to excess of water is prevented to the utmost at this range. Thus the appropriate cement pastes and mortars for the investigation of setting process are prepared and summarized in Table 2-4.

Type		Abbreviation	w/c	s/c	Admixture (%/cement)
Gray OPC Saint Vigor CEM I 52.5	cement paste	C35	0.35	-	-
		C45	0.45	-	-
		C30SP	0.30	-	2% SP*
	mortar	M42	0.42	2.0	-

	cement paste	<b>M38SP</b>	<b>0.38</b>	<b>2.0</b>	<b>1% SP</b>
		<b>C35SF</b>	<b>0.35</b>	<b>-</b>	<b>10% SF**</b>
		<b>C45SF</b>	<b>0.45</b>	<b>-</b>	<b>10% SF</b>
<b>White OPC Cruas</b> <b>CEM I 52.5</b>	cement paste	<b>WC35</b>	<b>0.35</b>	<b>-</b>	<b>-</b>
		<b>WC38</b>	<b>0.386</b>	<b>-</b>	<b>-</b>
		<b>WC40</b>	<b>0.40</b>	<b>-</b>	<b>-</b>
		<b>WC50</b>	<b>0.50</b>	<b>-</b>	<b>-</b>

**\*SP: super-plasticizer (cement addition), \*\*SF: silica fume (cement replacement)**

**Table 2-4: Mix design and abbreviations for the investigation of setting process.**

## 2.2.4 Repair mortars

Repair mortars with rapid setting process, good adhesion properties on both dried and humidified surfaces, excellent thermal compatibilities with a thickness over 2 cm, high resistance to abrasion and to penetration, etc., are appropriate for repair purposes [13].

It is worth mentioning that, a typical s/c ratio of mortar is 3.0 for on-site application. But in this thesis, the reference mortar is selected with an s/c ratio equal to 2.0, due to the requirements to stabilize cement matrix with aggregates and to avoid evident segregation. Bleeding phenomenon has been observed for a gray OPC mortar with w/c ratio at 0.42 and s/c ratio at 2.0. Therefore w/c ratio needs to be controlled under 0.40 to avoid any effects due to an excess of water, and to limit moisture transfer at the interface within repair mortar in contact with concrete.

To focus on moisture transfer in repair systems and to choose appropriate methods for investigating the repair procedure, two kinds of mortars with representative properties and a relatively low price that allows industrial application [6], are selected as follows:

1. Reference repair mortar: of w/c ratio equal to 0.30 and s/c ratio equal to 2.0, with super-plasticizer (SP) 0.3%/c in mass;
2. SAP-modified repair mortar: of w/c ratio equal to 0.30 and s/c ratio equal to 2.0, with SAP/c ratio equal to 0.2% and SP/c ratio equal to 0.3% in mass. Aldrich® from Sigma-Aldrich is selected, this SAP absorbs 29 gram of 1% saline solution per gram of dry powder which corresponds to a reduction of w/c ratio at about 0.05 at casting time.

The workability of both materials was verified by slump test to ensure a convenient use on old concretes, to avoid side flow and sedimentation.

### 2.2.5 UHPFRC matrix and with aramid fibers

The application of Ultra High Performance Fiber Reinforced Concretes (UHPFRC) on conventional concrete is frequently observed in the construction fields of roads and bridges. This kind of materials has extremely low permeability and outstanding mechanical properties. These points harden the composite structures in critical zones subjected to aggressive agents from environment and to significant stresses. They promise long-term durability which helps to avoid multiple interventions on structures during their service lifetime [25].

They are suitable for the application on new structures, as well as for rehabilitation of existing reinforced concrete structures. For example, thin overlays in replacement of waterproofing membranes, prefabricated elements such as kerbs, and steel rebars coated with concrete. As shown in Figure 2.5, UHPFRC serves for protection in case 1 as well as protection associated with improved mechanical performance in case 2 [26]. Both thicknesses are comparable to the designed repair systems (3 cm of repair mortar on 5 cm of concrete) in this thesis.

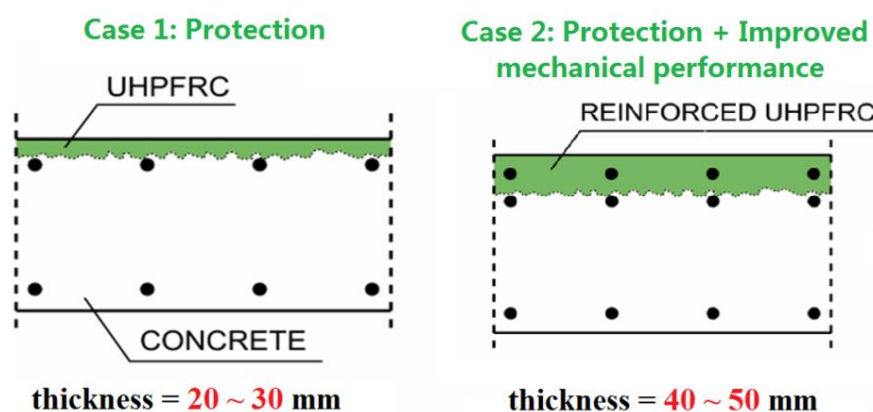


Figure 2.5: Application of UHPFRC materials on conventional concrete

The same composite systems as shown in Figure 2.2 are prepared with UHPFRC materials (strain hardening matrix, and with aramid fibers) on concrete M25. The mix design is shown in Table 2-5 [27]. Note that the w/c ratio is 0.180, the content of silica fume (SF) is 26% (replacement of cement) and the SP/c ratio is 2.5%.

Raw materials	Quantities (kg/m <sup>3</sup> )	Information
OPC	1112	CEM I 52.5 N PM ES from Lafarge (Le Teil)
Sand	643	Fontainebleau type MN30 Quartz; D <sub>max</sub> < 0.5 mm
Silica fume	289	Zirconium from SEPR
Superplasticizer	28	Zementol TKK (SL) ; Polycarboxylate-25% Solids content
Total water	200	
Aramid fiber	42	Technora; 20 mm 800 dtex fibres
Air	40	4% air

**Table 2-5: Composition of UHPFRC with aramid fibers**

Finally to observe different properties of moisture transfer during hydration process of UHPFRC materials to those of repair mortars, the same conditions of substrates are conserved in order to compare both cases. By using aramid fibers Technora® instead of steel fibers within mix design of conventional UHPFRC, NMR experiments are performed successfully.

### **2.2.6 Technical details of casting procedure**

Casting procedure for cement pastes and mortars corresponds to a standard preparation method in Navier group by using a paste mixer Heidolph RZR 2041. The solid compounds of cement and sand are pre-mixed, and then added into water and other liquid admixtures. The mixing times of entire mixture are 30 seconds by hand, 30 seconds at 130 rpm (revolution per minute), and 90 seconds at 260 rpm in this thesis.

For specimens containing SP such as C30SP, M38SP, etc., the bleeding effects reduce the effective w/c ratio. NMR, thermocouple monitoring and Vicat needle measurements are performed since casting, the conventional method to avoid sedimentation by using a rotation procedure is impossible to be applied.

SAP powder is difficult to be mixed homogeneously at dry state, due to its small quantity by comparing to that of cement and sand. Thus liquid phase (SAP in gel form, pre-mixed with water and SP) is firstly prepared, and then solid phase is added.

A 5 L Perrier mixer was used for UHPFRC materials because small mixer is not suitable for this kind of mix design and also for proposes to unify experimental conditions to those in MCS group in EPFL. Cement and SF were dry mixed for 2 minutes, and then sand was added and mixed for another 2 minutes with a speed of 61.5 rpm. Water and SP were added and entire mixture was mixed for approximately 7 minutes with a speed of 123 rpm. Finally, aramid fibers were added and mixed for one minute with the speed of 61.5 rpm to get a homogenous state without destroying fiber structures [27].

These cement pastes, mortars and UHPFRC specimens were casted in cylindrical-shaped plastic containers (volume ~ 250 mL) with dimensions of 6.3 cm in inner diameter and 7.5 cm in average height. These specimens were devoted to NMR measurements and sealed by using caps to avoid any drying after casting. Each specimen was duplicated with the same geometry for temperature monitoring.

Truncated conical metallic molds (volume ~ 200 mL) with dimensions of 7.0 / 8.0 cm in inner diameter on top / bottom and 4.0 cm in height were used for Vicat needle tests. The specimens were protected by a waterproofing membrane and conserved in water bath after casting. For repair mortars and UHPFRC materials in composite systems, specimens were casted on concrete substrate as shown in Figure 2.2.

## **2.3 Selected techniques during different stages of hydration**

Non-destructive and conventional techniques are used for various cement-based materials at different ages during hydration. The main objectives of this thesis are to better understand the mechanisms of moisture transfer, and its influences on mortar hydration process. Thus free water profiles (depletion combined with moisture transfer), setting times, and microstructural evolution are prior investigated.

At early ages of mortar hydration, NMR/MRI is used to investigate water mobility, setting process, and moisture transfer. GRA is used to measure the density profiles. Vicat needle is used to investigate setting and hardening times. Thermocouple is used to follow temperature.

After repair procedure, it also serves to investigate microstructure and permeability properties of repair systems. GRA is used to investigate immersion properties and total porosity at different heights. MIP is used to investigate total porosity and PSD within the same systems.

Concerning the long-term durability, repair systems are indicated by carbonation and chloride penetration. GRA is used to investigate carbonation profiles, while phenolphthalein indicator to measure final carbonation depth. Dosage is used to measure the concentration of chloride ions at different heights by drilling specimens within the repair systems.

In conclusion, this methodology is relatively fast to capture rapid hydration evolution, and also relatively accurate to characterize key parameters since early age until hardening. It is equally important to preview durability after the repair procedure. In order to provide a convenient way aimed at the investigation of all these properties, aforementioned techniques as hydration time evolves will be detailed in following sections.

### **2.3.1 For the investigation of only cement pastes and mortars**

#### **2.3.1.1 NMR relaxometry**

NMR technique initially results in a spectroscopy to study materials which investigates the interaction of electromagnetic radiation with specimen's nature. It exploits magnetic

properties of certain atomic nucleus, thus it determines physical and chemical properties of atoms or molecules and can provide detailed information about structure, dynamics, reaction state, and chemical environment of molecules [28]. There exist another type of spectrometers so called imaging, which allow measuring relaxation time and obtaining images of proton density (MRI) by performing spatial arrangements (will be described in section 2.3.2.1).

The simplest presentation to describe NMR principles is two-state vector formalism. Spin is an intrinsic property of elementary particles (electrons, quark) or compounds (proton, neutron, and nucleus). Proton spin (equal to  $\pm 1/2$ ) can be related to a magnetized needle. Each spin can be assigned by a magnetic moment:  $\vec{\mu} = \gamma \hbar \vec{I}$ . Where  $\gamma$  is gyromagnetic ratio of nucleus equal to  $26.75 \times 10^7 \text{ rad} \cdot \text{T}^{-1} \cdot \text{s}^{-1}$  for proton,  $\hbar$  is Planck's constant equal to  $6.626 \times \frac{10^{-34}}{2\pi} \text{ J} \cdot \text{s}$ ,  $\vec{I}$  is spin magnetic moment. NMR allows the observation of nuclear spins. The characteristic frequency resonance or angular Larmor frequency,  $\omega_0$  is related to a magnetic field  $B_0$ :  $\omega_0 = \gamma B_0$  [29]. It is necessary to consider quantum mechanics under more complex conditions. When a specimen is inserted into a static magnetic field  $\vec{B}_0$ , where a radiofrequency (RF) field  $\vec{B}_1$  is added perpendicularly, three separate phenomena occur:

- **Polarization:**  $\vec{B}_0$  is applied to guide spins which will align with  $\vec{B}_0$  in parallel or antiparallel ways. Two energy levels are created, with a gap of  $\Delta E = \gamma \hbar B_0$  as shown in Figure 2.6 (a). According to Boltzmann statistics, surplus of spins stay on most stable energy level. This creates a resulting magnetization denoted as  $\vec{M}$ . In fact, individually proton spins are not perfectly aligned according to  $\vec{B}_0$ , they rotate with precession phenomenon around magnetic field with Larmor frequency:  $\nu_0 = \frac{\gamma B_0}{2\pi}$  as shown in Figure 2.6 (b).
- **Resonance:** By using a coil,  $\vec{B}_1$  is applied perpendicularly to  $\vec{M}$ . Magnetization rotates into perpendicular plane, thus  $\vec{M}$  precesses around  $\vec{B}_1$ , then rotating field is resonated with magnetization. The phenomenon of double precession is thus shown in Figure 2.6 (c). Following the rotating by a RF pulse, magnetization has a longitudinal component  $M_z$  and a transverse component  $M_{xy}$ .

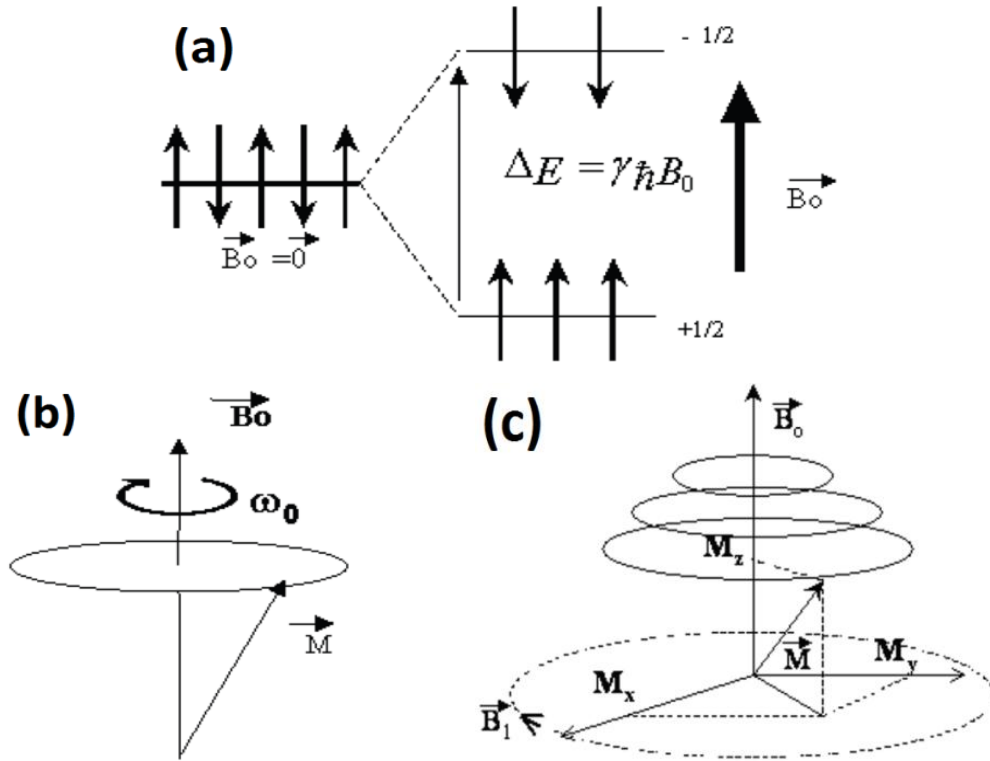


**Figure 2.6: Polarization: (a) by magnetic field  $\vec{B}_0$ , energy levels of spin  $\pm 1/2$ ; (b) Precession of magnetic moment with angular velocity around  $\vec{B}_0$ ; Resonance: (c) phenomenon of double precession.**

- **Relaxation:** after discontinuation of an external solicitation, system returns to its equilibrium following two relaxation phenomena according to the specimen's nature. This creates a regrowth of  $\vec{M}$  following  $\vec{B}_0$  during a time  $T_1$  as shown in Figure 2.7 and a phase shift of spins in transverse plane (disappearance of  $M_{xy}$ ) during a time  $T_2$  in Figure 2.8.

Longitudinal magnetization returns to equilibrium value as:  $M_z(t) = M_0 (1 - e^{-\frac{t}{T_1}})$ , where  $M_0$  presents the resulting magnetization at equilibrium. This spin-lattice relaxation is characterized by time  $T_1$ , which corresponds to the interactions of spins with environment.

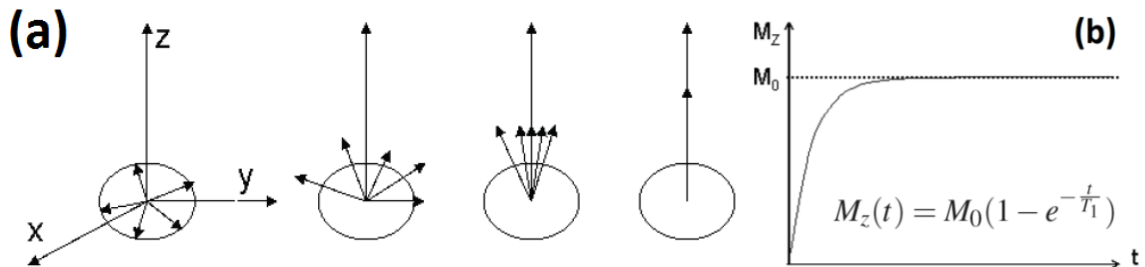


**Figure 2.7:  $T_1$  relaxation: (a) Regrowth of magnetization in longitudinal plane; (b) Characterization.**

Transverse magnetization decreases and disappears rapidly following the shape:  $M_{xy}(t) = M_0 e^{-\frac{t}{T_2}}$ . This spin-spin relaxation time is characterized by  $T_2$ , which corresponds to the interactions between spins. Nucleus return to equilibrium state by transmitting accumulated energy stored in the form of RF wave at Larmor frequency.

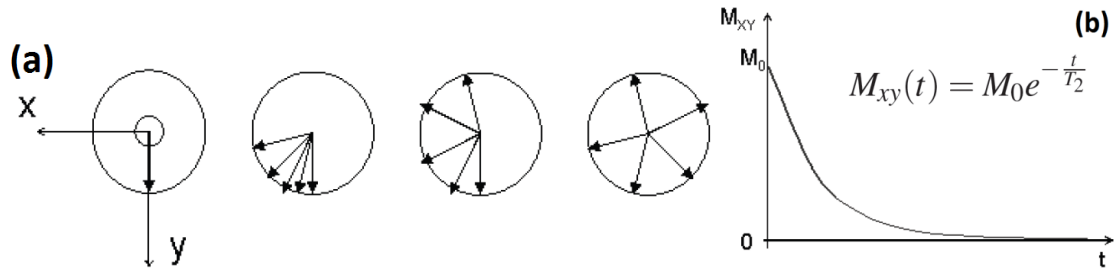


**Figure 2.8:  $T_2$  relaxation: (a) Phase shift of spins in transverse plane; (b) Characterization.**

NMR relaxometry has been used to investigate cement-based materials by Dr. Robert Blinc since the period of 1978 - 1986. And corresponding SPI sequence (MRI) was firstly designed by Dr. Bruce Balcom at 1995. The vertical imaging spectrometer DBX 24/80 Bruker, which was installed in 1999 by Navier group, is a similar design to commonly-encountered medical devices. This NMR/MRI device is successfully dedicated to investigate materials in civil engineering, thus as columns porous saturation and de-saturation velocity profiles for granular flows [30], rheology of fluids (liquids, pastes, granules) with the insertion of a rheometer [31], moisture transfer within porous solids (soil, rocks, cement pastes, concrete) [32], etc.

**Parameters:** In this thesis, the spectrometer is equipped with a birdcage radio-frequency coil possessing an inner diameter of 20 cm, which provides the capacity to investigate centimeter-size specimens, i.e., bulk materials with negligible edge effects. NMR experiments were operated at  $\nu_0$  equal to 0.5 T, i.e., 20 MHz proton, with a gradient strength of  $50 \text{ mT m}^{-1}$ , i.e.,  $5 \text{ G cm}^{-1}$ . Such a low magnetic field limits the effect of heterogeneity and it is suitable for porous media such as cement-based materials. NMR experiments were performed with enough sensitivity and high signal-to-noise (s/n) ratio (close to 1000 in hardened cement-based materials, and even higher in fresh ones). The main drawbacks of these applied parameters are long duration to perform radio-frequency pulses ( $110 \text{ } \mu\text{s}$  for hard  $\pi/2$  pulse) and  $40 \text{ } \mu\text{s}$  dead time between pulse and signal acquisition [33]. Before each measurement, antenna is adjusted by calibrating its natural frequency (tuning) and optimizing its agreement in impedance (matching). The height of the sample holder is adjusted depending on



specimens' sizes, in order to be positioned in the middle of antenna, within the homogenous magnetic field which results in optimal experimental conditions.

Nevertheless, NMR signal intensity is still sufficient and the duration of one measurement usually lasts several minutes, which is suitable to capture rapid cement hydration. The longitudinal ( $T_1$ ) and transverse ( $T_2$ ) relaxation times are measured by using series of elementary instructions called "sequence", which is related to synchronized elements on RF antenna and gradient coils. It allows exciting magnetization of specimen to obtain necessary information. According to feasibility tests as shown in Table 2-3, both relaxation times of several cement pastes have been investigated:  $T_1$  measurement is more stable, accurate and informative than  $T_2$  measurement for heterogeneous materials, thus the investigation of  $T_1$  is prior to be used in this thesis.  $T_1$  distribution is also influenced by internal rigidity and hence setting process according to Faure *et al.* [34].

Two NMR **methods of characterization** were selected to investigate the water mobility related to  $T_1$  and the depletion kinetics of free water (with most important mobility). The experiments were carried out at a constant room temperature of  $20 \pm 0.1$  °C and their protocols are detailed as follows:

- **Method (1)**:  $T_1$  distribution was obtained with an Inversion Recovery (IR) sequence and after the conversion of relaxation signal into a continuous distribution by inverse Laplace transform as shown in Figure 2.9.

This sequence is firstly performed by a  $180^\circ$  pulse which inverts longitudinal magnetization. And then it recovers during an inversion time ( $t_i$ ) before recording in a transverse plane by a  $90^\circ$  pulse. It depends on  $t_i$  between RF pulses and repetition time (TR). The signal is presented in form:  $S = M_0 * (1 - 2e^{-\frac{t}{T_1}})$ . Final results were obtained through data treatment by a self-developed computer program [33] based on method which performs the same function as the well-known CONTIN program in NMR research described by Provencher [35] and Whittall [36]. The duration to perform one measurement is about 10 minutes.

The evolution of  $T_1$  distribution was continuously monitored since casting (from 0 to 3 days). Data treatment was obtained by assuming 256 different pre-defined  $t_i$  values which are logarithmically distributed between 75  $\mu$ s and 100 ms. Aforementioned parameters were selected by considering the initial  $T_1$  distribution at casting time ( $t \approx 0$ ) of the studied cement pastes and mortars. Although  $T_1$  diagram evolves with time and admixtures in formula,  $t_i$  values are fixed to compare different materials.

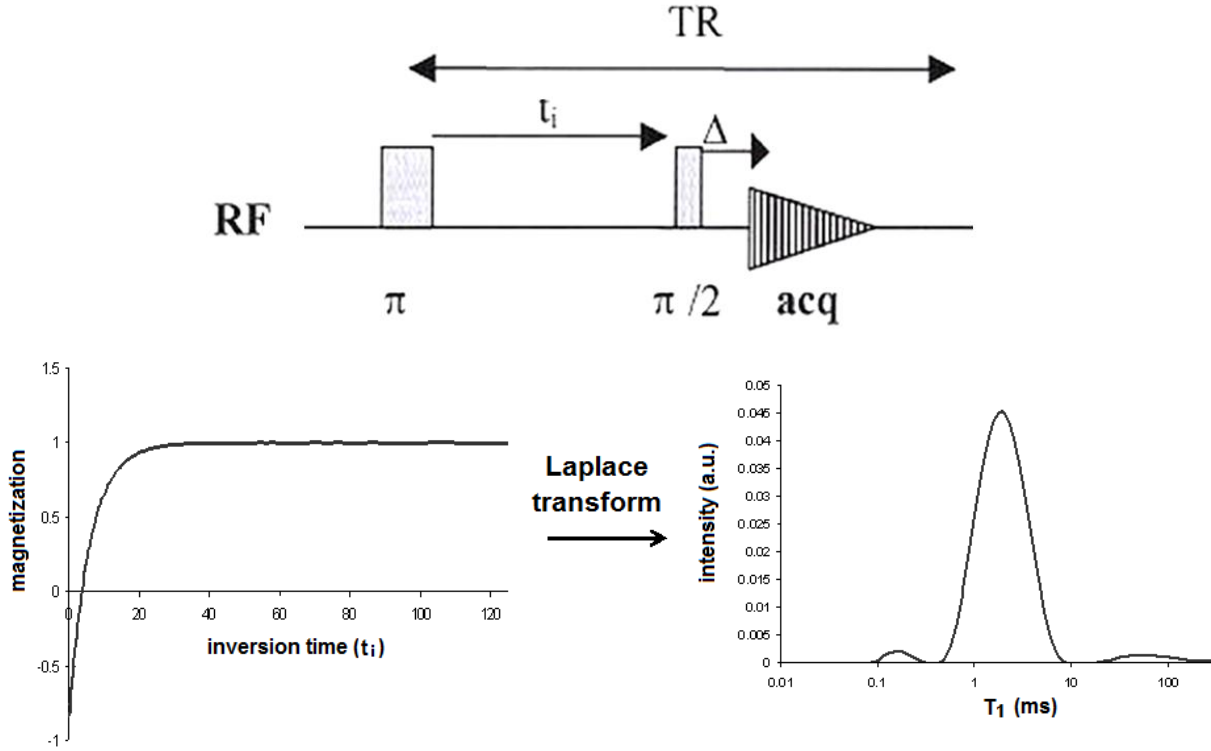


**Figure 2.9: Inversion recovery sequence and the conversion by inverse Laplace transform.**

- **Method (2):** Global free water content was assessed with a simple one pulse-acquisition sequence, i.e., one signal acquisition (so called FID, Free Induction Decay).

FID signal is consecutive to an excitation of single RF of  $\pi/2$  after its return to equilibrium, as shown in Figure 2.10. By using a reception coil (antenna of perpendicular axis to  $B_0$ ), the information is collected point by point. This signal is a damped sinusoid, which has an exponential envelope  $e^{-t/T_2}$  in a homogeneous field. This sequence can be repeated and then involves with TR, which represents the duration between each cycle. Between each  $\pi/2$  pulse, it is necessary to set TR large enough (usually equal to  $5T_1$  to acquire 99% of signal) to allow full relaxation of magnetization. The duration to perform one measurement is 2 seconds.

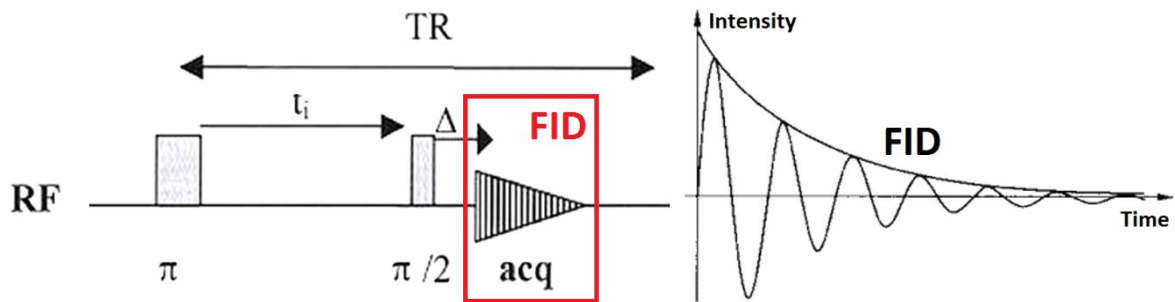


**Figure 2.10: FID acquisition sequence and acquired signal with exponential envelope.**

The inversion Laplace transform of relaxation data is approximate to these data as a sum of mono-exponential components as presented in equation 2.1. Where  $s(t_i)$  is the experimental curve. Its values were obtained by correcting phase of each FID signal at each  $t_i$  (except the disturbing 6 points which are deleted at the very beginning, this method of data treatment will be discussed in section 3.2.1.4):

$$S(t_i) \approx S_\infty - \sum_p a_p \exp(-\frac{t_i}{T_p}) \quad (\text{Equation 2.1})$$

By comparing Figures 2.9 and 2.10,  $T_1$  distribution and FID acquisition can be successively obtained. The signal amplitude, i.e., intensity of FID ( $I_{\text{FID}}$ ) is proportional to the surface under  $T_1$  distribution curves and to the content of water molecules, thus related to global free water content within the whole specimen.

Taking into account the requirements for continuous NMR measurements during hydration, considering the necessity to capture rapid development of percolation properties since very early age until hardening, and preventing useless and heavy data treatments with excessively frequent experiments, the time delays between two different measurements for both methods (1) and (2) are set to 30 minutes from 0 to 1 days, and 2 hours from 1 to 3 days.

### **2.3.1.2 Conventional techniques**

It was not possible to measure a sample temperature within spectrometer. In order to follow the kinetics of exothermic chemical reactions during setting, independent samples were monitored under the same condition as during NMR experiments: they were prepared using the same composition, protocol and size, constant room temperature of  $T_0 = 20 \pm 0.1$  °C, in sealed condition and free thermal contact with surrounding air. Temperature evolution was monitored from 0 to 3 days by embedding sensors (T-type thermocouple [37]) at three different positions within each sample just after casting, so as to get the first measurements as soon as possible, to monitor setting process as shown in Figure 2.11 (a): near the top, inside the core and near the bottom. Temperature was recorded continuously for a couple of hours and thus determined by the average of three monitored values. The time delay between two measurements is set to one minute. It corresponds to a system where free heat-exchange between specimens and environment exists, and typical time  $t_{\text{cool}}$  needed by the sample to exchange heat with air will be discussed in section 3.2.1.2.

Setting process was monitored from 0 to 2 days by a Vicat needle equipped with four positions as shown in Figure 2.11 (b). This technique is applied to principally investigate initial and final setting times, average values were taken into account. The time delay between two measurements is set to 16 minutes 12 seconds. Moreover, the specimens were protected by thin membranes of waterproofing oil which avoid surface drying or wetting with environment. During measurements, the specimens were isolated in water bath at a constant temperature of  $20 \pm 0.01$  °C. It corresponds to free heat-exchange condition with water bath, and presents evident difference from that for NMR and thermocouple. Temperature increase accelerates hydration reactions during and after setting, but it is supposed to slightly influence hydration process before setting [38]. For example, the maximum of temperature is 31 °C for gray cement paste of  $w/c = 0.35$  and 37 °C for white cement paste of  $w/c = 0.386$ , but the initial setting time is similar for each specimen by both Vicat needle and NMR techniques. Thus the difference between different heat-exchange conditions is negligible. According to [39] and [40], initial setting time of Portland cement detected by Vicat needle is correlated to chemical reactions during induction period when weak heat release exists.

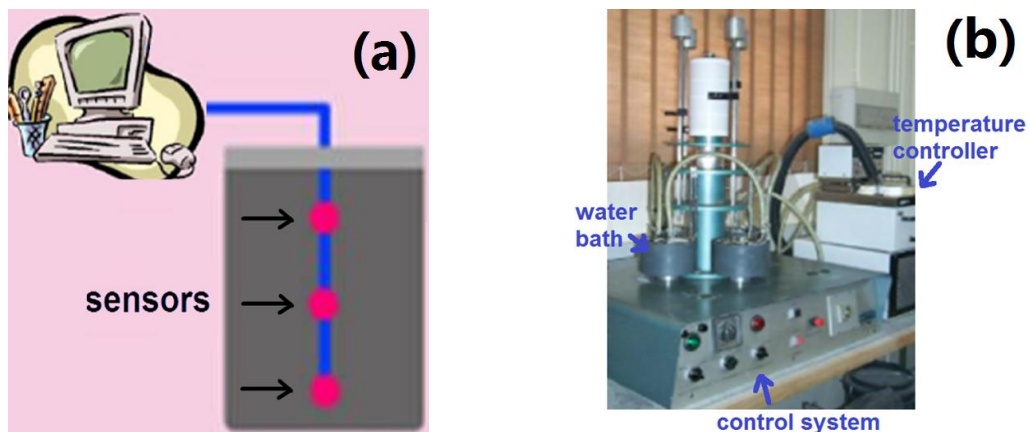


**Figure 2.11: (a) Schematic diagram of thermocouple; (b) Photo of Vicat needle equipment.**

### **2.3.1.3 Numerical simulations**

A numerical and analytical model of multi-kinetics hydration, which is based on Powers' theory and developed in IFSTTAR, was used in this thesis to simulate capillary water content during hydration process. This modeling is based on the description of coupled hydration with each clinker phase ( $C_3S$ ,  $C_2S$ ,  $C_3A$ , and  $C_4AF$ ). The kinetics is controlled by three consecutive steps: (1) dissolution of the clinker phases, (2) nucleation-growth of hydration products, (3) reduction of the reaction rates due to ion diffusion through the layer of hydration products around cement grains.

The hydration kinetics are fitted to data reported by Lothenbach *et al.* [41], where hydration rates for each clinker phase were determined by a semi-quantitative XRD for a w/c = 0.5 cement paste made of CEM I 42.5. The identified kinetic parameters are in agreement with those purposed by Bernard *et al.* [42], where the effects of temperature and water depletion on hydration kinetics were also taken into account. The reaction rate for each clinker phase is thermo-activated (according to the Arrhenius law  $h_i = \exp\left(-\frac{E_{ai}}{RT}\right)$  for the temperature dependence of reaction rates [43], where  $E_{ai}$  is the activation energy of phase “i”, R is the gas constant (8.314 J/molK). These numerical simulations were consistent with experimental data provided in Nguyen’s thesis [44].

The hydration model allows two kinds of simulation, i.e., either (1) the water content which corresponds to the initial water minus chemically-bound water and C-S-H gel water by assuming a C-S-H porosity of 28%, or (2) the water content which corresponds to the initial water minus chemically-bound water. Data provided by Bentz *et al.* [45] have also been used to assess the evolution of free water content during hydration. By using the loss of ignition technique, the evolution of the degree of hydration ( $\alpha$ ) from 1 to 100 days for two OPC cement pastes of w/c = 0.35 and 0.435 are followed. The free water content is then determined via the Powers' model which allows a quantitative description of the volumetric distribution of free water, gel water and chemically-bound water according to  $\alpha$ . This model makes it possible to verify the numeric modeling from  $\alpha$ , which is assimilated from the numeric modeling. The content of free water in mass (in percentage) is thus given by the following equation according to Jensen *et al.* [46]:

$$water\% = 100 \cdot (1 - 3.15 \cdot 0.42 \cdot (\frac{1}{3.15 \cdot w/c + 1})) \cdot \alpha \quad \text{(Equation 2.2)}$$

This hydration modeling is applied since casting until more than 100 days to monitor the free water content within cement-based materials. These results were compared to the intensity of FID evolution during hydration. For further purposes, it is more convenient to predict the evolution in long term after repair works, by this numerical model rather than experiments.

## 2.3.2 For the investigation of repair systems

### 2.3.2.1 At early age (since casting until 28 days)

#### *MRI - SPI sequence (moisture profiles)*

MRI is a medical imaging technique by using scanners in strong magnetic fields and radio waves to form images. Since the end of 20<sup>th</sup> century, MRI has been widely developed in

various domains such as food science, detection of petroleum, construction materials in civil engineering such as cement-based materials, soils, and rocks, etc.

MRI sequences are more developed and complex than NMR sequences. Indeed, an additional parameter is involved to locate spatially signal: linear gradients of magnetic field, which results in a linear variation in applied direction. Spatial information coding is made by applying three gradients of magnetic induction successively: a slice selection gradient (GSS), a phase encoding gradient (GPE), and a read gradient (GR). Gradients are shown in Figure 2.12 and characterized by intensity, power, direction, application moment and duration. GSS allows selecting a section (perpendicular to interior volume) by applying a selective RF pulse in this plane. All spins within magnet precess at the same Larmor angular frequency  $\omega_0$  without gradients. Lines (phases) and columns (frequencies) are defined within selected slice. GPE is applied in a perpendicular direction to perform a phase encoding. GPE allows selecting different lines within section plane. It induces phase shifts of protons in each line. Frequency coding or GR: is applied during signal record in a perpendicular direction to the first two ends of spatial encoding information. Similarly GR selects section columns by increasing spin precession speeds in each column.

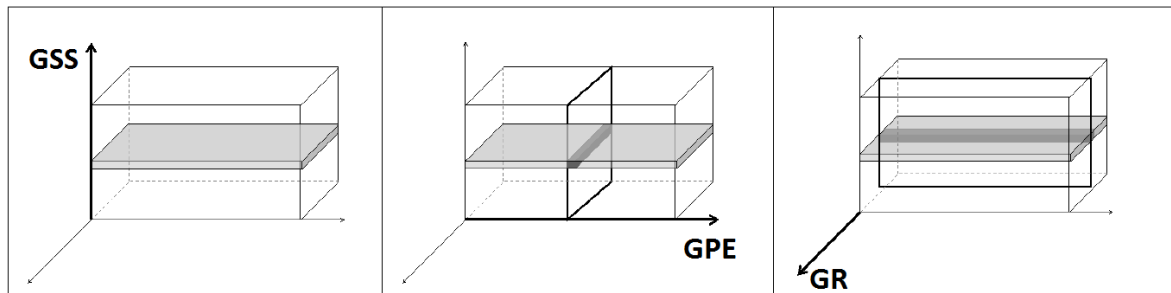


**Figure 2.12: Schematic of imaging gradients: x = GSS, y = GPE, z = GR.**

In general, MRI is applied to obtain a spatial representation of water distribution within cement matrix. Signal intensity is related to localized density of proton, thus information of free water content. The moisture profiles are thus obtained by the application of a rapid one-dimensional (1D) single point imaging (SPI) sequence, which was firstly developed by Emid and Creydon [47], and largely improved by Balcom *et al.* [48, 49, 50]. Except this acquisition, images and intensity profiles in 2 or 3 dimensions are also possible by applying additional magnetic field gradients which enables a spatial coding. But there exist several disadvantages: perturbed results, distortion problem, strong gradients also cause to vibration, and acquisition duration becomes too long. To overcome these problems, a fast SPI sequence named SPRITE (Single Point Ramped Imaging  $T_1$  Enhancement) which significantly reduces

noise, is developed by using a gradient of staircase type (shaped gradients) [51]. It is relatively fast to follow rapid hydration process with good resolution, and frequently applied to investigate cement-based materials: hydration and drying [52], or freeze / thaw [53].

In this thesis, a single gradient field is applied in order to reduce experimental durations. Broadband pulse excites the transverse magnetization that is encoded in line for a fixed time  $t_p$ . One complex point is acquired by FID after RF for each applied gradient value. Unlike conventional imaging methods, the obtained profiles are not susceptible to distortions caused by inhomogeneity in  $B_0$  field. This sequence is dedicated to materials exhibiting short  $T_1$  like cement-based materials as reported by Prado *et al.* [49]. The signal intensity is defined by equation 2.3 and the timing diagram sequence is shown in Figure 2.13:

$$S = \rho \exp\left(-\frac{t_p}{T_2^*}\right) * \left[ \frac{1 - \exp\left(-\frac{TR}{T_1}\right)}{1 - \cos\theta \exp\left(-\frac{TR}{T_1}\right)} \right] * \sin\theta \quad (\text{Equation 2.3})$$

Where  $\rho$  is spin density,  $t_p$  is phase encode time,  $T_2^*$  is apparent spin-spin relaxation time,  $TR$  is repetition time between successive pulses. In this thesis,  $\theta$  is  $\pi/8$ .

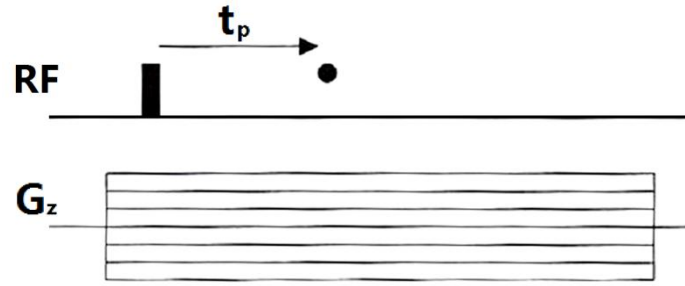


Figure 2.13: One-dimensional SPI sequence.

Since casting, free water often shows a high mobility and gives rise to relatively longer relaxation times. When hydration occurs, water becomes less mobile and results in much shorter relaxation times and a corresponding signal loss. As  $TR$  is long enough by comparing to  $T_1$  within cement matrix (in this thesis,  $TR \approx 5T_1$  initial value since casting),

$\left[ \frac{1 - \exp\left(-\frac{TR}{T_1}\right)}{1 - \cos\theta \exp\left(-\frac{TR}{T_1}\right)} \right] * \sin\theta$  is approximately equal to 1, thus  $S \approx \rho \exp\left(-\frac{t_p}{T_2^*}\right)$ . Calculation by

inverse Fourier transform performed by an appropriate program allows obtaining a longitudinal profile of the water distribution. These measures enable to monitor cement pastes during the first hours of hydration. Moisture profiles are monitored with a sufficient resolution of 2 mm. Note that the duration to do one measurement is about 6 minutes.

### GRA (density profiles)

The transport properties of liquid water within cement-based materials are quantitatively monitored by GRA, which is a non-destructive technique of characterization, frequently used to measure the density of inert specimen. It is based on the acquisition of gamma-ray absorption from a radioactive source Cesium 137 (correlating to 660 keV radiation) as shown in Figure 2.14 (a), and widely applied in civil engineering to follow density evolution and carbonate profiles [15].

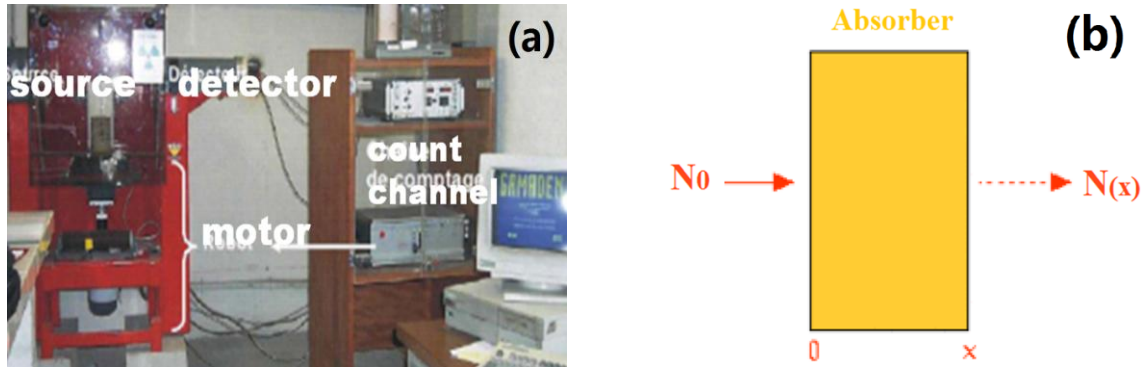


**Figure 2.14: (a) GRA equipment at IFSTTAR; (b) Gamma-ray absorption principle**

$N_0$  and  $N(x)$  are respectively the number of incident photons in air and of photons having passed through the specimen, along the gamma rays' path with thickness  $x$  (cm), and  $\rho$  ( $\text{g}\cdot\text{cm}^{-3}$ ) is the density of material. While  $\mu$  ( $\text{m}^2\cdot\text{g}^{-1}$ ) is the characteristic coefficient of mass absorption, it depends on constituents and can be calculated from formulation. For example,  $\mu = 0.0776 \text{ m}^2\cdot\text{g}^{-1}$  for M25 concrete. Encountered loss of gamma rays' intensity:  $\Delta N = N_0 - N(x)$  removed from the incident  $N_0$ , is proportional to residual  $N(x)$  according to Beer-Lambert law as shown in Equation 2.4 [54]:

$$\Delta N = N_0 (1 - e^{-\mu\rho x}) \quad N(x) = N_0 e^{-\mu\rho x} \quad (\text{Equation 2.4})$$

These equations reveal several effects which were involved in this thesis, such as: (1) Effect of density: the lower is  $\rho$ , the less attenuation is provided for interactions between radiation and specimen molecules; (2) Effect of thickness: the thicker is  $x$ , the greater is the absorption.

At early age, density evolution within repair mortar is variable caused by decreased water content due to hydration reactions and the increased density with the formation of hydration products [55]. However in old concrete, the variations are related to the moisture transfer from repair mortar towards concrete bulk and potential re-hydration of non-hydrated compounds. These results can be compared to water profiles obtained by SPI sequence, which will be detailed in sections 4.1.4.



### 2.3.2.2 At middle age (since 2 months)

#### **GRA (total porosity)**

The experimental protocol is proposed [56] to obtain information on water porosity after repair procedure. The repair systems after two months of mortar hydration need to be firstly pretreated, in order to stop hydration process before experiments. They were demolded and dried in an oven for 3 to 4 weeks, with constant temperature controlled at 45 °C in order to avoid thermal dehydration. The drying process is completed until the specimens reach a constant mass (followed by measurement up to  $\Delta \text{mass} < 0.5\%$  per day). It is often required to use a vacuum oven as shown in Figure 2.15 (a), in order to reduce the influence of carbonation, which alters the microstructure during drying.

The specimens are then saturated in vacuum by distilled water during 3 days; the equipment is shown in Figure 2.15 (b). The difference of GRA results between dried and saturated states is used to demonstrate the distribution of total porosity. The principle is shown in Figure 2.15 (c) and described by Equation 2.5 as follows:

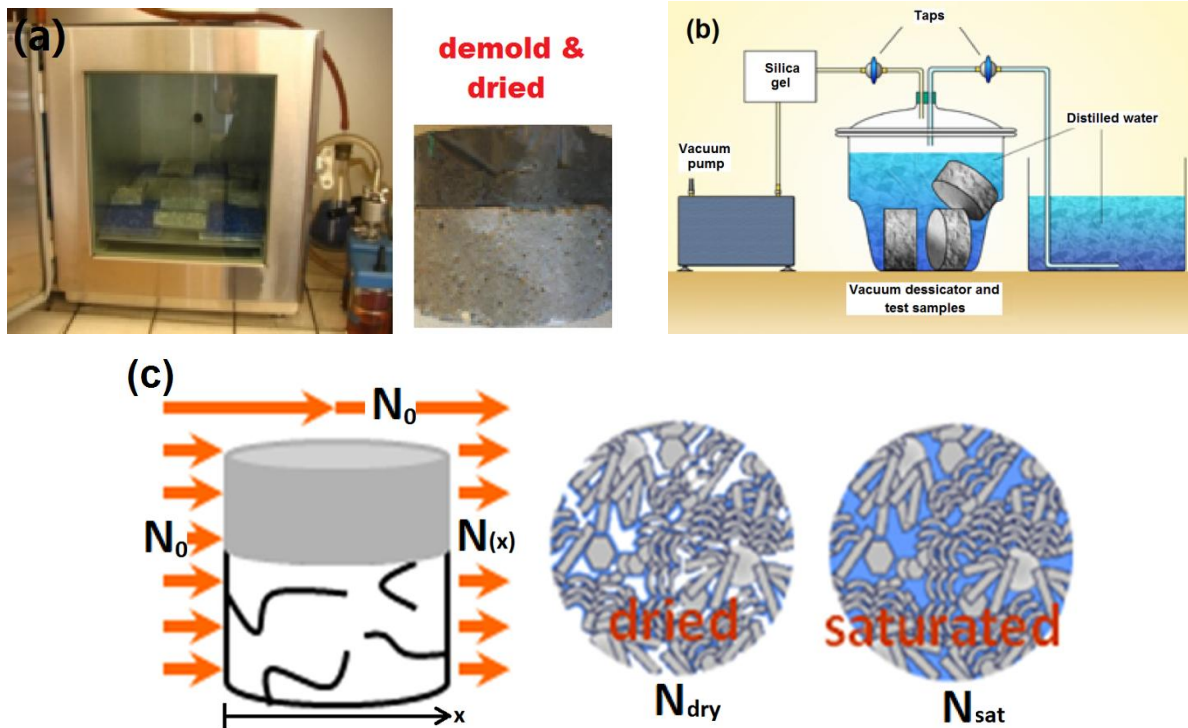


**Figure 2.15: Determination of water porosity by GRA: (a) Drying at 45 °C in vacuum oven; (b) Saturating in vacuum by distilled water; (c) Principle of calculating the total porosity.**

The total porosity at different heights of the whole specimen can be easily calculated:

$$\text{porosity } \phi = \frac{1}{\rho_w \mu_w l} \ln \left( \frac{N_0^{\text{sat}} N^{\text{dry}}}{N^{\text{sat}} N_0^{\text{dry}}} \right) \quad (\text{Equation 2.5})$$

At each measurement,  $\phi$  presents the total porosity,  $\rho_w$  and  $\mu_w$  are respectively the density and mass absorption coefficient of water at room temperature.  $N_0^{\text{sat}}$  and  $N^{\text{sat}}$  are the numbers of incident and residual gamma rays protons at saturated state; while  $N_0^{\text{dry}}$  and  $N^{\text{dry}}$  are the numbers of incident and residual protons at dried state.

It is worth mentioning that, this porosity is different to the conventional total porosity after 105 °C drying, thus the results are much lower than accurate results but still close to. It is helpful to understand the evolution during repair procedure within both mortar and concrete, without destructing microstructure. These results can be compared to the total porosity values obtained by MIP, and will be detailed in sections 4.2.

### ***MIP (total porosity & PSD)***

After 45 °C drying in vacuum oven of the whole repair systems, cracked specimens at different heights are dried to completely remove water, in order to investigate total porosity and PSD by MIP. It is often recommended to use liquid nitrogen by sublimation from ice directly to water vapor, which involves a relatively fast procedure [57]. Specimens are cut into different layers, and then cracked into small pieces as shown in Figure 2.16 (a). Free water and gel water within cement matrix are frozen and removed in vacuum as shown in Figure 2.16 (b). These pretreated specimens need to be labelled and conserved in desiccators before experiments to avoid carbonation with environment.

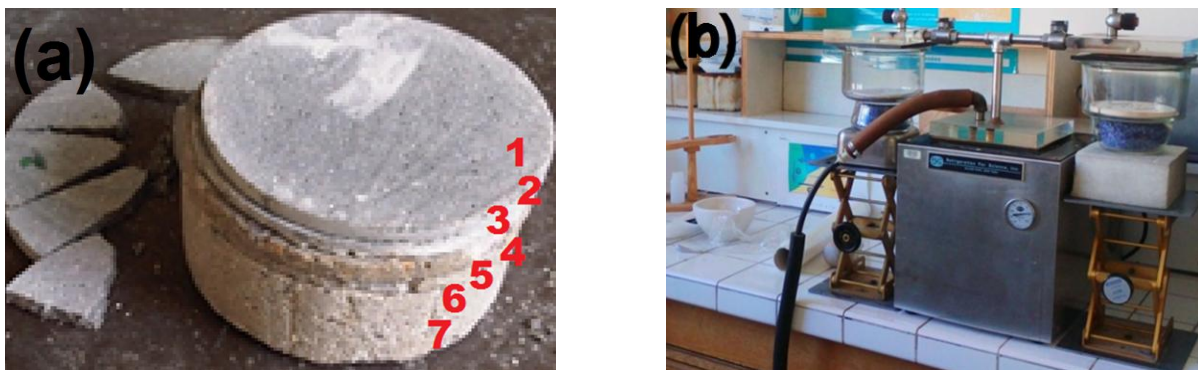


**Figure 2.16: Sample preparation before MIP tests: (a) Cut to different layers; (b) Freeze-drying.**

MIP technique is widely used to estimate micro and macro-porosity within cement-based materials. The principle is based on physical phenomenon that a non-reactive, non-wetting fluid, will not penetrate pores until sufficient pressure is applied to force its entrance. From a practical point of view, the quantification of accessible porosity is investigated by submerging specimens in confined quantity of mercury. At different stages, pore sizes are related to

injection pressures, which are hydraulically increasing during experiments. The mercury diminution is detected and measured by penetrometer based on a capacitance system. The displaced amount is equal to that filling the pores.

The equipment is composed of two different parts with low and high pressures as shown in Figure 2.17: “Pascal 140” ( $0.01 \text{ KPa} \leq P_{\text{Hg}} \leq 100 \text{ KPa}$ ) and “Pascal 440” ( $0.1 \text{ MPa} \leq P_{\text{Hg}} \leq 400 \text{ MPa}$ ), related to the capacity to explorer broad range of pores from 1.8 nm to 60  $\mu\text{m}$  [58].



**Figure 2.17: Mercury porosimetry equipment of “Pascal 140” and “Pascal 440”.**

This distribution does not take into account the micro-porosity of C-S-H ( $r_p < 2 \text{ nm}$ ) and the macro-porosity of air bubbles ( $r_p > 60 \mu\text{m}$ ). However; the obtained results provide information on PSD and the corresponding curves of porosity are still close to total porosity.

The pores are supposed in cylindrical shape and their mean  $r_p$  is calculated by Washburn’s equation which describes capillary flow in porous materials as shown in Equation 2.6:

$$r_p = - \frac{2\sigma_{\text{Hg}} \cos\theta_{\text{Hg}}}{P_{\text{Hg}}} \quad (\text{Equation 2.6})$$

$P_{\text{Hg}}$  is the average of incremental pressure at each stage.  $\sigma_{\text{Hg}} = 0.474 \text{ N}\cdot\text{m}^{-1}$  is surface tension, while  $\theta_{\text{Hg}} = 141.3^\circ$  is the contact angle between mercury and solid surface.

After MIP experiments, mercury intrusion curve is obtained. It presents cumulative volume of introduced mercury according to radius of accessible pores. By logarithmic differentiation, distribution of porous volumes in function of  $r_p$  is investigated:  $dV/d\log(r_p)$ .

This technique is suitable to investigate cement pastes and mortars, but its application for concrete need to be delicately operated because of the heterogeneity between aggregates and cement matrix. To solve this problem, it is recommended to increase the repeatability by taking parallel tests and to avoid aggregates during sampling.

It is worth mentioning that, considering the investigation of relaxation times ( $T_1$  and  $T_2$ ) by NMR, moisture and density profiles by MRI and GRA, it is useful to get information in a

non-destructive way especially at early stages of hydration. There exist three advantages over conventional destructive methods (such as: Vicat needle, Thermocouple, MIP, BET, etc.):

- (i) To avoid heavy repetitions of sample preparation with continuous measurements;
- (ii) No need of complex pretreatments (ex: drying potentially disrupts microstructure);
- (iii) No intrusion of liquid or gas (there exists a wide PSD ranging from micro to macro within cement matrix, which plays an important role on its properties. Non-destructive techniques are more informative for small pores, as microstructure is protected).

### **2.3.2.3 After repair procedure (since 2 months until long term)**

#### ***Water immersion***

As the repair systems will be placed in solution by chloride penetration tests, it is interesting to firstly investigate the immersion profiles by GRA. It is also interesting to compare these results to total porosity, which reveals both microstructure and moisture transfer properties after a repair procedure. When hydration time of the repair mortar reaches 2 months, the repair system is demolded and then put in oven at 45 °C during 3 - 4 weeks for drying until a constant mass. Then it is coated with self-adhesive aluminum paper and a bit silicone is applied to avoid water leakage throughout small crackings directly into concrete by lateral side. Finally this system is placed in GRA apparatus, and distilled water is filled from top of mortar to investigate its immersion properties. This protocol is shown in Figure 2.18 as follows, while it is simulated 1D water transfer from outside to repair mortar and then into concrete bulk. The evolution of density profiles directly reflects water immersion curves, which is related to the performance of moisture transfer properties [16].

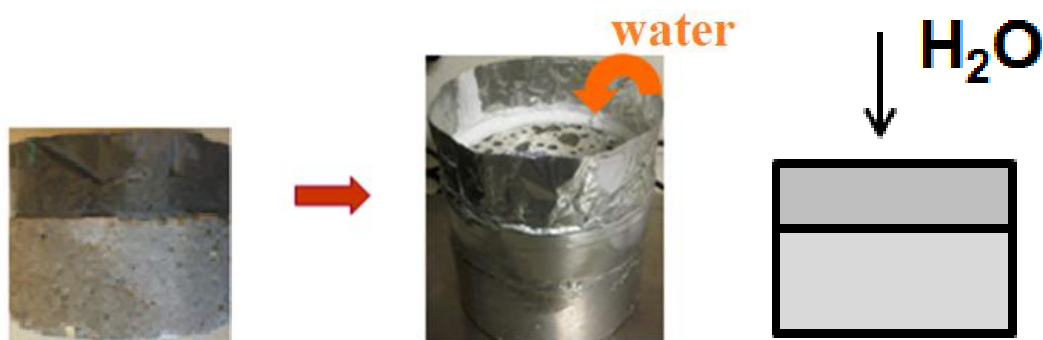


**Figure 2.18: Protocol of water immersion test**

#### ***Carbonation***

Principle of accelerated carbonation experiments consists in introducing carbon dioxide into a container with controlled conditions. The concentration of 10 % CO<sub>2</sub> is applied in this thesis

to avoid an excessively rapid carbonation and to obtain an appropriate carbonation rate. The RH is set to 53 % and temperature at  $20 \pm 1$  °C, which corresponds to optimal environmental conditions for accelerated carbonation [59].

Because non-destructive condition at 45 °C is not sufficient to obtain a complete and fast drying, specimens are pre-dried at 105 °C during 48 h before carbonation to eliminate residual free water and stop hydration. Prepared specimens are coated with aluminum paper; only top surface is exposed to environment, and then positioned as shown in Figure 2.19.

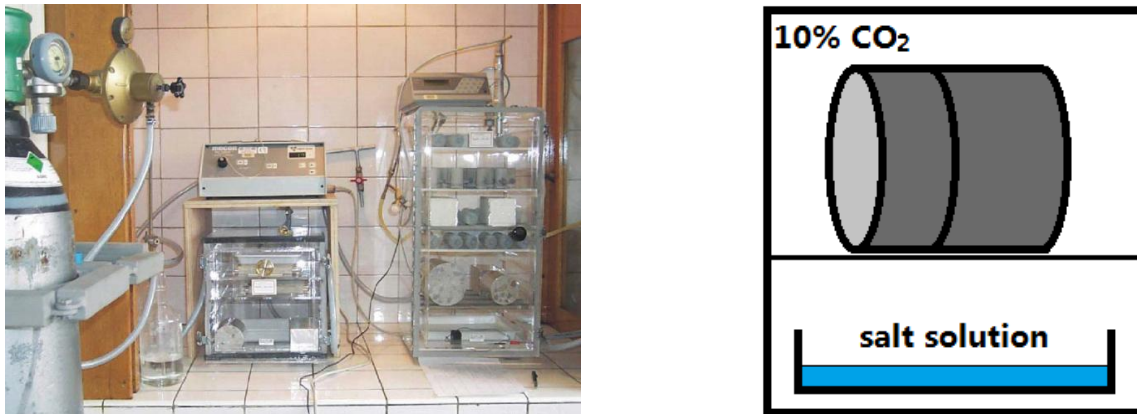


**Figure 2.19: Equipment of accelerated carbonation**

Generally, each specimen is monitored respectively at 0, 9, 14, 28 and 56 days after carbonation by GRA to obtain carbonation profiles in function of carbonation duration. This non-destructive measurement allows an in-situ monitoring of carbonation process [60].

After 56 days of carbonation procedure, phenolphthalein indicator is applied on each specimen to determine carbonation depth (destructive).

### ***Attack by chloride ions***

Repair systems are protected with resin at bottom and lateral surface, except the top surface is exposed to chloride solution, in order to obtain a simple 1D diffusion condition. Principle of accelerated diffusion of chloride ions is shown in Figure 2.20 as detailed and investigated in Wang's thesis [16]. According to water immersion tests, the liquid penetration is relatively slow to the repair systems by comparing to conventional concrete.



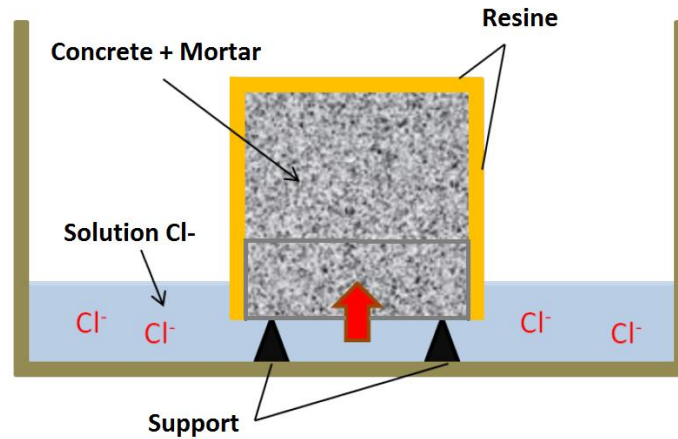


**Figure 2.20: Container of chloride ions diffusion**

The chloride solution is renewed every 14 days in order to avoid the shortage of chloride ions in solution (ideal situation is supposed as unlimited large and at a constant concentration, thus this solution is prepared with an intensified concentration of 160 g/L NaCl and 40g/L NaOH, i.e., pH ~ 13, to strengthen the penetration in this thesis).

Each specimen is grinded respectively at various durations of penetration by a grinding tool (BOSCH equipment) at different layers. To compare their resistances to chloride ions diffusion, different repair systems and reference concretes are multiply prepared for each experiment. The specimens are taken from middle position to avoid boundary effect.

Then the grinded powders are respectively dissolved into acid solution (nitric acid of 0.13 mol/L and 3.2 mol/L for free and total chloride contents) to obtain chloride contents at different layers. This procedure is shown in Figure 2.21 [61] by three different steps. These solutions are titrated and then chloride content is thus calculated and determined.



**Figure 2.21: Dosage of chloride ions concentration**

## **2.4 Global overview**

In this chapter, repair systems are designed, for the purposes to avoid evaporation to environment and to focus on moisture transfer during mortar hydration.

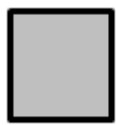
The mix design formulas of studied concrete (M25), cement pastes (for the investigation of feasibility and setting process), repair mortars (reference mortar and SAP-modified mortar) and UHPFRC materials (with and without aramid fibers) are detailed.

Different techniques in relation to different ages of hydration are presented.

For cement pastes and mortars for the investigation of setting process, relaxation time (NMR), temperature (thermocouple) and setting time (Vicat needle) are monitored since casting. Water depletion is compared to numerical modeling.

For mortars and UHPFRC materials, moisture profiles (MRI and GRA) are monitored since casting. After repair procedure, total porosity (GRA and MIP), PSD (MIP), penetration properties of water (immersion), carbonation and chloride ions are monitored.

In conclusion, four various configurations are designed to investigate various systems at different periods during hydration, and the parameters determined by different techniques are detailed. They help to well understand this methodology of investigation:



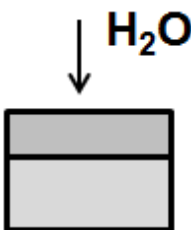
**Mortars and cement pastes**, studied hydration time is from **0 to 3 days** and some measurements at **7, 14, 28 and 90 days**.

NMR is applied to investigate the evolution of water mobility; Vicat needle is applied to investigate the setting and hardening times; Thermocouple is applied to investigate internal temperature evolution of cement-based materials.



**Mortars or UHPFRC materials on concrete M25**, studied hydration time is **0 to 3, and 7, 14, 28 days**.

MRI is applied to investigate moisture profiles; GRA is applied to investigate density profiles.



**Mortar + concrete M25**, studied hydration time is **2 to 4 months**.

GRA is applied to investigate total porosity and immersion profiles; MIP is applied to investigate total porosity and porous distribution.



↑ **Cl<sup>-</sup> ou CO<sub>2</sub>**

**Mortar + concrete M25**, studied hydration time is **2 to 4 months**.

GRA is applied to investigation carbonation profiles; Phenolphthalein is applied to investigate final carbonation depth. Concentration titration at different layers is applied to investigate the free and total penetration profiles of chloride ions.






### 3. Chapter 3: Monitoring of setting process at early age of hydration

#### Summary

<b>3.1 Definition of mechanical and chemical setting times .....</b>	<b>79</b>
<b>3.2 Monitoring of <math>T_1</math> / <math>I_{FID}</math> to monitor water mobility and free water content - NMR relaxometry as a probe for setting process and water depletion.....</b>	<b>81</b>
3.2.1 Compared with results obtained by thermocouple (temperature), Vicat needle (setting time) and numerical modeling (water depletion).....	81
3.2.1.1 Mechanical setting time related to the percolation of solid network....	81
3.2.1.2 Chemical setting time related to hydration reactions and temperature evolution.....	86
3.2.1.3 Comparison of mechanical and chemical setting times.....	87
3.2.1.4 Effect of FID data treatment methods.....	89
Selection of capillary peak for FID acquisition .....	89
Deletion of different points of FID acquisition.....	92
3.2.2 Numerical simulation as a probe for free water depletion.....	94
<b>3.3 NMR results for various cement pastes / mortars .....</b>	<b>95</b>
3.3.1 Cement pastes made of gray and white OPC.....	95
3.3.2 Effect of the addition of standard sand (cement paste vs. mortar) .....	97
3.3.3 Effect of the addition of super-plasticizer .....	99
3.3.4 Effects of the replacement of cement by silica fume.....	103
<b>3.4 Global overview .....</b>	<b>106</b>

---

 The monitoring of **setting times** is an important investigation during **hydration process**, especially at **early age** when the hydration reactions are active and complex. The application of **NMR relaxometry** helps to develop a **non-destructive** and **multiplex** way to investigate *in situ* different setting times and the evolution of **free water content**

within cement-based matrix; while conventional techniques of characterization are generally destructive and monotonous to obtain results.

The NMR results can be compared to those obtained by **conventional techniques** (temperature by thermocouple, setting times by Vicat needle) and **a numeric modeling** (water depletion). Different materials were concerned to explore the **effects of additions** (super-plasticizer, silica fume, etc.) and the various properties of different formulas (made of white cement, standard sand, etc.). This analytical procedure helps to better understand the mechanisms of moisture transfer and to develop the complete methodology of characterization.

By monitoring the relaxation decay of protons, Korb *et al.* [62] measured longitudinal relaxation time  $T_1$  as a function of magnetic field strength to provide microstructural evolution information during ongoing hydration. Results reported by Nestle *et al.* [63] explained how to determine the degree of hydration by transverse relaxation experiment ( $T_2$  is frequently applied in NMR techniques as shown in [64], [65]).

Furthermore, results reported by Faure *et al.* [33] showed that the evolution of optimum  $T_1$  value (localization of the optimum of  $T_1$  diagram) according to time is correlated with well-acknowledged 4-age hydration process since early age: *dissolution*, *induction*, *setting* and *hardening*. This evolution was compared with temperature monitoring and electrical conductivity data available in literature. In brief, intrinsic relation between microstructural evolution and hydration process was described. By considering the presence of iron compounds in studied cement-based materials made of gray OPC,  $T_1$  monitoring is less affected than  $T_2$  monitoring [66]. An analysis of  $T_1$  has thus been privileged in this thesis.

In the continuity of aforementioned aspects, this chapter is intended at studying setting process, water depletion and hydration kinetics by NMR measurements for various cement-based materials. NMR results were compared to percolation properties of solid network (Vicat needle test) and temperature variations during early age of hydration (from 0 to 3 days). Moreover, water depletion kinetics was assessed thanks to numerical simulations by using an analytical hydration model and was compared to the evolution of NMR signal amplitude.

This chapter is thus divided into two parts:

Firstly, NMR results (evolution of the optimum  $T_1$  value and of NMR signal amplitude which is referred as  $I_{FID}$  in following sections) are compared to conventional techniques and numerical simulations. Cement pastes made of gray or white OPCs are investigated.

Secondly, as NMR relaxometry is proved as a non-destructive and relevant method to identify setting times and water depletion during hydration, the effects on hydration process and the evolution of microstructure involving the addition of sand, super-plasticizer and silica fume are respectively investigated by NMR analyses.

### **3.1 Definition of *mechanical* and *chemical* setting times**

NMR analytical method and the definition of different setting times are illustrated by experimental data for the  $w/c = 0.35$  cement paste made of gray OPC (C35) in Figures 3.1.

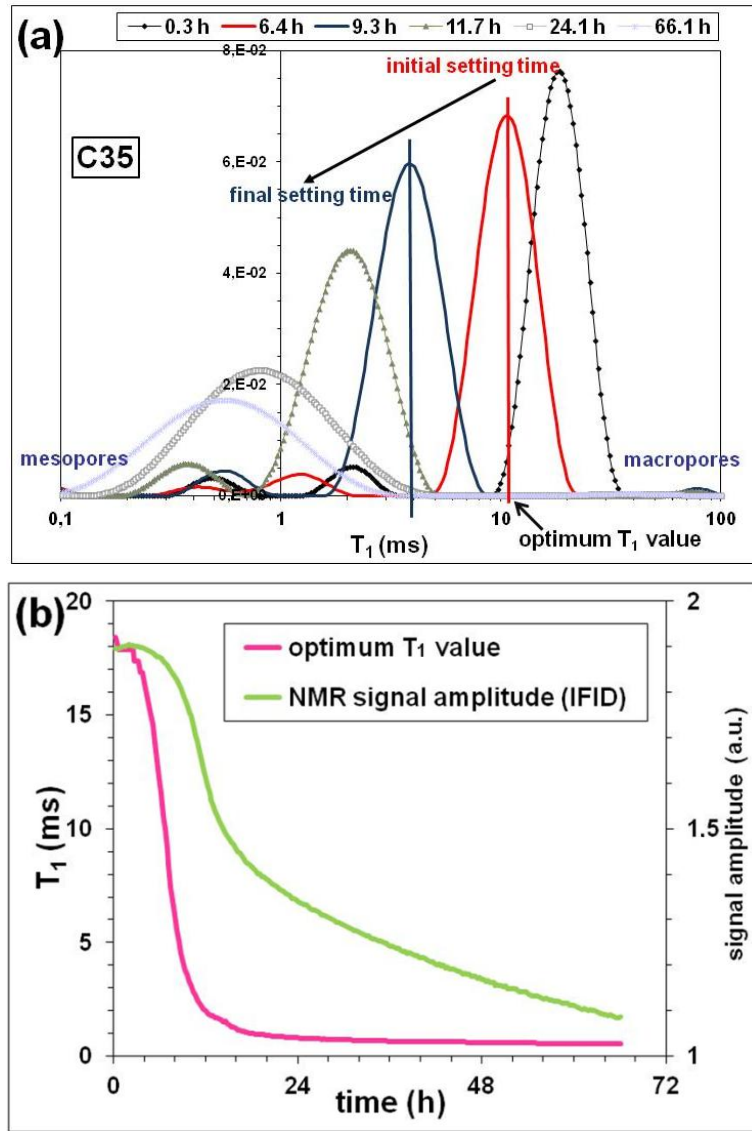


**Figure 3.1: Cement paste made of gray OPC at  $w/c = 0.35$  (C35): (a) continuous  $T_1$  distribution during hydration and identification of optimum  $T_1$  value; (b) monitoring of optimum  $T_1$  value and of NMR signal amplitude  $I_{\text{FID}}$  since  $t = 0$  until 66 h.**

In Figure 3.1 (a), continuous NMR measurements allow the monitoring of  $T_1$  diagram since casting time until 66 hours. The development of  $T_1$  distribution shows the evolution of water mobility during hydration, and the increase of internal rigidity and matrix surface area [33]. The optimum  $T_1$  value is defined as the  $T_1$  value at the maximum of  $T_1$  diagram at every instant during hydration. For example, the optimum  $T_1$  value is 10.6 ms at 6.4 hours of hydration (initial setting time obtained by Vicat needle) as shown in Figure 3.1 (a). Thus the shift of  $T_1$  diagram evolves towards smaller times as water mobility reduces.

The evolution of the optimum  $T_1$  value and of  $I_{\text{FID}}$  is shown in Figure 3.1 (b) since casting until 66 hours. Decrease in optimum  $T_1$  value during hydration illustrates the transition of free

water from large pores (about 1  $\mu\text{m}$ , initially located between cement grains) to smaller pores (about 1 - 100 nm, related to the pores within layered network of C-S-H and to the intrinsic porosity of C-S-H). The reduction of pore size causes an increase in the confinement level, and thus a decrease in mobility of water molecules. This mechanism has been extensively described by means of numerical simulations according to Korb *et al.* [67]. On the other hand, the decrease in  $I_{\text{FID}}$  corresponds to water depletion due to hydration reactions.

Generally, the percolation threshold of solid network is detectable by the analysis of optimum  $T_1$  value [33] which depends on PSD [68]. Therefore, the relaxation rate  $1/T_1$  and the optimum  $T_1$  value are considered as mechanical indicators of setting, and these results can be compared with Vicat needle data. The kinetics of hydration is accessible through the rate of water depletion obtained by the analysis of  $I_{\text{FID}}$ . Consequently,  $I_{\text{FID}}$  stands for a chemical indicator of hydration process, as it is related to chemical reactions.

In this thesis, the time corresponding to the maximum of the derivative of optimum  $T_1$  value ( $dT_1/dt$ ) is defined as a *mechanical* setting time and the time defined by the maximum of  $I_{\text{FID}}$  derivative ( $dI_{\text{FID}}/dt$ ), is supposed to represent a *chemical* setting time. Note that both maxima are set equal to unity for normalization purpose. The analyses of different systems are facilitated by considering these two denoted setting times and derived parameters. These experimental results will be detailed in section 3.3.

## **3.2 Monitoring of $T_1$ / $I_{\text{FID}}$ to monitor water mobility and free water content - NMR relaxometry as a probe for setting process and water depletion**

### **3.2.1 Compared with results obtained by thermocouple (temperature), Vicat needle (setting time) and numerical modeling (water depletion)**

#### **3.2.1.1 Mechanical setting time related to the percolation of solid network**

A cement paste made of gray OPC of  $w/c = 0.35$  (C35) (see Figures 3.2) and a cement paste made of white OPC of  $w/c = 0.386$  (WC38) (see Figures 3.3) are investigated by the analysis of the optimum  $T_1$  value and the relaxation rate  $1/T_1$  according to hydration time. By comparing NMR results to those of Vicat needle test, setting process is thus investigated and intrinsic relationship between these two techniques will be revealed.

WC38 was prepared with a minimal  $w/c$  ratio according to properties of this white cement.

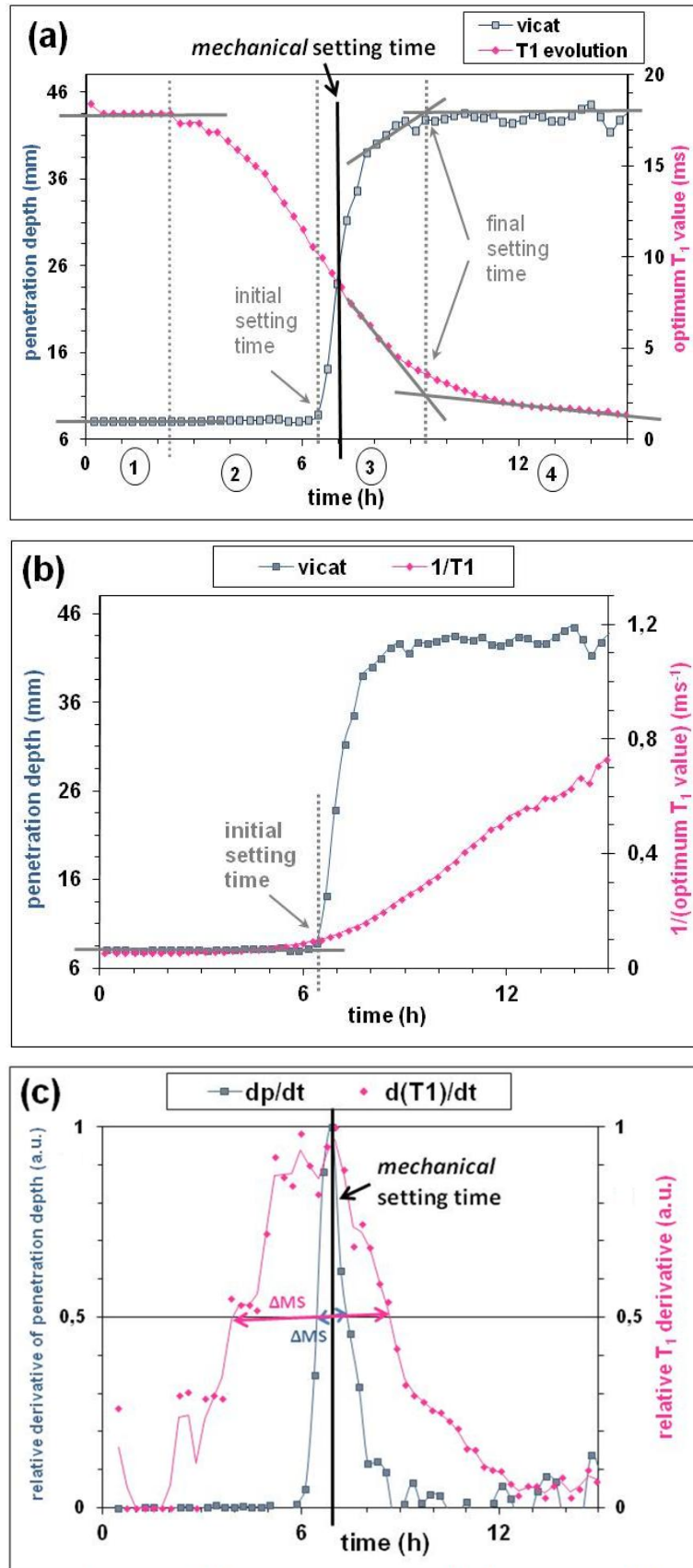
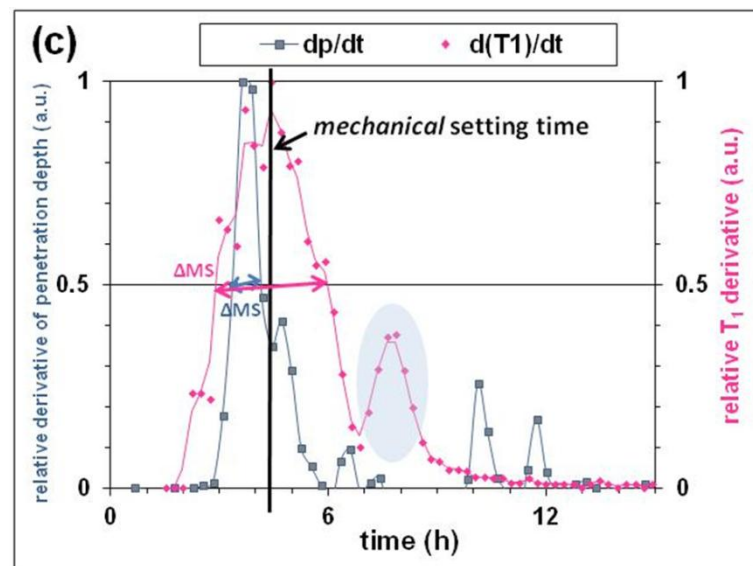
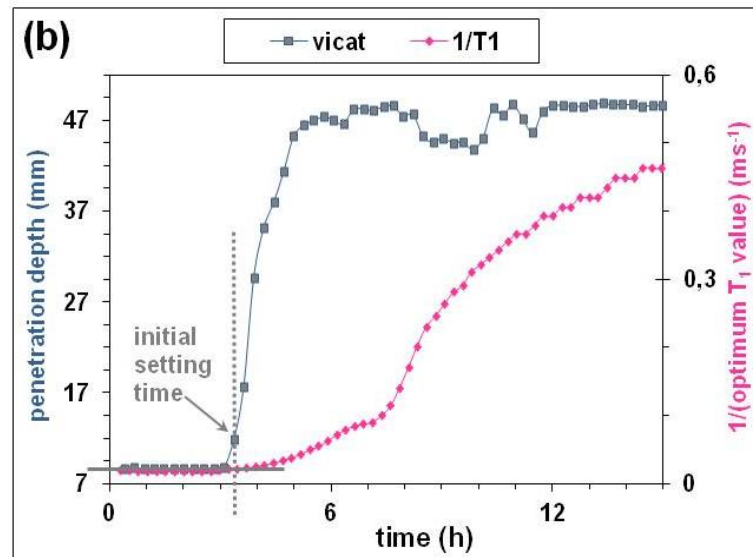
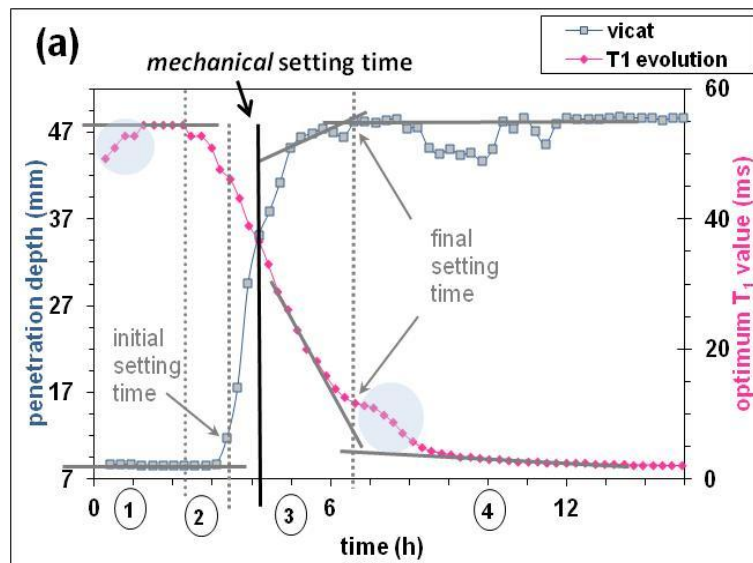


Figure 3.2: Cement paste made of gray OPC of w/c = 0.35 (C35):(a) evolution of optimum  $T_1$  value compared to the penetration depth of Vicat needle; (b) evolution of  $1/T_1$  compared to penetration depth; (c)  $T_1$  derivative ( $dT_1/dt$ ) compared to penetration depth derivative ( $dp/dt$ ).





**Figure 3.3: Cement paste made of white OPC of w/c = 0.386 (WC38): (a) evolution of optimum  $T_1$  value compared to the penetration depth of Vicat needle; (b) evolution of  $1/T_1$  compared to penetration depth; (c)  $T_1$  derivative ( $dT_1/dt$ ) compared to penetration depth derivative ( $dp/dt$ ).**

The evolution of the optimum  $T_1$  value is monitored and compared to the penetration depth of Vicat needle in Figures 3.2 (a) and 3.3 (a) for these two cement pastes. It can be observed that in each case, the two curves cross between the initial and final setting times measured by the Vicat needle test. The classic four hydration periods can be identified thanks to the combination of these two techniques: (1) dissolution, from casting until the initial decrease of  $T_1$ ; (2) dormant period, from the initial decrease of  $T_1$  until the initial setting time measured by Vicat needle; (3) setting, from the initial setting time measured by Vicat needle until the intersection of slopes for the Vicat and  $T_1$  evolution curves (this time is usually defined in the case of the Vicat needle test as the final setting time); (4) hardening, after the final setting time. The decrease of  $T_1$  during step (2) is observed before the percolation of the solid network related to the setting detected by Vicat needle. This phenomenon is attributed to the progressive formation of hydrated compounds around cement grains, and to the associated reduction in the mobility of water molecules due to an increase of the confinement level.

The evolution of the relaxation rate  $1/T_1$  is also compared to the penetration depth of Vicat needle in Figures 3.3 (b) and 3.3 (b). It is noticeable that the increase of both curves begins simultaneously, at about 6.4 and 3.2 hours for C35 and WC38, respectively. This time is correlated with the initial setting time detected by Vicat needle and represents the increase of internal rigidity of the solid network.

In Figures 3.2 (c) and 3.3 (c), the evolution of the time derivative of the optimum  $T_1$  value (noticed  $dT_1/dt$ ) is presented and compared to the derivative of the penetration depth of Vicat needle (noticed  $dp/dt$ ). The maximum of both derivations occurs exactly at the same time for C35 and WC38. As described before in section 3.1, this time is defined here as the *mechanical* setting time.

It should be remarked that there is an important difference between the widths of both curves. Consequently, the full width at half maximum (FWHM) will be also studied for each material as an indicator of hydration. The difference in FWHM is explained by the fact that the Vicat needle test is a macroscopic measurement able to detect the percolation of the solid network, whereas  $T_1$  monitoring is more related to a microscopic investigation able to detect small

variations of water mobility and internal rigidity before the percolation of the solid network due to the fact that the hydrated compounds become closer and closer.

In the case of WC38, there exists a pre-induction period before the dormant period, showing an initial increase in the optimum  $T_1$  value as shown in Figure 3.3 (a). On one hand, this phenomenon has already been explained in the literature [33] [69] by the formation of an ettringite barrier around cement grains which creates a gap between paramagnetic  $C_4AF$  phases and the surrounding free water in the bulk porosity. On the other hand, according to Scrivener *et al.* [7], ettringite crystals are forming in solution at early age. The formation of an ettringite barrier seems doubtful. At early age (1 - 2 h) of hydration, the formation of an amorphous layer of hydrated compounds which is directly in contact with cement grains was identified as AFm phase by Minard *et al.* [70]. This early increase of  $T_1$  is not observed in the case of C35 as shown in Figure 3.2 (a) due to a lower content of  $C_3A$  by comparing to the case of WC38 (2.6 % in gray OPC vs. 10.8 % in white OPC) and thus the formation of AFm is certainly not observed.

Moreover, there exists a shoulder effect in the evolution of the optimum  $T_1$  value just after the final setting time, as illustrated in Figure 3.3 (a). This feature is also reflected by a peak in Figure 3.3 (c) on the  $T_1$  derivative diagram. This phenomenon has also been demonstrated through temperature monitoring. It is related to a specific step during the hydration process, which corresponds to the transformation of ettringite into AFm when gypsum has been depleted. Given that the formation of AFm is related to changes of the compositions of the pore solution, and that AFm crystals are characterized by a different morphology than ettringite crystals, it is reasonable to expect a modification of the  $T_1$  diagram. Generally, gypsum depletion is observed after 9 - 15 h if  $C_3A$  is in excess (here the gypsum depletion is detected around 7 - 8 h through the presence of the shoulder effect on the  $T_1$  diagram). This shoulder effect related to the formation of AFm is even stronger if the  $C_3A$  content of the cement is high [33]. As a matter of fact, this phenomenon is not observed in the case of cement pastes made of the studied gray OPC which is characterized by a lower  $C_3A$  content than the cement pastes made of a white OPC (see Figures. 3.2 (a) and 3.2 (c)).

The evolution of the optimum  $T_1$  value or  $1/T_1$  (providing information at the micro-scale) and of the penetration depth of Vicat needle (information at the macro-scale) are in good agreement. It seems that there is an intrinsic relationship between the percolation properties detected by these both techniques. Nevertheless, it is worth mentioning that  $T_1$  monitoring is

more relevant than Vicat needle. Indeed, the  $T_1$  monitoring allows the distinction between the dissolution, dormant and nucleation-growth periods (see Figure 3.2 (a)). It is explained by the fact that the  $T_1$  monitoring is more sensitive to the formation of the solid network which controls the mobility of water molecules at the micro-scale and occurs earlier than the percolation of the solid matrix.

### 3.2.1.2 Chemical setting time related to hydration reactions and temperature evolution

As aforementioned, the same cement pastes C35 and WC38 are also studied through the investigation of NMR signal amplitude  $I_{\text{FID}}$ . These results are compared to temperature evolution as shown in Figures 3.4.

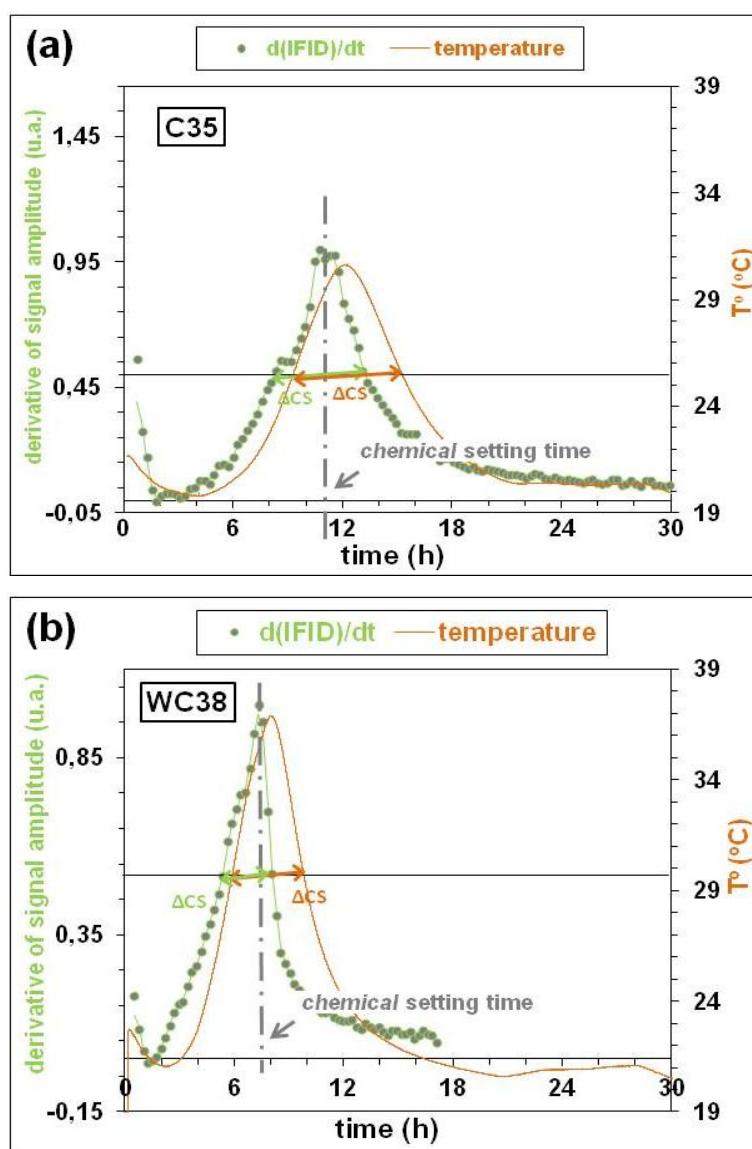


**Figure 3.4:** Time derivative of NMR signal amplitude  $dI_{\text{FID}}/dt$  and temperature evolution: (a) for  $w/c = 0.35$  gray OPC cement paste (C35); (b) for  $w/c = 0.386$  white OPC cement paste (WC38).

The  $I_{FID}$  derivative ( $dI_{FID}/dt$ ) is related to the rate of free water depletion during hydration. It allows a better visualization of the signal variations and therefore the different steps of water depletion. Its comparison with the temperature evolution is shown in Figures 3.4 (a) and 3.4 (b) for both studied cement pastes. The widths of both curves are similar, which reveals the intrinsic relationship between water depletion and temperature evolution which are both recognized as chemical indicators of hydration.

There exists a reasonable correlation between the maximum of  $dI_{FID}/dt$  and the temperature peak. As described in section 3.1, the time corresponding to the maximum of both curves is defined as *chemical* setting time.

Nonetheless, it is worth mentioning that the slight shift which is observed between both curves is attributed to the delay between the instantaneous heat release directly caused by the exothermic hydration reactions, and the real temperature increase which is monitored by means of the average data of the three embedded sensors (top, core and bottom positions).

When the typical time  $t_{cool}$  needed by the sample to exchange heat with air and homogenize its inner temperature is smaller than the typical evolution time of heat produced by chemical reactions, under such conditions, it can be shown by means of basic heat transfer theory and that [33]:  $T(t) \approx T_0 + \frac{\alpha}{C_p * t_{cool}} * q(t)$ , where  $T(t)$  is measured temperature by thermocouple,  $C_p$  is specific heat per unit volume of sample at constant pressure,  $q(t)$  is the volume power density produced by chemical reactions, and  $\alpha$  is equal to 1 in this thesis. It can be assumed that the temperature is homogeneous inside the sample at each step of chemical reactions. The maximal temperature increasing is no more than 15 °C. Taking  $q_{max} = 100$  and 4 J/cm<sup>3</sup>/K, respectively, as typical orders of magnitude for maximal  $q(t)$  and  $C_p$ ,  $t_{cool} \approx \frac{C_p * \Delta T}{q_{max}} \approx 45$  min is estimated. It is much smaller than the typical evolution time of  $T(t)$  curves (i.e., a few hours), but still hinders the acquisition of temperature rather than by NMR signal amplitude  $I_{FID}$ .

### **3.2.1.3 Comparison of mechanical and chemical setting times**

It is clearly observed in Figures 3.4 that, a shift between the *mechanical* and *chemical* setting times. As expected, this shift is various according to the mix design as shown in Figures 3.5 for cement pastes made of gray OPC of w/c = 0.35 (C35) and 0.45 (C45). Experimental results and analyses are summarized in Table 3-1.

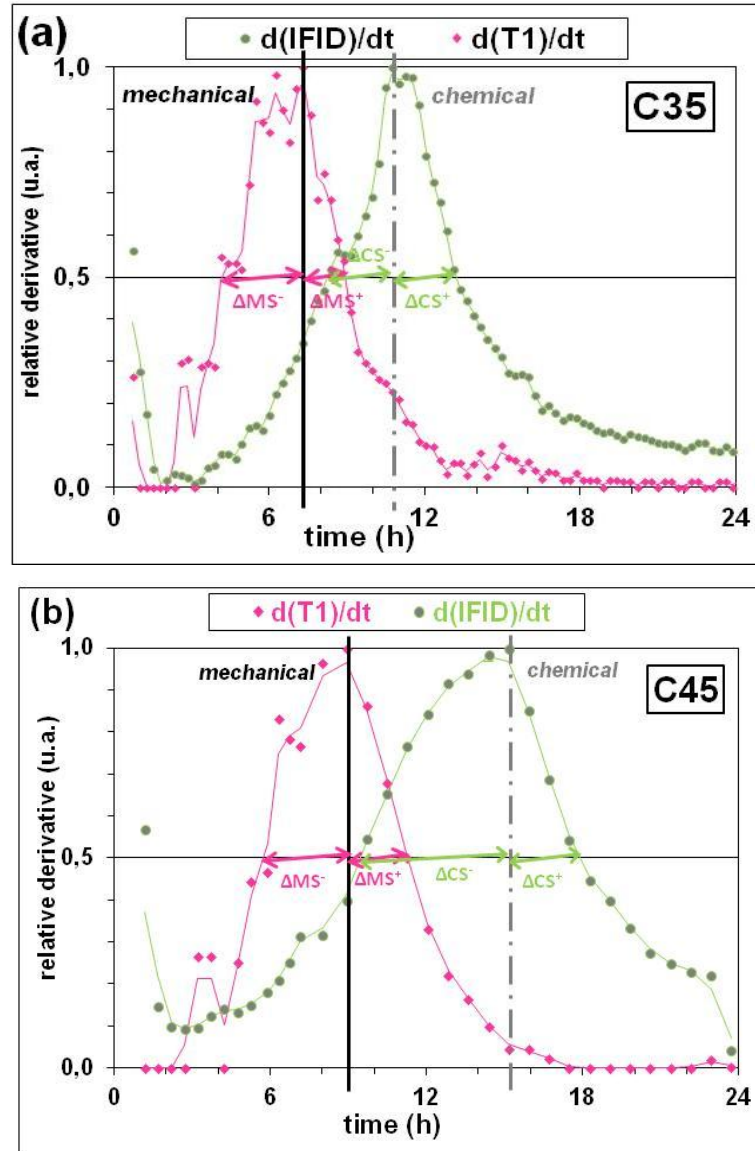


Figure 3.5: Time derivative of optimum  $T_1$  value  $dT_1/dt$  and NMR signal amplitude  $dI_{FID}/dt$  for cement pastes made of gray OPC of  $w/c =$  (a) 0.35 (C35) and (b) 0.45 (C45).

w/c	MS: <i>mechanical</i> setting time (h)	CS: <i>chemical</i> setting time (h)	CS-MS (h)	full width at half maximum (h)			
				$\Delta MS$		$\Delta CS$	
				$\Delta MS^-$	$\Delta MS^+$	$\Delta CS^-$	$\Delta CS^+$
0.35	7.3	10.7	3.4	4.8		5.0	
				3.1	1.7	2.6	2.4
0.45	9.0	14.4	5.4	5.4		8.4	
				3.1	2.3	4.9	3.5

Table 3-1: *Mechanical* and *chemical* setting times and full width at half maximum ( $\Delta MS$ ,  $\Delta CS$ ) determined on  $dT_1/dt$  and  $dI_{FID}/dt$  diagrams (pre-peak durations:  $\Delta MS^-$ ,  $\Delta CS^-$ , post-peak durations:  $\Delta MS^+$ ,  $\Delta CS^+$ ) for cement pastes made of gray OPC of  $w/c = 0.35$  (C35) and 0.45 (C45).

The setting process seems hindered with the increase of w/c ratio. The acceleration period detected by  $dI_{\text{FID}}/dt$  is indeed much longer for C45. This phenomenon illustrates the prolonged germination phase and development of hydration products, and the longer duration of water depletion at high w/c ratio. It should be noted that the *chemical* setting time occurs usually after the *mechanical* setting time.

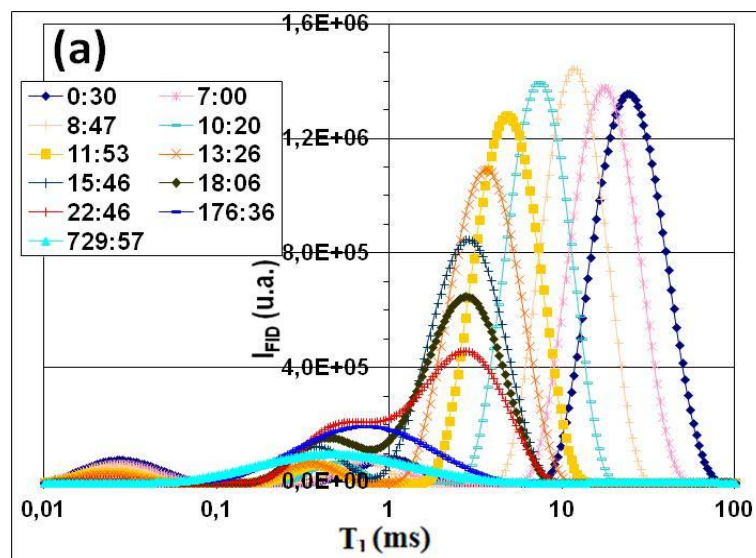
However, it should also be kept in mind that there is no intrinsic correlation between the *mechanical* setting time corresponding to the percolation of the solid network, and the *chemical* setting time corresponding to the maximum rate of water depletion or to the peak of heat release. The presence of two setting times is related to natural properties of cement-cased materials. For example, in the case of an extremely diluted cement paste (very high w/c ratio), the *mechanical* setting time may never occur (no percolation of the solid network) whereas the *chemical* setting (maximum of temperature increase) remains possible.

In section 3.3, this simple and relevant method for the determination of the *mechanical* and *chemical* setting times by NMR tools will be applied for various mix designs to investigate the setting process, hydration kinetics and water depletion mechanisms.

#### **3.2.1.4 Effect of FID data treatment methods**

##### ***Selection of capillary peak for FID acquisition***

By accumulating  $I_{\text{FID}}$  in function of time, the evolution of free water content during hydration is monitored. The acquisition number of FID signal is 1024 points. An analytical example for an OPC gray cement paste of w/c = 0.45 (C45) is shown in Figures 3.6 (a), (b), and (c).



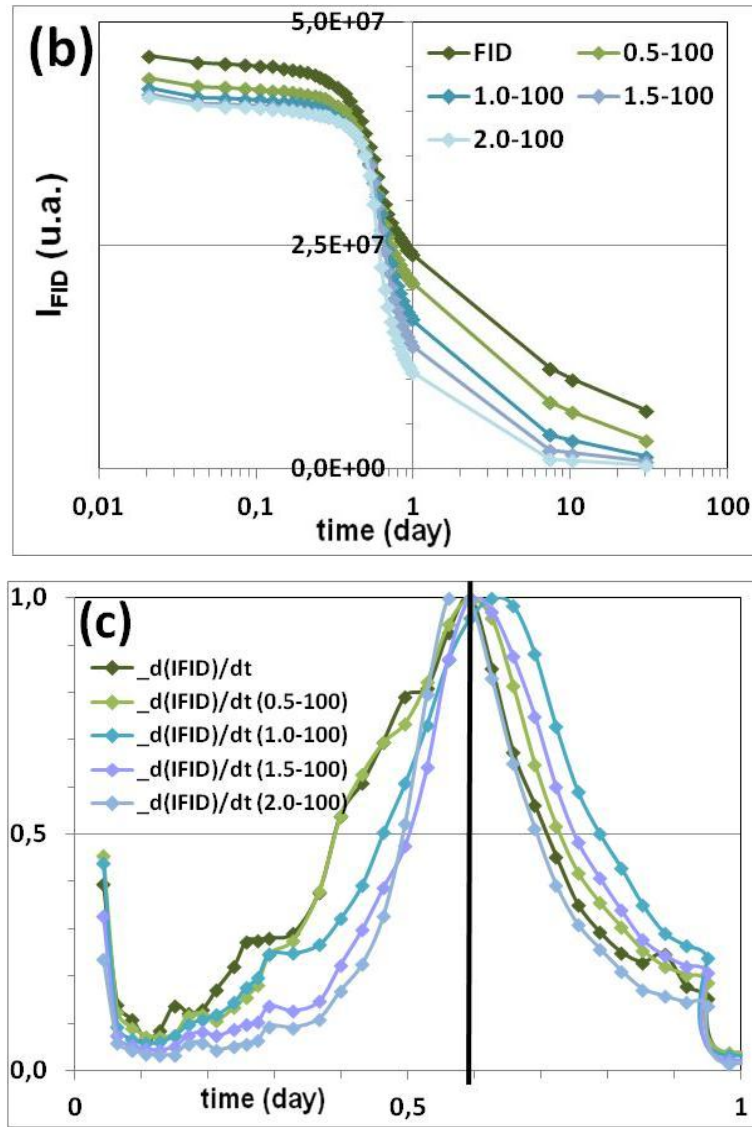


**Figure 3.6: Cement paste made of gray OPC of w/c = 0.45: (a) Distribution of FID intensity (b) FID diagrams according to the range of  $T_1$  accumulation by the distinguish of capillary / physically-bound water (c) Time derivative of  $I_{FID}$  according of the range of  $T_1$  accumulation.**

The distribution of FID acquisition following hydration time is generated based on these acquisitions by Fourier transform as in the case of 6 deleted-points profiles, as shown in Figure 3.6 (a). Since very early age from 30 minutes to about 30 days after mixing, the optimum peak evolves towards smaller value of  $T_1$ .

It can be observed that in this case, the peak which is corresponding to capillary water occurs at  $T_1 > 1$  ms. The  $T_1$  peak observed in the range of 1 ms - 100 ms corresponds to capillary pores according to literatures ([71], [72], [73]), consequently the peak of  $I_{FID}$  observed in this range corresponds to water in capillary pores as well. According to this assumption, FID

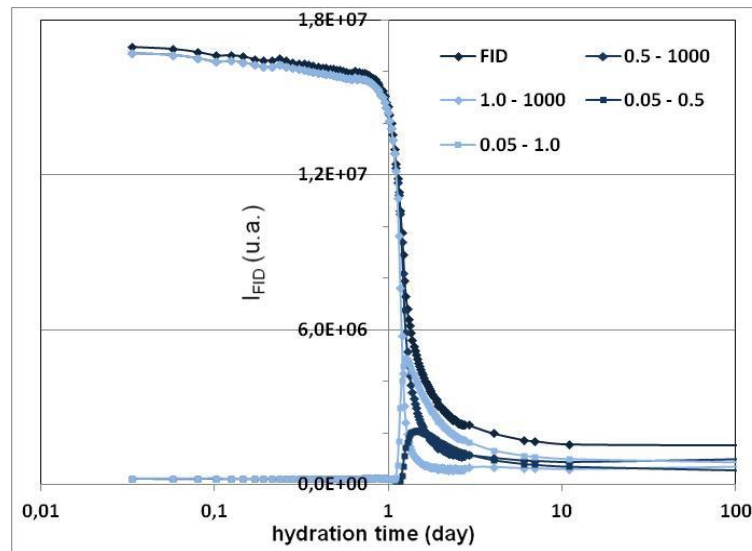
intensity is divided into 2 parts. Different NMR signals can be determined by an accumulation of  $I_{\text{FID}}$  distribution below and above a given threshold value  $T_{\text{lim}}$ .

Four different  $T_{\text{lim}}$  values have thus been tested: 0.5 ms, 1.0 ms, 1.5 ms, and 2.0 ms. Diagrams of  $I_{\text{FID}}$  accumulation between each of these  $T_{\text{lim}}$  values and 100 ms are illustrated in Figure 3.6 (b). It highlights that the higher is  $T_{\text{lim}}$ , the faster intensity of NMR signal amplitude ( $I_{\text{FID}}$ ) decreases and the kinetics of water depletion until reaching complete hydration. But these evolutions are observed as in same performance during water depletion process.

This trend reflects that the accumulation of the  $I_{\text{FID}}$  distribution from  $T_1 = 1.0$  ms to 100 ms mainly represents free capillary water, which is supposed to be almost completely depleted in long term of hydration. In this case, the  $w/c = 0.45$  is characterized as slightly exceeding the stoichiometric  $w/c = 0.42$  corresponding to a complete consumption of free water necessary for the formation of chemically-bound water and gel water.

The time derivative of each selected FID curve is illustrated in Figure 3.6 (c). Although the shape of each curve is slightly different, the *chemical* setting times defined as the optimum of  $d(I_{\text{FID}})/dt$  are consistent despite of different  $T_{\text{lim}}$  values. This result shows that the definition of a *chemical* setting by means of the optimum of  $d(I_{\text{FID}})/dt$  appears representative of the free water depletion.

This data treatment can also be applied for UHPFRC without fibers as shown in Figures 3.7:





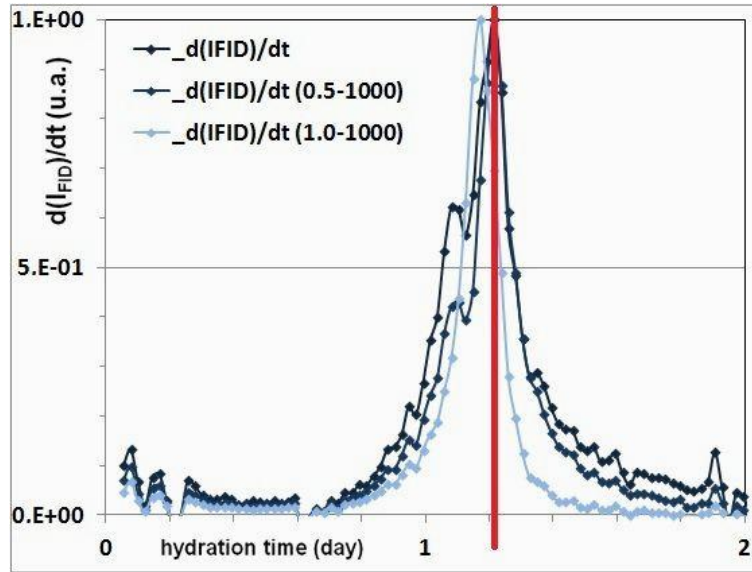


**Figure 3.7: UHPFRC without fibers: (a) FID diagrams according to the range of  $T_1$  accumulation by the distinguish of capillary / physically-bound water (b) Time derivative of  $I_{FID}$  according of the range of  $T_1$  accumulation.**

The different NMR signals can be determined by an accumulation of the  $I_{FID}$  distribution below and above a given threshold value  $T_{lim}$ . Two different threshold values  $T_{lim}$  have been tested: 0.5 ms and 1.0 ms; the diagrams of  $I_{FID}$  accumulation between each of these  $T_{lim}$  values and 100 ms are illustrated in Figure 3.7 (a) for UHPFRC without fibers. It highlights that the higher is  $T_{lim}$ , the faster is the kinetics of water depletion until reaching a complete consumption of water.

The time derivative of each selected FID curve is illustrated in Figure 3.7 (b). The shapes of each curve are quite similar, the *chemical* setting times defined as the optimum of  $d(I_{FID})/dt$  are constant despite of different  $T_{lim}$  values.

#### ***Deletion of different points of FID acquisition***

By the accumulation of  $I_{FID}$  in function of time, the evolution of proton content, i.e., free water content during hydration can be monitored. The acquisition number of FID signal is 1024 points in this thesis. The profiles are generated based on these acquisitions by Fourier transform as in the case of 6 deleted-points profiles.

Because the first six-points are usually not useful in the treatment, the application of Fourier transform begins from 7 to 1024 points of FID acquisition [33]. It can also be applied to delete the first 10, 20, 30, 50, 100, 150, 200 points, etc. to generate different profiles.

The comparison between the deletions of 6, 50, 100 points is shown in Figure 3.8 (a) for an OPC gray cement paste of  $w/c = 0.45$  (C45). And the derivations of these profiles are presented in Figure 3.8 (b).

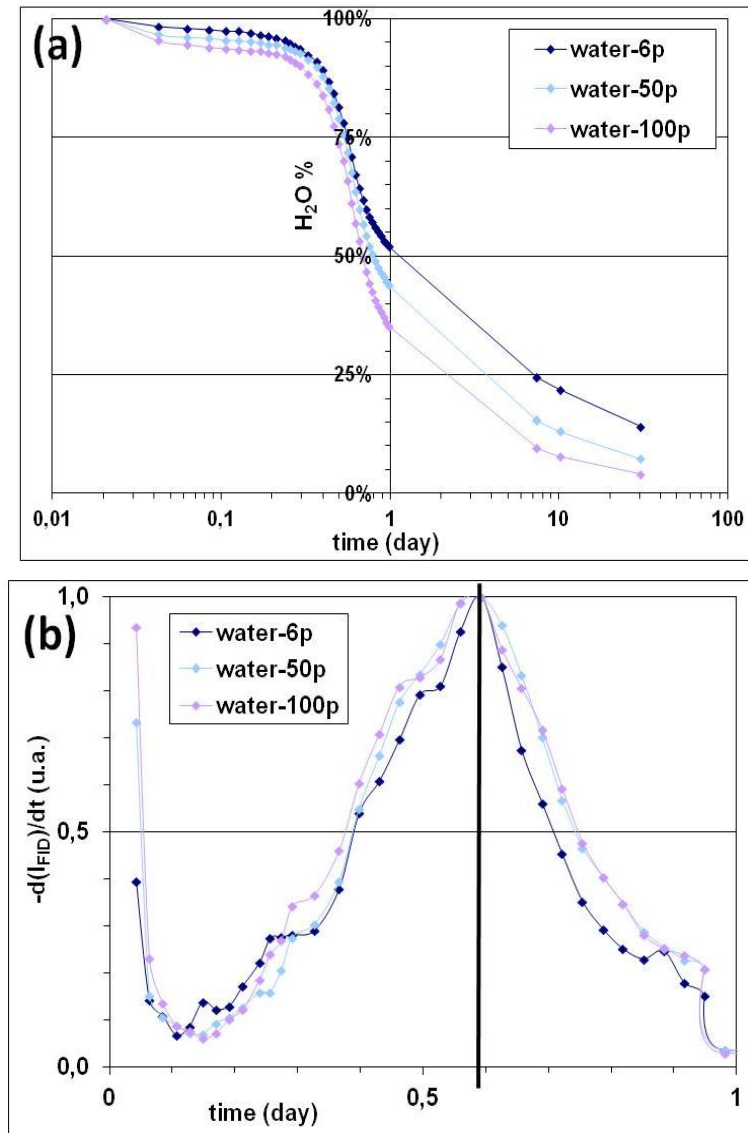


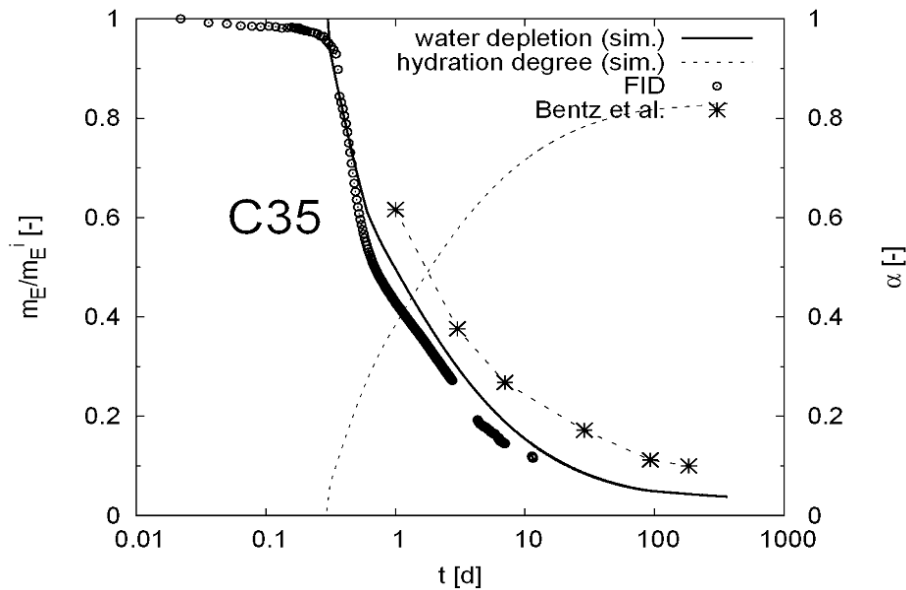
**Figure 3.8: Cement paste made of gray OPC of  $w/c = 0.45$ : (a) Effect of deleted points of FID acquisition; (b) Derivation of  $I_{FID}$  in different conditions of deleted points**

The intensity of  $I_{FID}$  decreases as the number of deleted points of FID acquisition increases. But these evolutions are observed in similar performance during water depletion process. Furthermore, as it was proved in aforementioned section, *chemical* setting time occurs at the time corresponding to the optimum value of the derivation of  $I_{FID}$  ( $d(I_{FID})/dt$ ) and of temperature evolution ( $T^\circ$ ). Although different numbers of deleted points are presented in this section, the optimum of  $-d(I_{FID})/dt$  occurs at the same time as shown in Figure 3.8 (b). This modification in data treatment does not change the *chemical* setting time.

### 3.2.2 Numerical simulation as a probe for free water depletion

Analytical tools and the numerical model of hydration presented in section 2.3.1.3 were used to verify that  $I_{FID}$  monitoring is a relevant way to quantify the water consumption during hydration. The same cement pastes C35 and C45 as described in section 3.2.1 are investigated in this section.

The hydration model allows the quantification of the mass fraction of water which has been consumed during hydration by calculating total amount of water in the mix design minus chemically-bound water. Hence this calculation represents the time evolution of free capillary water plus gel water which is assumed embedded inside the layered microstructure of the C-S-H. Note that the determination of gel water is carried out by considering a C-S-H porosity of 28% [74]. In Figures 3.9 (a) and 3.9 (b),  $m_E/m_E^i$  represents the water content normalized by the initial water content of the fresh material in the case of two OPC pastes of  $w/c = 0.35$  and  $0.45$ . The global water depletion assessed by  $I_{FID}$  is well in agreement with the simulations.



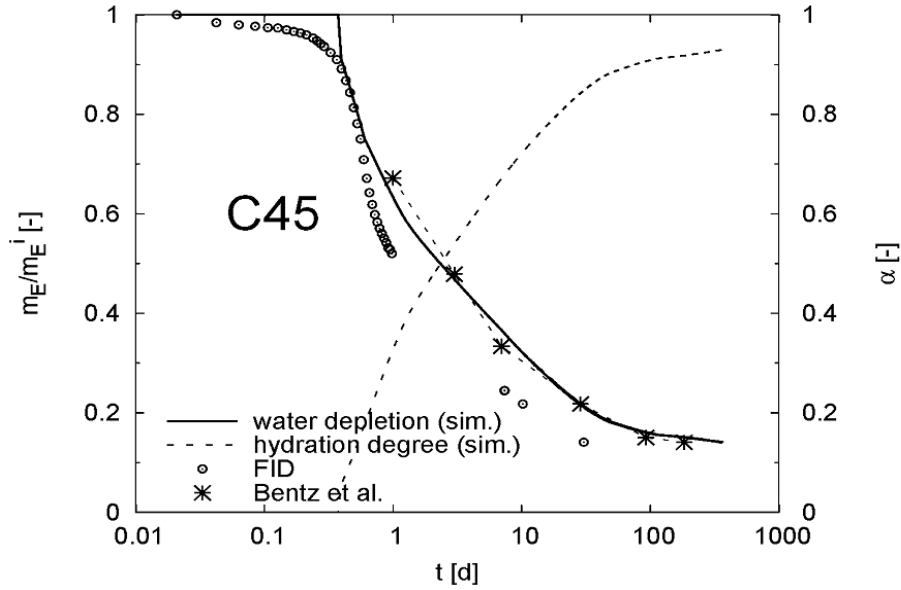


**Figure 3.9: Monitoring of  $I_{FID}$ , simulated kinetics of water depletion, and indirect assessment of the time evolution of the water consumption from data provided in [48]. Case for cement pastes made of gray OPC of w/c = (a) 0.35 (C35) and (b) 0.45 (C45).**

Data provided by Bentz *et al.* [45] were been used to assess water consumption during hydration. The authors have assessed the evolution of the degree of hydration  $\alpha$  from 1 to 100 days for two OPC cement pastes of w/c = 0.35 and 0.435. By considering that 1 g of cement binds 0.3 g of water chemically, the amount of free water plus gel water can be assessed and the water depletion kinetics can be plotted as illustrated in Figures 3.9. A similar method has been used by Friedmann *et al.* [75]. But in a reverse way to determine the degree of hydration from the NMR signal intensities.

Note that the difference in w/c between 0.45 (in this thesis) and 0.435 (in [45]) is not important enough to generate significant discrepancies. The simulations and the indirect assessment of water depletion kinetics from the provided data show a quite satisfactory agreement with  $I_{FID}$ . These results confirm the possibility to use the NMR signal amplitude  $I_{FID}$  to assess the kinetics of water consumption from early age to long term of hydration. The analysis of  $I_{FID}$  is a relevant tool to determine the *chemical* setting by monitoring  $dI_{FID}/dt$ .

### **3.3 NMR results for various cement pastes / mortars**

#### **3.3.1 Cement pastes made of gray and white OPC**

Three cement pastes made of white OPC of w/c = 0.35 (WC35), 0.40 (WC40) and 0.50 (WC50) were investigated by using the aforementioned analytical methods. The *mechanical*

and *chemical* setting times for each material are presented in Figure 3.10 and summarized in Table 3-2. The settings times for cement pastes made of gray OPC are recalled in Table 3-1.

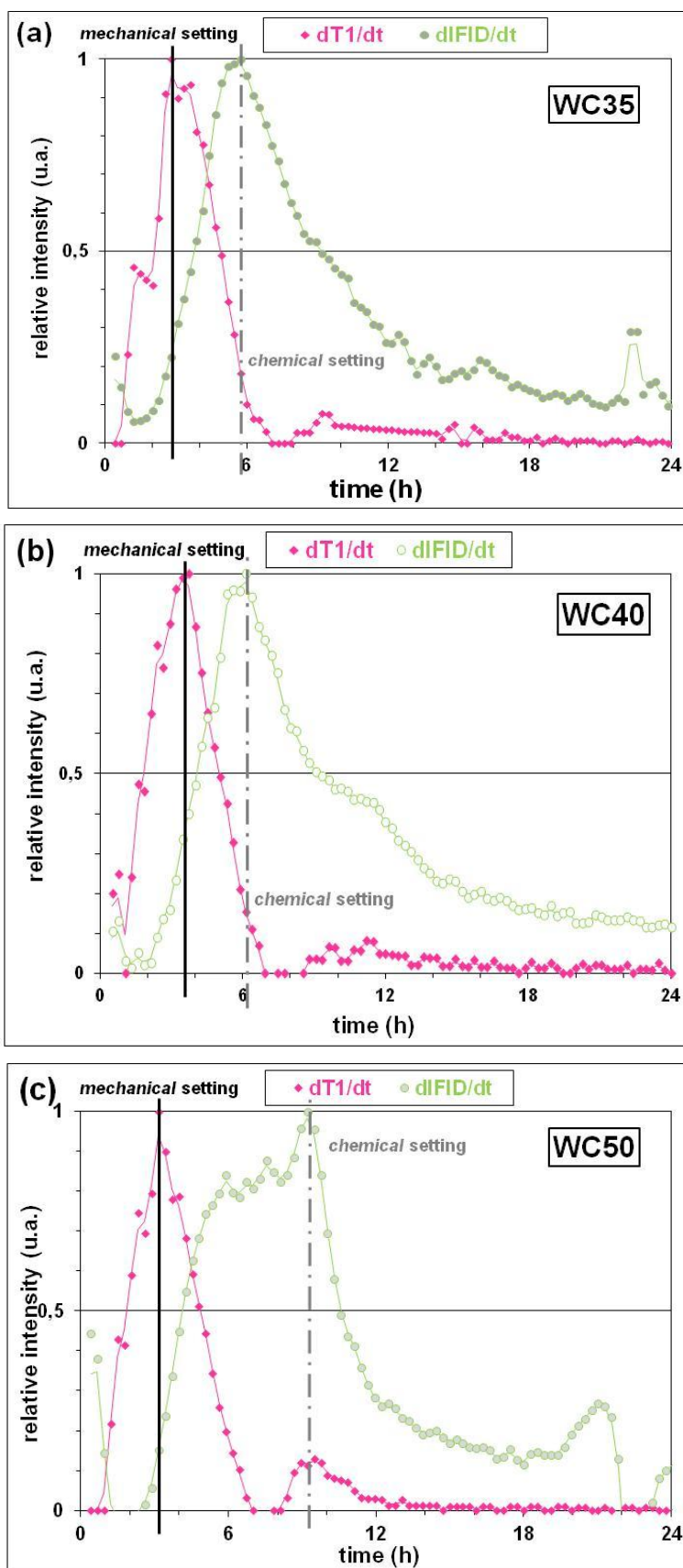


**Figure 3.10: Time derivative of optimum  $T_1$  value  $dT_1/dt$  and NMR signal amplitude  $dI_{FID}/dt$  for cement pastes made of white OPC of w/c = (a) 0.35 (WC35); (b) 0.40 (WC40); (c) 0.50 (WC50).**

w/c	MS: <i>mechanical</i> setting time (h)	CS: <i>chemical</i> setting time (h)	CS-MS (h)	full width at half maximum (h)			
				$\Delta MS$		$\Delta CS$	
				$\Delta MS^-$	$\Delta MS^+$	$\Delta CS^-$	$\Delta CS^+$
0.35	2.8	5.7	2.9	2.9		5.4	
				0.8	2.1	1.9	3.5
0.40	3.5	6.1	2.6	3.2		5.0	
				1.6	1.6	2.1	2.9
0.50	3.2	9.2	6.0	3.0		6.5	
				1.3	1.7	5.1	1.4

**Tableau 3-2: Mechanical and chemical setting times and full width at half maximum ( $\Delta MS$ ,  $\Delta CS$ ) determined on the  $dT_1/dt$  and  $dI_{FID}/dt$  diagrams (pre-peak durations:  $\Delta MS^-$ ,  $\Delta CS^-$ , post-peak durations:  $\Delta MS^+$ ,  $\Delta CS^+$ ) for the cement pastes made of white cement WC35 (w/c = 0.35), WC40 (w/c = 0.40) and WC50 (w/c = 0.50).**

As expected, the setting process is hindered with the increase of w/c. Compared with the cement paste C35 made of gray OPC, the *mechanical* settings time for WC35 are shorter. This was explained by the fact that there is a higher content of  $C_3A$  in white cement than in gray cement in section 3.2.1. In Tables 3-1 and 3-2, the FWHM of the  $dT_1/dt$  and  $dI_{FID}/dt$  peaks are indicated ( $\Delta MS$  and  $\Delta CS$ , respectively) (see Figure 3.2 (c), 3.3 (c) for the definition of  $\Delta MS$ , Figures 3.4 for that of  $\Delta CS$ ). The determination of these values is illustrated on each  $dT_1/dt$  and  $dI_{FID}/dt$  diagram. Note that the durations of the pre-peak ( $\Delta CS^-$  and  $\Delta MS^-$ ) and post-peak periods ( $\Delta CS^+$  and  $\Delta MS^+$ ) around the *chemical* or *mechanical* setting times are also identified (see Figure 3.6 (b) for the definition of  $\Delta MS^-$ ,  $\Delta MS^+$ ,  $\Delta CS^-$ ,  $\Delta CS^+$ ).  $\Delta CS^-$  and  $\Delta MS^-$  corresponds to the duration of the acceleration period of hydration (nucleation-growth step) while  $\Delta CS^+$  and  $\Delta MS^+$  corresponds to the deceleration period (diffusion-control step). The use of white OPC accelerates the pre-peak phase due to a high content of  $C_3A$  compared to the gray OPC. On the other hand, the post-peak period is longer in the case of white cement.

### 3.3.2 Effect of the addition of standard sand (cement paste vs. mortar)

A cement paste and a mortar made of gray OPC were prepared to investigate the effect of sand addition on hydration process. The *mechanical* and *chemical* setting times for each material are presented in Figures 3.11 and summarized in Table 3-3. Two different mix

designs are prepared: (C35): w/c = 0.35 cement paste, (M42): w/c = 0.42 s/c = 2.0 mortar. Since it is necessary to take into account the absorption capacity of sand (3% of water in weight is absorbed by standard sand), equivalent effective w/c ratio is equal to 0.36 as in a cement paste for this mortar.

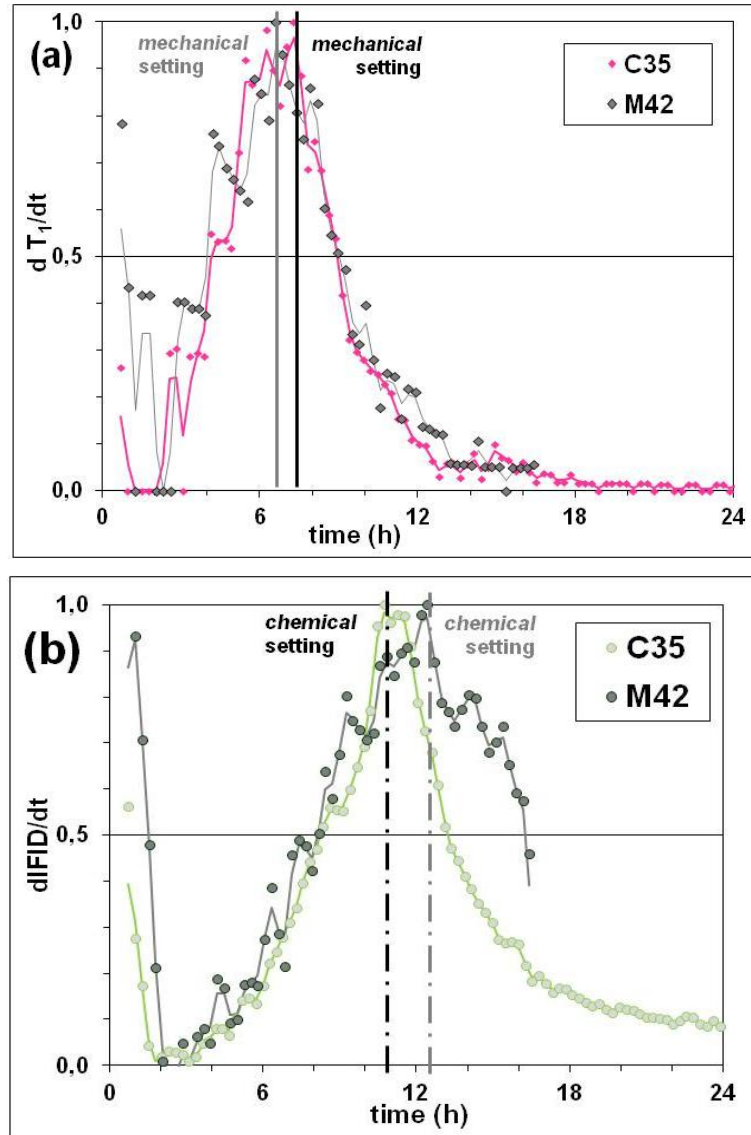


**Figure 3.11: Time derivative of optimum  $T_1$  value  $dT_1/dt$  and NMR signal amplitude  $dI_{FID}/dt$  for the w/c = 0.35 cement paste (C35) and the w/c = 0.42 mortar of s/c = 2.0 (M42).**

w/c	MS: <i>mechanical</i> setting time (h)	CS: <i>chemical</i> setting time (h)	CS-MS (h)	full width at half maximum (h)			
				$\Delta MS$		$\Delta CS$	
				$\Delta MS^-$	$\Delta MS^+$	$\Delta CS^-$	$\Delta CS^+$
C35	7.3	10.7	3.4	4.8		5.0	
				3.1	1.7	2.6	2.4
M42	6.6	12.4	5.8	5.0		8.2	

				2.5	2.5	4.2	4.0
--	--	--	--	-----	-----	-----	-----

**Tableau 3-3: *Mechanical and chemical setting times and full width at half maximum ( $\Delta MS$ ,  $\Delta CS$ ) determined on the  $dT_1/dt$  and  $dI_{FID}/dt$  diagrams (pre-peak durations:  $\Delta MS^-$ ,  $\Delta CS^-$ , post-peak durations:  $\Delta MS^+$ ,  $\Delta CS^+$ ) for C35 and M42 (mortar).***

In Figures 3.11 (a) and 3.11 (b), the *mechanical* and *chemical* setting times occur similarly for C35 and M42. The *mechanical* setting times are almost the same. This phenomenon demonstrates that the presence of sand does not influence the *mechanical* setting process (percolation of the solid network).

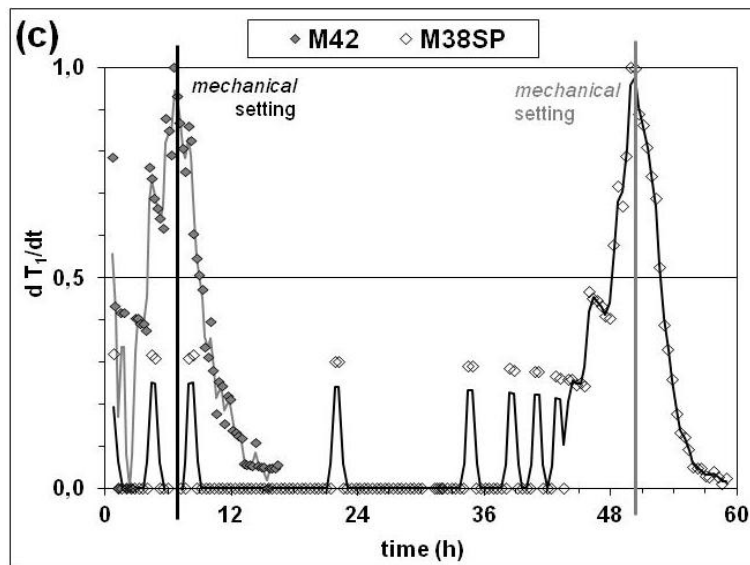
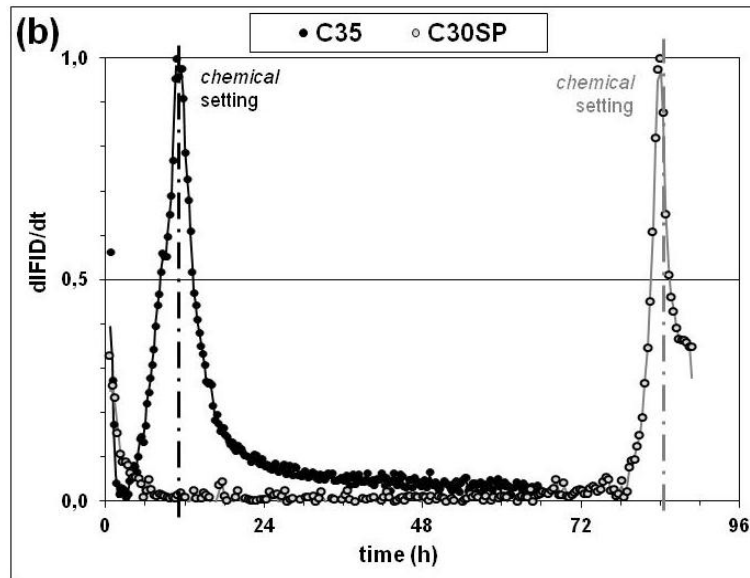
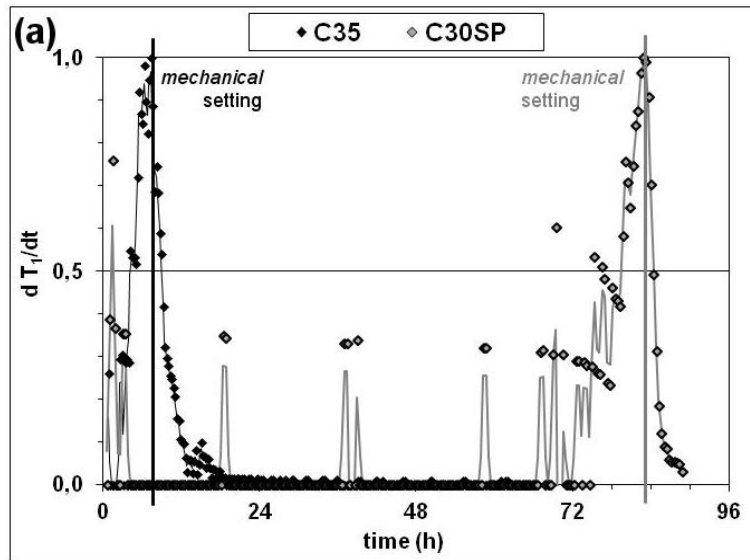
Nonetheless, considering *chemical* setting, the rate of water depletion during the prolonged deceleration period is slightly reduced in the case of M42. The addition of sand increases the delay in chemical reactions after setting because the sand releases pre-absorbed water into the cement matrix. The presence of sand also hinders the diffusion of water and ions between the bulk porosity and the non-hydrated cement grains [76].

### 3.3.3 Effect of the addition of super-plasticizer

Two cement pastes and two mortars made of gray OPC were prepared to investigate the effects of a water-reducer super-plasticizer (SP). The *mechanical* and *chemical* setting times for each material are presented in Figures 3.12 and summarized in Table 3-4. The studied mix designs are presented as follows:

- \* (C35):  $w/c = 0.35$  (cement paste).
- \* (C30SP):  $w/c = 0.30$  (cement paste with 2% SP).
- \* (M42):  $w/c = 0.42$  and  $s/c = 2.0$  (mortar).
- \* (M38SP):  $w/c = 0.38$  and  $s/c=2.0$  (mortar with 1% SP).





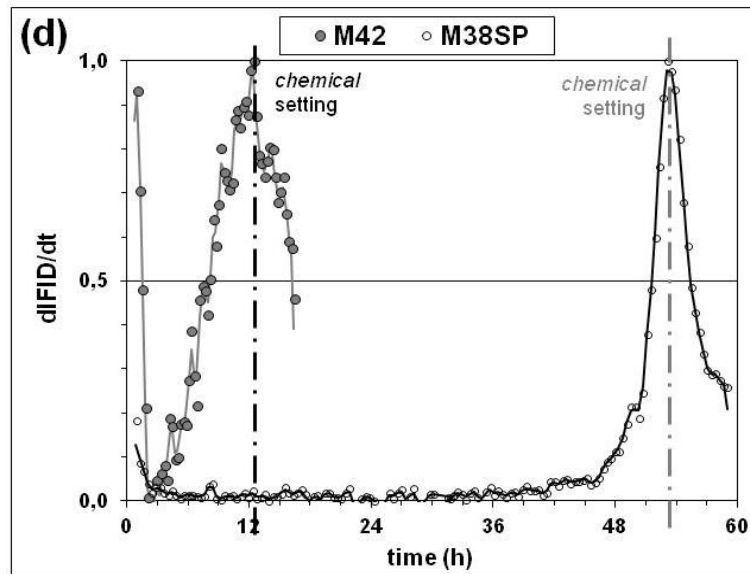


**Figure 3.12: Effect of the addition of super-plasticizer: (a)  $dT_1/dt$  and (b)  $dI_{FID}/dt$  for C35 and C30SP; (c)  $dT_1/dt$  and (d)  $dI_{FID}/dt$  for M42 and M38SP.**

w/c	MS: <i>mechanical</i> setting time (h)	CS: <i>chemical</i> setting time (h)	CS-MS (h)	full width at half maximum (h)			
				$\Delta MS$		$\Delta CS$	
				$\Delta MS^-$	$\Delta MS^+$	$\Delta CS^-$	$\Delta CS^+$
C35	7.3	10.7	3.4	4.8		5.0	
				3.1	1.7	2.6	2.4
C30SP	82.9	84.1	1.2	5.4		2.7	
				3.8	1.6	1.5	1.2
M42	6.6	12.4	5.8	5.0		8.2	
				2.5	2.5	4.2	4.0
M38SP	49.9	53.1	3.2	5.0		3.8	
				2.2	2.8	1.5	2.3

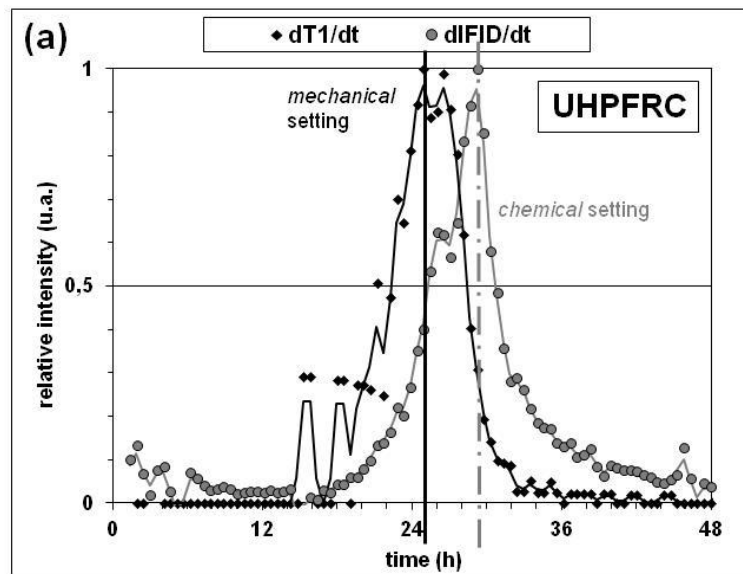
**Table 3-4: Mechanical and chemical setting times and the full width at half maximum ( $\Delta MS$ ,  $\Delta CS$ ) determined on the  $dT_1/dt$  and  $dI_{FID}/dt$  diagrams (pre-peak durations:  $\Delta MS^-$ ,  $\Delta CS^-$ , post-peak durations:  $\Delta MS^+$ ,  $\Delta CS^+$ ) for C35, C30SP, M42 and M38SP.**

It is impossible to maintain the identical effective w/c ratio if SP is added due to phenomena of bleeding and sedimentation. To preserve an adequate workability, w/c must be reduced. Water content was reduced by 10 - 15% thanks to with super-plasticizer characteristics and according to cement content of the recipe. This section is aimed at providing a qualitative analysis of the setting process and water depletion in these various mix designs.

In Figures 3.12 (a) and 3.12 (b), the addition of SP entails an evident delay of the *mechanical* and *chemical* setting times corresponding to a prolonged induction period. However, after initial setting has been reached,  $dI_{FID}/dt$  evolution shows that the rate of water depletion is accelerated around the *chemical* setting time for C30SP compared with C35, and for M38SP compared with M42. This is illustrated in Table 3-4 by focusing on the full width at half maximum ( $\Delta CS$ ). However, it seems that the full width at half maximum of the *mechanical* setting ( $\Delta MS$ ) is slightly affected by the presence of SP as shown in Figures 3.12 (c) and 3.12 (d), as well as in Table 3-4. The prolonged induction period in the presence of SP has already been observed in the literature [77], as well as the possible acceleration of the germination phase which is generally related to the dispersion effect of the SP on the cement grains [78]. It is also possible that the prolonged dissolution period due to the presence of SP allows an accumulation of ions inside the pore solution and a delayed homogeneous diffusion of ions according to [75] which leads to an accelerated nucleation and growth of hydration products.

In UHPFRC of quite low  $w/c = 0.180$  [27], it has also been observed that *mechanical* setting occurs earlier than *chemical* setting. The *mechanical* and *chemical* setting times for each material are illustrated in Figures 3.13 and the values are summarized in Table 3-5. The studied mix designs are:

- \* UHPFRC:  $w/c = 0.18$  with 2.5% super-plasticizer and 26% silica fume;
- \* UHPFRC + fibers: UHPFRC without fibers with 4% (in volume) of aramid fibers (length = 20 mm and diameter = 0.8mm).



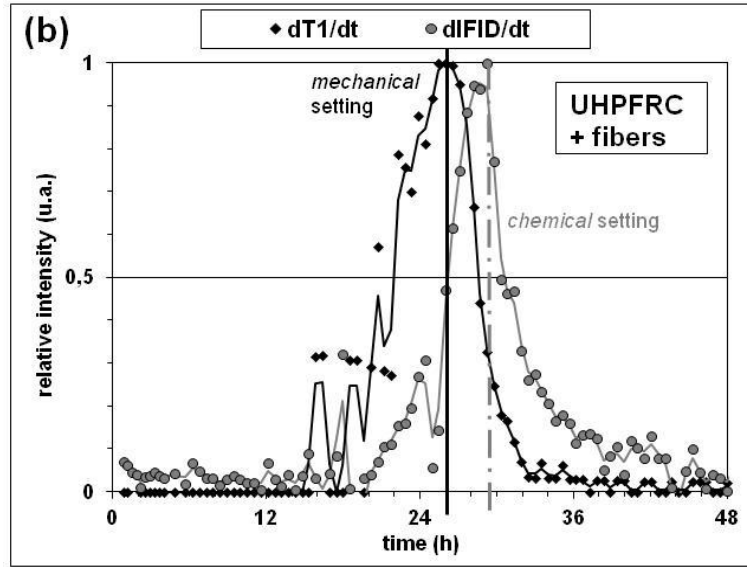


Figure 3.13: Time derivative of optimum  $T_1$  value  $dT_1/dt$  and NMR signal amplitude  $dI_{FID}/dt$  for (a) UHPFRC and (b) UHPFRC + fibers.

w/c	MS: <i>mechanical</i> setting time (h)	CS: <i>chemical</i> setting time (h)	CS-MS (h)	full width at half maximum (h)			
				$\Delta MS$		$\Delta CS$	
				$\Delta MS^-$	$\Delta MS^+$	$\Delta CS^-$	$\Delta CS^+$
UHPFRC	24.9	29.2	4.3	6.2		5.4	
				2.7	3.5	3.9	1.5
UHPFRC + fibers	26.0	29.2	3.2	7.3		4.2	
				4.3	3.0	3.1	1.1

Table 3-5: *Mechanical and chemical* setting times and full width at half maximum ( $\Delta MS$ ,  $\Delta CS$ ) determined on the  $dT_1/dt$  and  $dI_{FID}/dt$  diagrams (pre-peak durations:  $\Delta MS^-$ ,  $\Delta CS^-$ , post-peak durations:  $\Delta MS^+$ ,  $\Delta CS^+$ ) for UHPFRC, UHPFRC + fibers.

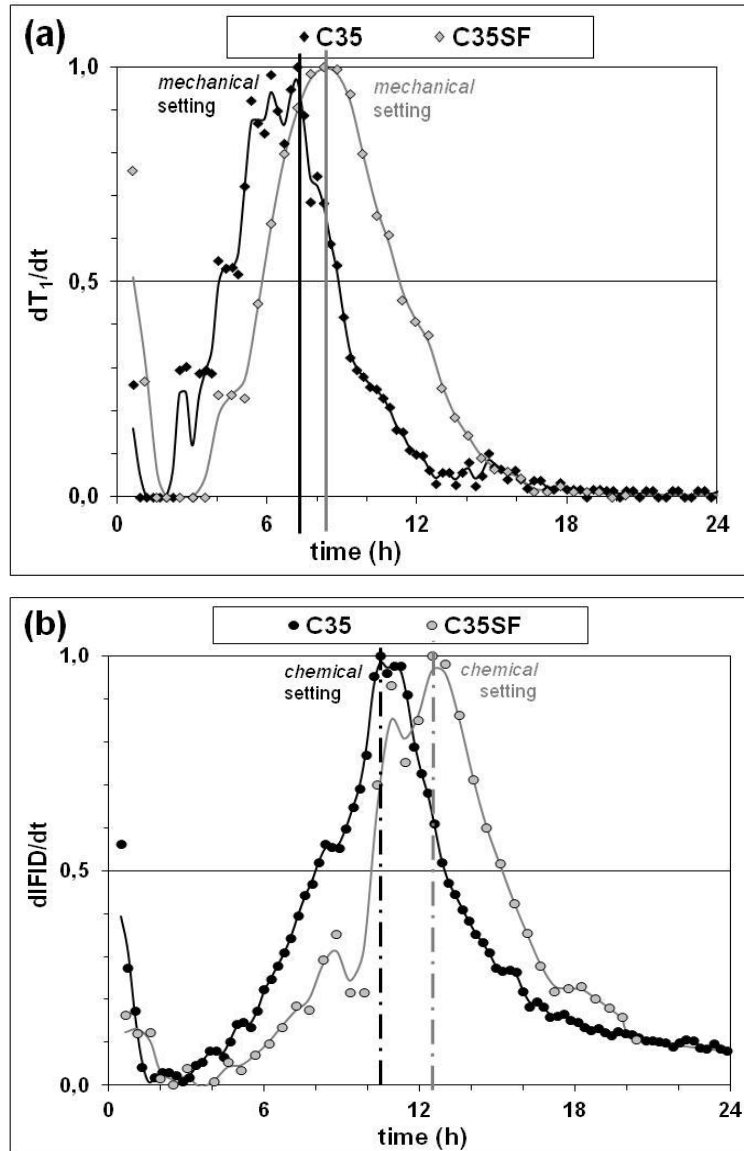
A prolonged induction period is observed whereas the post-peak period is accelerated around the *chemical* setting (see Figure 3.13 (a)). Note that the addition of aramid fibers slows down the setting from the *mechanical* point of view (see Table 3-5) because of the release of pre-absorbed water after initial setting time.

### 3.3.4 Effects of the replacement of cement by silica fume

Four cement pastes made of gray OPC were prepared to investigate the effects of silica fume (SF) on the hydration process. The *mechanical* and *chemical* setting times for each material are presented in Figures 3.14 and summarized in Table 3-6. The various mix designs are presented as follows:

- \* (C35): w/c = 0.35 (cement paste).
- \* (C35SF): w/c = 0.35 (cement paste) and 10% cement replaced by SF (in mass).
- \* (C45): w/c = 0.45 (cement paste).
- \* (C45SF): w/c = 0.45 (cement paste) and 10% cement replaced by SF (in mass).

These measurements are carried out by monitoring both derivatives of the optimum  $T_1$  value and of the NMR signal amplitude  $I_{\text{FID}}$  during the first 24 hours after casting.



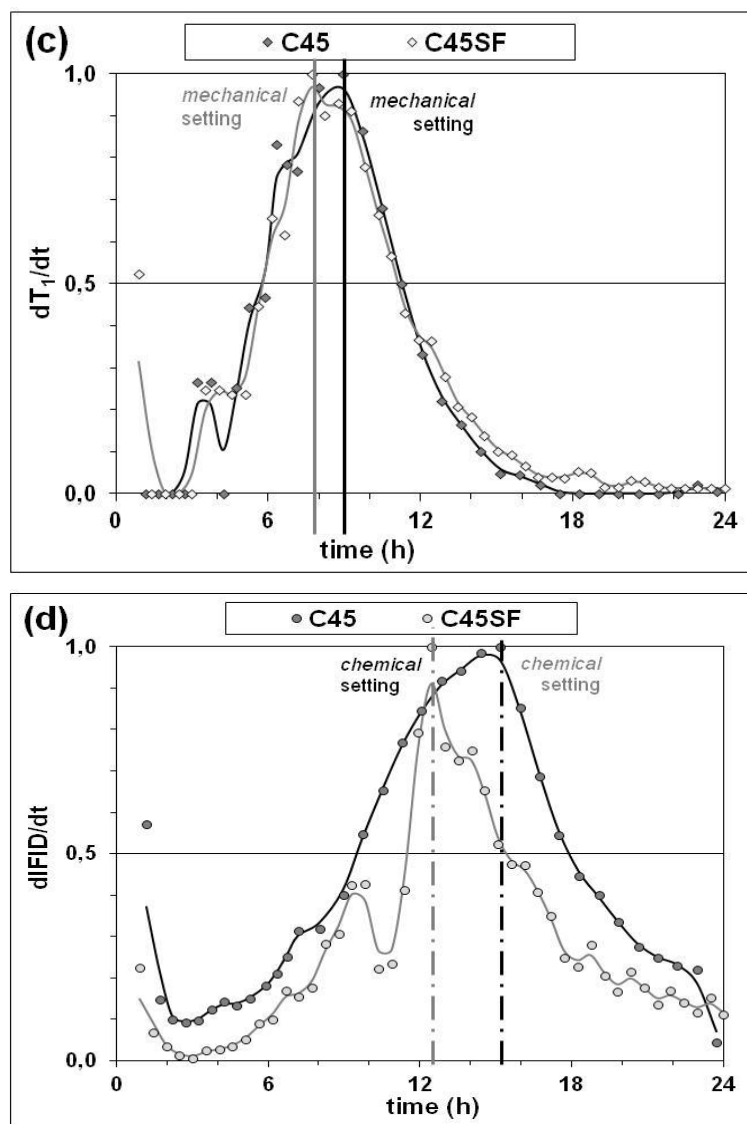


**Figure 3.14: Time derivative of (a) optimum  $T_1$  value  $dT_1/dt$  and (b) NMR signal amplitude  $dI_{FID}/dt$  for C35 and C35SF; Time derivative of (c) optimum  $T_1$  value  $dT_1/dt$  and (d) NMR signal amplitude  $dI_{FID}/dt$  for C45 and C45SF.**

w/c	MS: <i>mechanical</i> setting time (h)	CS: <i>chemical</i> setting time (h)	CS-MS (h)	full width at half maximum (h)			
				$\Delta MS$		$\Delta CS$	
				$\Delta MS^-$	$\Delta MS^+$	$\Delta CS^-$	$\Delta CS^+$
C35	7.3	10.7	3.4	4.8		5.0	
				3.1	1.7	2.6	2.4
C35SF	8.3	12.5	4.2	5.5		5.3	
				2.5	3.0	2.6	2.7
C45	9.0	14.4	5.4	5.4		8.4	
				3.1	2.3	4.9	3.5
C45SF	7.7	12.4	4.7	5.3		3.8	

				1.9	3.4	0.9	2.9
--	--	--	--	-----	-----	-----	-----

**Table 3-6: Mechanical and chemical setting times and full width at half maximum ( $\Delta MS$ ,  $\Delta CS$ ) determined on the  $dT_1/dt$  and  $dI_{FID}/dt$  diagrams (pre-peak durations:  $\Delta MS^-$ ,  $\Delta CS^-$ , post-peak durations:  $\Delta MS^+$ ,  $\Delta CS^+$ ) for C35, C35SF, C45 and C45SF.**

As shown in Figure 3.14 (b), the dormant period is prolonged with 10% silica fume replacement for C35SF compared with C35. The delay in hydration was explained by Langan *et al.* [79], due to the dissolution of silica fume and the formation of a gel-like Ca-poor Si-rich layer [80] on the cement grains surface. This layer inhibits water diffusion to the non-hydrated cement grains. Moreover, silica fume has a lower water demand than cement which apparently increases the w/c ratio during the dormant and acceleration periods. Therefore the acceleration rate is reduced.

On contrary, as shown in Figure 3.14 (d), hydration is accelerated with 10% silica fume replacement in the case of a higher w/c = 0.45. Actually, for a higher w/c ratio, the space between the cement grains is increased and filled with water. The higher availability of water accelerates the dissolution of the gel-like layer which hinders dissolution of the cement grains. Due to the breakdown of the initial hydration products and the exposure of additional surface of cement grains to water, the nucleation of hydration products starts earlier.

Moreover, the adsorption of  $Ca^{2+}$  by silica fume to its surface during the dormant period reduces the concentration of  $Ca^{2+}$  in solution and leads to pump effect which accelerates the dissolution of the cement grains.

On the whole, the addition of silica fume slows down the *chemical* setting due to an increase of the induction period for cement paste of low w/c ratio (0.35) whereas it accelerates it if w/c is high (0.45 in the present research and 0.50 in Langan's work). Both phenomena have been verified by calorimetry experiments in [80].

It is worth mentioning that, as shown in Figures 3.14 (a) and (c), the *mechanical* setting time is also hindered with 10% silica fume replacement in the case of w/c = 0.35, and accelerated if w/c = 0.45.  $\Delta MS$  and  $\Delta CS$  seem not to be affected by the presence of silica fume.

### **3.4 Global overview**

The *mechanical* and *chemical* setting times (MS and CS, respectively), and related full width of half maximum ( $\Delta MS$  and  $\Delta CS$ , respectively) are summarized in Figures 3.15 for the studied materials.

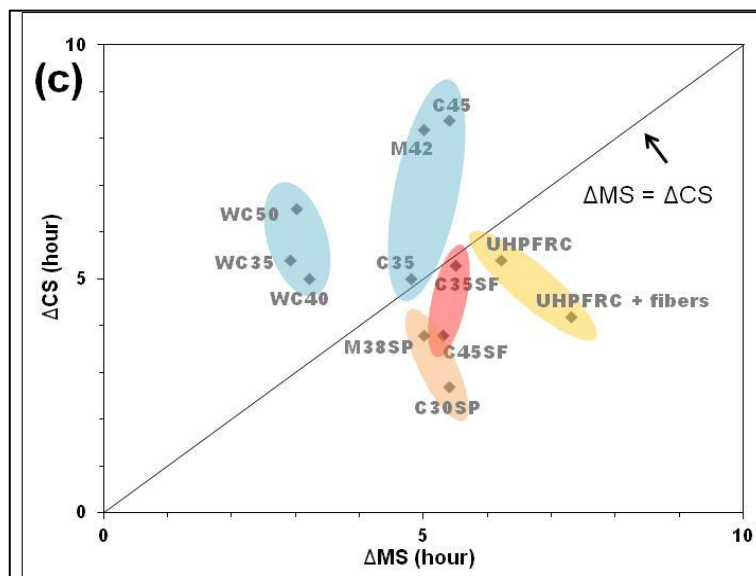
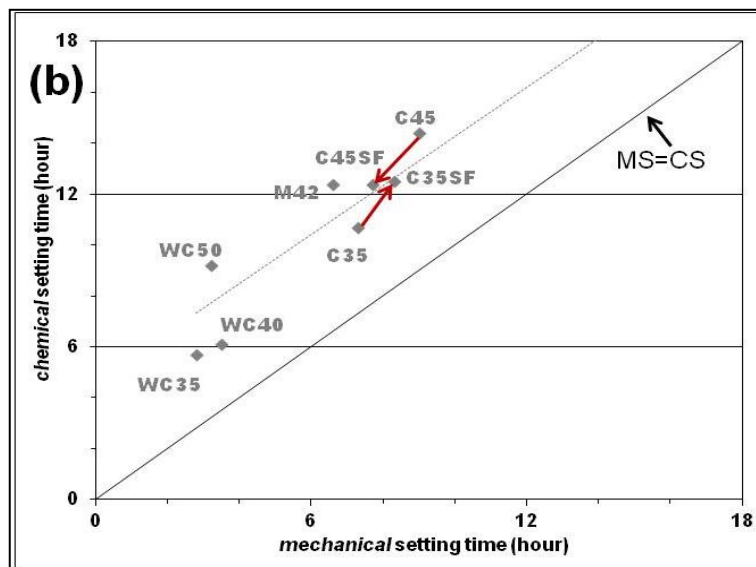
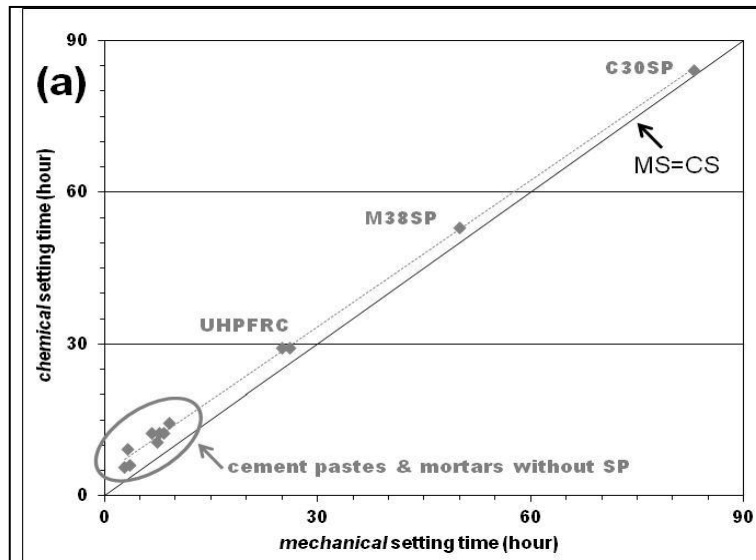




**Figure 3.15: Analysis of the relation (a) between *mechanical* (MS) and *chemical* (CS) setting times for various mix designs; (b) zoom in cement pastes and mortars without super-plasticizer; (c) analysis of the relation between the full width at half maximum of MS and CS.**

The *mechanical* setting times occur systematically earlier than the *chemical* setting times for all the studied materials. The relationship between both setting times seems linear as shown in Figure 3.15 (a). Figure 3.15 (b) represents a zoom for materials without super-plasticizer. As illustrated throughout the present paper, the use of white OPC accelerates the setting compared with gray OPC. The effect of the presence of silica fume on the hydration kinetics is complex and can lead to an acceleration effect (high w/c) or a deceleration effect (low w/c). Obviously, the addition of super-plasticizer severely delays the setting as it is illustrated here for ultra high performance matrix [81].

Figure 3.15 (c) provides an overview of the width of the *mechanical* and *chemical* settings ( $\Delta MS$  and  $\Delta CS$ , respectively) for all the studied materials.  $\Delta CS$  seems shorter than  $\Delta MS$  if materials containing super-plasticizers and silica fume are considered while it is the contrary if materials made of OPC are considered.

Thus by considering obtained results, both setting times are important parameters, to study setting process in a fast and accurate way. The NMR relaxometry is proved as a convenient method for the investigation of cement hydration procedure. According to experimentations, the results obtained by NMR relaxometry are corresponding to those by other techniques. And by comparing to conventional techniques, it is *in-situ*, non-destructive and informative.

The continuous NMR measurements allow the monitoring of **setting process** and **water depletion** since casting until hardening. The evolution of **optimum  $T_1$  value** has been applied to monitor the **percolation** of the solid network and shown as a relevant ***mechanical indicator*** of setting. The evolution of the **NMR signal amplitude  $I_{FID}$**  has been assessed to monitor the **global free water content** during hydration and used as a ***chemical indicator*** of hydration.

NMR data have been complemented thanks to the results obtained by **conventional techniques** and the **numerical simulation** from the *mechanical* and *chemical* points of view. The optimum  $T_1$  value is correlated with the results provided by Vicat needle. The  $I_{FID}$  is consistent with the data obtained by the numerical simulation and illustrated from the literature. Time derivative of the  $I_{FID}$  is also correlated with the temperature variations. The non-destructive NMR relaxometry has more advantage as it allows an *in situ* study of setting **from the very early age** without any pretreatment.

***Mechanical*** and ***chemical setting times*** correspond to the maximum of both derivatives of optimum  $T_1$  value and  $I_{FID}$ , respectively. The NMR measurements also allow the determination of the duration of acceleration (nucleation-growth) and deceleration (diffusion-control) periods around the setting times.

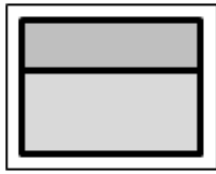
Based on NMR methods, various effects related to the formula (**admixtures**) on the **kinetics of setting** and hydration have been investigated: delayed initial setting time and an acceleration of the pre-peak and post-peak periods is observed when the super-plasticizer is added; the setting process in the case of silica fume replacement of cement is accelerated when w/c ratio is high enough, and decelerated when w/c is low.



## ***4. Chapter 4: Investigation of moisture transfer and its impact on hydration and microstructure of repair systems, during and after a repair procedure***

### **Summary**

<b><u>4.1 During early ages of repair procedure (0 - 28 days)</u></b>	<b>114</b>
4.1.1 Investigation of moisture profiles by SPI sequence	114
4.1.1.1 Reference repair mortar on initially-dried M25	116
4.1.1.2 Reference repair mortar on initially-saturated M25	118
4.1.1.3 Repair mortar with SAP on initially-dried M25	121
4.1.1.4 Conclusion	124
4.1.2 Application of characterized methodology on UHPFRC materials	124
4.1.2.1 UHPFRC matrix and with fibers on initially-dried M25	125
4.1.2.2 UHPFRC matrix and with fibers on initially-saturated M25	129
4.1.2.3 Fresh UHPFRC matrix ( $w/c = 0.16$ ) on fresh concrete M25 ( $w/c = 0.84$ )	132
4.1.3 Relations between SPI integration and FID - global free water content and chemical setting times	134
4.1.4 Investigation of moisture transfer within old concrete by density profiles	137
4.1.4.1 Reference repair mortar on initially-dried M25	137
4.1.4.2 Comparison with SPI profiles	138
<b><u>4.2 After 90-day repair procedure</u></b>	<b>140</b>
4.2.1 Total porosity determined by GRA	140
4.2.2 Total porosity and porous distribution determined by MIP	143
4.2.3 Repair efficiency and preview of durability	147
4.2.3.1 Profiles of water immersion by GRA (wetting properties)	147
Reference repair mortar and with SAP on initially-dried M25	147
Reference repair mortar on initially-saturated M25	149
4.2.3.2 Carbonation profiles and penetration depth	150
4.2.3.3 Accelerated $Cl^-$ diffusion profiles	152
<b><u>4.3 Global overview</u></b>	<b>153</b>

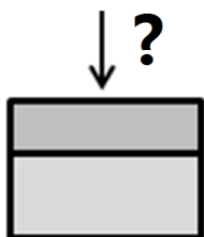


The **moisture profiles** within repair mortar and concrete during early stages of hydration have been investigated by Single Point Imaging (**SPI**) sequence of MRI technique. This sequence is operated with appropriate frequency and provides the possibility to follow complex evolution during hydration. As evaporation to the atmosphere is avoided in this thesis, there exists no exchange with environment. **Water depletion** within a repair mortar, as well as **moisture transfer** at the interface between the repair mortar and the old concrete, occur simultaneously within the whole system. Thus moisture profiles which represent free water content at different heights (at a scale of 2 mm) for various composite systems are monitored with accuracy.

This evolution is also characterized by **density profiles** at a scale of 3-10 mm through **GRA** technique. These profiles present the couplings of water content and hydrated compounds, and can be compared to aforementioned results obtained through SPI sequence.

The **microstructural evolution** after the repair procedure is investigated by GRA and **MIP** (total porosity and PSD) techniques, at different heights within various repair systems.

And this methodology can also be applied for **high performance concretes**, such as UHPFRC without and with fibers. These materials are widely applied on conventional substrate, and function as a concrete cover of protection or reinforcement, during bridge and road constructions [25 - 27].



Requirements of essential repair works are to **extend service lifetime** of reinforced concrete structures, in order to achieve a better **long-term durability** and also to avoid massive

reconstruction for economic purposes. After a repair procedure, most of macro-pores within concrete bulk are filled with **newly hydrated compounds**. While repair mortar forms a multiple protection on concrete cover, which more or less **prevents the passage of aggressive agents** from the environment into the system. It is interesting to investigate the repair systems under various conditions such as water immersion, chloride diffusion and accelerated carbonation. The objective is to understand better the repair efficiency, which is related to different repair materials and saturation states of substrates.

In this thesis, moisture transfer is mainly investigated in various composite systems, where exist the effects of both hydration reactions and microstructural formation. Both non-destructive MRI (SPI profiles) and GRA (density profiles) techniques were applied to monitor the profiles of free water content and density evolution at different heights of composite systems (since casting until 28 days). Especially to mention that, moisture transfer is focused on at macroscopic level, at the interface between repair mortar and concrete during early ages of a repair procedure (0 - 3 days).

Both GRA (non-destructive) and MIP (destructive) techniques were applied at micro scales to respectively monitor the profiles of total porosity and PSD, at different heights of repair system after 90 days when the microstructure is completely stabilized.

This methodology is applied both on “repair mortar on old concrete” and “UHPRFC on old and fresh concrete” systems, and will be detailed in sections 4.1.1 and 4.1.2.

#### **4.1 During early ages of repair procedure (0 - 28 days)**

##### **4.1.1 Investigation of moisture profiles by SPI sequence**

The related configuration of repair systems to SPI profiles is designed as shown in Figure 4.1. It is recalled that, moisture transfer at the mortar - concrete interface, its impacts on mortar hydration and microstructure, internal water depletion within repair mortar, are respectively investigated. The diameter of this representative system is 11 cm, and the height is 3 cm for the mortars and 5 cm for the old concrete.

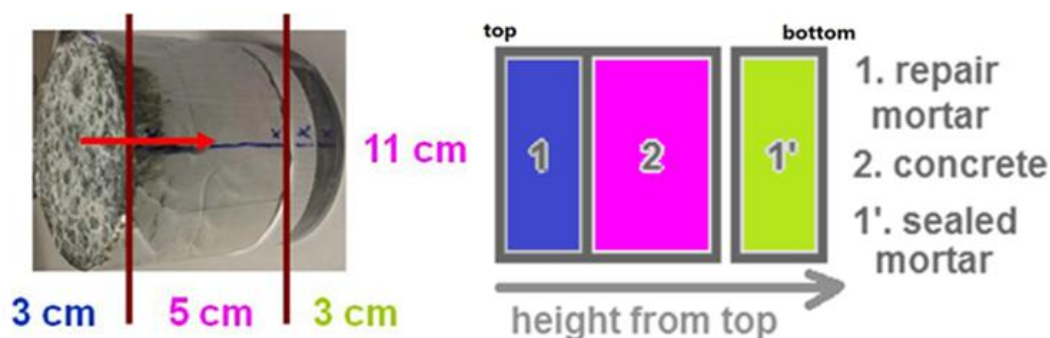


**Figure 4.1: Configuration of repair system and SPI profiles**

Three **repair systems** were thus studied:

1. Reference mortar ( $w/c = 0.30$  and  $s/c = 2.0$ ) on initially-dried concrete (pre-dried at  $45^{\circ}\text{C}$  during 28 days);

2. Reference mortar on initially-saturated concrete (pre-dried at 45 °C for 28 days and then vacuum-saturated in distilled water during 3 days);
3. Repair mortar with SAP ( $w/c = 0.30$  and  $s/c = 2.0$ ) on initially-dried concrete.

The second case is aimed at simulating a more realistic repair work in construction field. Indeed deteriorated concrete surface is commonly wetted and then patched with repair mortar, in order to prevent rapid moisture transfer from the fresh mortar to the old concrete. Depending on different formulas and properties of materials, excess water at the mortar - concrete interface can also influence the hydration process of the repair mortar being in contact with the wetted concrete. The resulted consequences are negative, since its microstructure becomes coarser. By considering these aforementioned aspects, both initially-dried and initially-saturated concretes, were investigated in this thesis to obtain critical results under laboratory conditions.

It is worth mentioning that, arbitrary values of NMR signal (a.u.) have no sense of absolute quantification, as they evolve with experimental conditions (preset parameters, etc.). SPI profiles and the evolution of its accumulated value (integration) can only be considered as relative results to compare local water content within different parts [34], and are respectively obtained to delicately explore physico-chemical interactions. The integration is obtained by averaging signal intensities of each part and related to the free water content within different materials. For quantitative analysis, the diagram is thus obtained by averaging signal intensities of each part and finally presented after normalization [82]: the initial water content (maximal intensity) is set to 100% before hydration begins (several minutes after casting and placing due to the limitations of experimental manipulation) for both mortars. The real-time water content within concrete (relative intensity) is proportional to the initial water content within mortars (maximal intensity), to obtain an overall review of moisture transfer during repair procedure.

In order to investigate aforementioned systems, TR is set to 100 ms ( $TR > 5T_1$ ) according to specimens' nature [33]. The initial  $T_1$  value is 14 ms for reference mortar, measured at casting time according to feasibility test. SN is set to 32,  $t_p$  is set to 130  $\mu s$ , and Rg is set to 16, in order to obtain accurate profiles under suitable experimental duration. The time to perform one measurement is about 10 minutes.

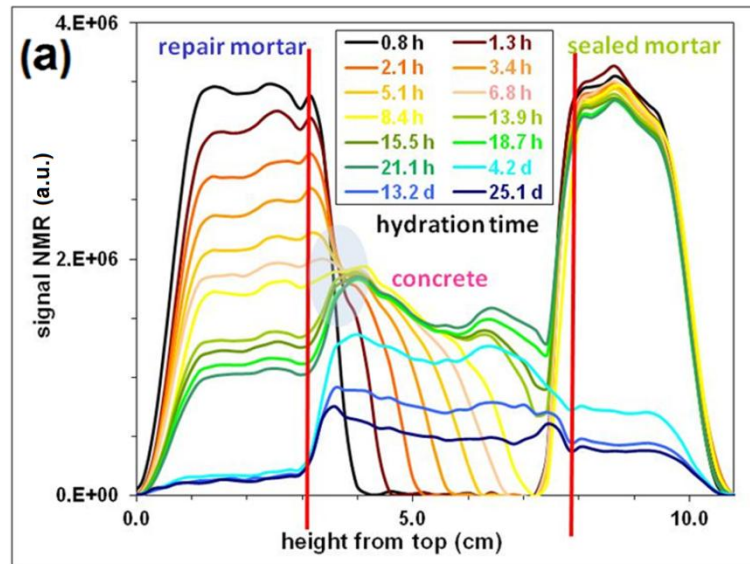


#### 4.1.1.1 Reference repair mortar on initially-dried M25

A reference repair mortar of  $w/c = 0.3$  and  $s/c = 2.0$  is applied on an initially-dried M25. Their formulas were detailed in section 2.2. The acquisition of SPI profiles starts from the very beginning of placing the repair system within the MRI apparatus. Normalized NMR signal intensities (a.u.) in function of height from top surface (cm), and their evolutions during hydration process are shown in Figure 4.2 (a).

The interface between the repair mortar and the old concrete, as well as the distinction between the repair system and the sealed mortar, are emphasized by red bold lines. The (1) repair mortar owns the same formula and quantity as the (1') sealed mortar, i.e., both mortars present the same diameter and height, thus the same volume. The slight difference is related to the inhomogeneity of magnetic field, although the system was adjusted in the middle of homogeneous area [33].

The accumulated values of global free water content within different parts are shown in Figure 4.2 (b) by the integration of SPI profiles. By comparing different intensities, it provides information to investigate moisture transfer separately from water depletion due to hydration reactions.



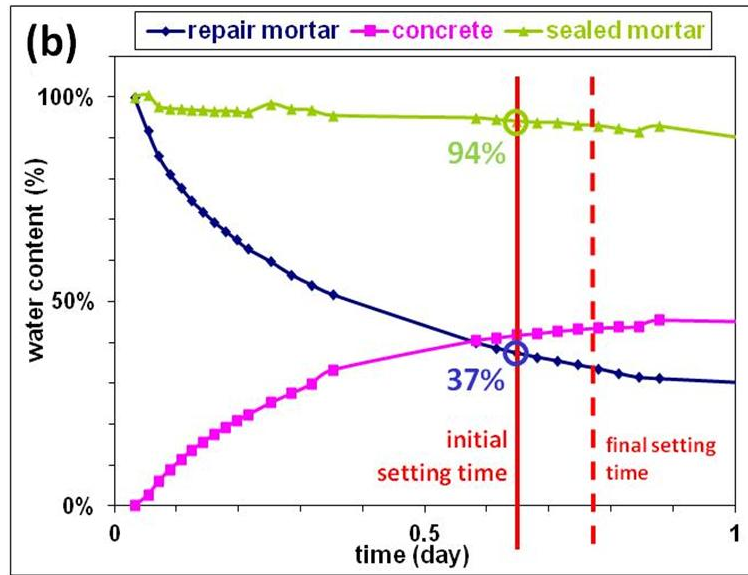


**Figure 4.2: Reference mortar on initially-dried concrete: (a) SPI profiles; (b) Integration of accumulated intensities.**

It is evident to observe from Figure 4.2 (a) that, water transfers continuously through the interface from repair mortar into initially-dried concrete during premier hours, and diffuses homogenously within each part. The effective w/c ratio is reduced since casting; it remains less water within the repair mortar at setting times than that within sealed mortar. This phenomenon may slow down the hydration process for the repair mortar by comparing to the sealed mortar according to Bentz [83]. For example, by comparing the cement pastes at w/c ratio of 0.35 (C35) and 0.45 (C45), the hydration process of C35 is hindered. By experimental results and modeling data, instantaneous hydration rate is linearly corresponding to the volume fractions of both water-filled porosity and unhydrated cement.

Figure 4.2 (b) illustrates that only 37% of free water is remained at 15 hours in repair mortar (corresponding to initial setting time determined by Vicat needle test as shown in section 3.2.1), while the sealed mortar consumes only 6% at the same time. Water diffuses into the concrete, and never comes back towards the repair mortar; while the “water reversion” is observed between UHPFRC and conventional concrete, this phenomenon will be detailed in section 4.1.2. Because the repair mortar has a w/c ratio equal to 0.30 and due to moisture transfer, the water content is strongly reduced and less than that in a cement paste with theoretically complete hydration at w/c = 0.42 [24]. This phenomenon leads to the insufficiency of available water for hydration reactions. Its microstructure should be coarser, and there exists non-hydrated cement grains. The formation of coarser porosity for passage of aggressive agents is assumed. These properties will be verified in section 4.2.

It is worth mentioning that, according to the verification after 2 months of hydration, there exists only 1.34% of mass loss within repair system (since 1797.67 g at placing until 1773.52 g at 63 days). Although it is well packed by a parafilm, the evaporation is not completely prevented. This difference is not evident by traditional techniques of characterization, but by SPI profiles which focus on free water content, it is interesting to take place the analysis as shown in Table 4-1.

Hydration time (day)		0.0	4.2	13.2	25.1
SPI intensities	concrete	0.20%	35.23%	22.57%	14.97%
	sealed mor.	100.00%	20.92%	13.04%	11.22%
	repair mor.	100.00%	7.46%	6.13%	5.72%
	con. + rep. mor.	100.00%	42.60%	28.65%	20.64%
	con. loss	-	-	12.66%	7.61%
	con. + rep. mor. loss	-	-	13.98%	8.02%
Mass verification	evap. loss			14.01%	8.82%

**Table 4-1: Effect of drying during hydration process of repair system by integrated intensities of SPI profiles and mass verification**

The mass loss by evaporation (14.01% from 4.2 to 13.2 days, and 8.82% from 13.2 to 25.1 days) is related directly to the differences between different hydration times of SPI intensities (while 13.98% and 8.02%) after hardening period. It is difficult to distinguish drying effect combined with hydration and moisture transfer before setting, for this propose the system should be improved to maintain its impermeability. This sensitive technique helps us to better understand the complex procedure in a delicate way.

#### **4.1.1.2 Reference repair mortar on initially-saturated M25**

Repair efficiency depends on the moisture gradient within repair systems and it is influenced by the initial saturation rates of concrete substrates. Appropriate condition is essential to improve adhesion properties and long-term durability. In order to quantify the repair procedure under different saturation rates, it is interesting to firstly review both critical conditions of reference repair mortars on initially-saturated (saturation level  $\approx 100\%$ ) and initially-dried (saturation level  $\approx 0\%$ ) M25 concretes.

The same reference repair mortar as presented in section 4.1.1.1 of  $w/c = 0.3$  and  $s/c = 2.0$  is applied on an initially-saturated M25. NMR signal (a.u.) in function of height from top surface (cm) of repair system, and its evolution during hydration is shown in Figure 4.3 (a). Identical color is applied for the profiles corresponding to the same hydration time as shown in section 4.1.1.1. The accumulation of free water content within different parts is shown in Figure 4.3 (b). The initial SPI integrations for both mortars are set to 100 %, and that for substrate is calculated at about 60%, which is corresponding to the water content proportional to that within repair mortar since placing.

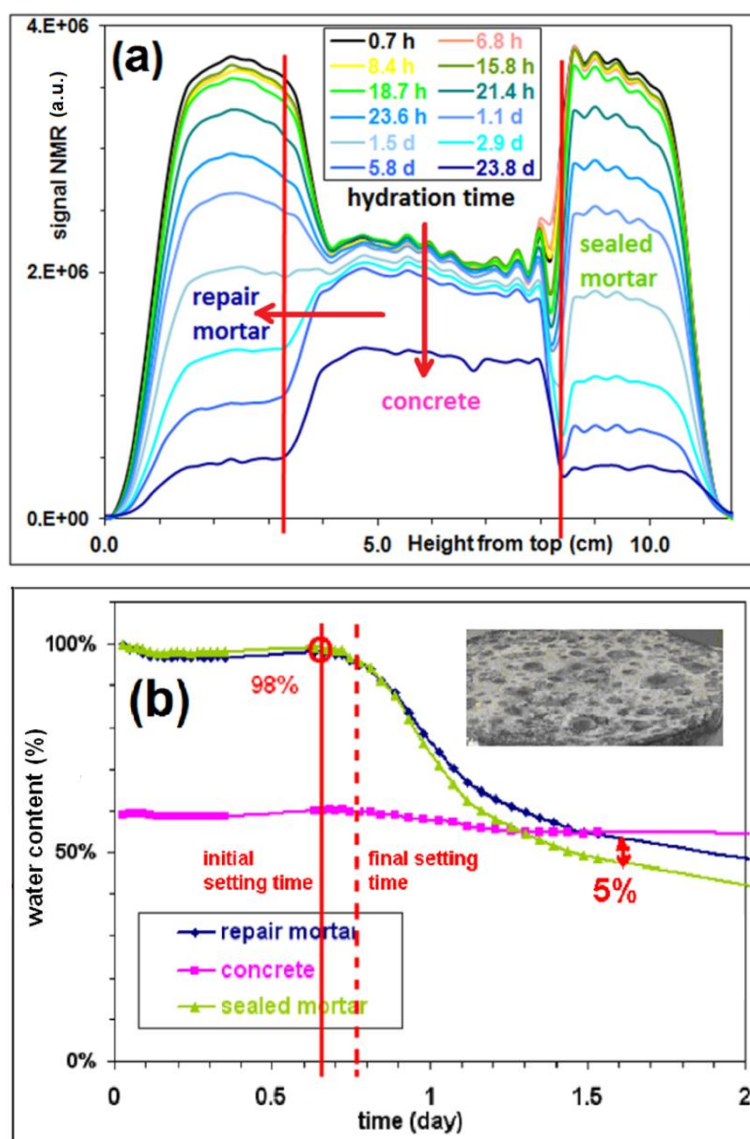


**Figure 4.3: Reference mortar on initially-saturated concrete: (a) SPI Profiles (b) Integration of accumulated intensities and bleeding at top surface of repair mortar.**

As shown in Figure 4.3 (a), the profiles of free water content within the repair mortar is similar to that observed within the sealed mortar. In Figure 4.3 (b), global water content

within different parts is accumulated and quantified. Before initial setting time, the evolution is similar in both repair and sealed mortars; but since final setting time at 18 hours, there exists more water within repair mortar; and this phenomenon is more evident since 3 days after casting. The concrete provides available water into the repair mortar due to a re-distribution of excess water within the whole system. This procedure introduces about 5% of excess water (by comparing to initial water content within repair mortar) after setting. This part of water deteriorates the microstructure and diffuses through the porosity of repair mortar onto the top surface. Macro pores are thus created after repair procedure as shown in the photo of Figure 4.3 (b).

By considering both systems as shown in section 4.1.1.1 and 4.1.1.2 (reference repair mortars on initially-dried or initially-saturated concretes), the optimization of substrate preparation is suggested to reach a suitable saturation rate after complete hydration procedure and before evident evaporation in long term (ca. 21 h and 5.5 d in this thesis with calculated rates between 64 % and 78 %). Thus moisture transfer, who deteriorates mortar hydration process, is hindered around setting and after hardening. Substrates need to be humidified homogeneously rather than surface wetting as described in conventional repair method based on empirism. By considering the surface preparation of substrates, especially by evaluating the optimum moisture condition, suitable RH level needs to be demonstrated by cohering saturation level within the sealed mortar and initially-saturated concrete in this thesis. These results also correspond to those obtained by Courard *et al.* [84] that saturation rates between 50 % and 90 % are required to achieve the optimal adhesion of mortars.

		/ ini. concrete	/ ini. mortar	/ ini. concrete	/ ini. mortar
<b>1. mor. ref + dried M25</b>	<b>time</b>	<b>21.1 h</b>		<b>5.3 d</b>	
	<b>SPI%</b>		<b>45.4%</b>		<b>33.5%</b>
<b>2. mor. ref + sat. M25</b>	<b>time</b>	<b>21.4 h</b>		<b>5.8 d</b>	
	<b>SPI%</b>	<b>100.2%</b>	<b>58.4%</b>	<b>89.6%</b>	<b>52.5%</b>
<b>1. /2. (%)</b>			<b>77.8%</b>		<b>63.9%</b>

**Table 4-2: Estimated saturation rate for optimized repair efficiency**

It is worth mentioning that, according to the verification after 1.5 months of hydration, there exists only 0.24% of mass lost within repair system (since 1976.99 g at placing until 1972.34 g at 44 days). Although it is well packed by a parafilm, the evaporation is not completely prevented. This difference is not evident by traditional techniques of characterization, but by

SPI profiles which focus on free water content, it is interesting to take place the analysis as shown in Table 4-3.

Hydration time (day)		0.0	2.9	5.8	23.8
SPI intensities	concrete	59.0%	53.8%	52.3%	36.1%
	sealed mor.	100.0%	30.6%	19.8%	11.6%
	repair mor.	100.0%	36.9%	25.5%	12.9%
	con. + rep. mor.	159.0%	90.7%	77.8%	49.0%
	con. loss	-	-	1.58%	16.16%
	con. + rep. mor. loss	-	-	12.93%	28.77%
Mass verification	evap. loss			2.08%	2.60%

**Table 4-3: Effect of drying during hydration process of repair system by integrated intensities of SPI profiles and mass verification**

The mass loss by evaporation (2.08% from 2.9 to 5.8 days, and 2.60% from 5.8 to 23.8 days) is far less than signal loss (while 12.93% and 28.77%) after hardening period, as the hydration procedure within repair mortar continues due to water transfer from concrete to repair mortar. It distinguishes the drying effect combined with hydration and moisture transfer, this sensitive technique provides more information rather than conventional techniques.

#### **4.1.1.3 Repair mortar with SAP on initially-dried M25**

The application of this polymer for construction proposes was initially purposed by Hansen and Jensen [24], referring to its water absorption properties of SAP within cement-based materials. The repair mortar of  $w/c = 0.3$ ,  $s/c = 2.0$  and additional  $SAP/c = 0.2\%$  in mass, is applied on an initially-dried M25. Normalized NMR signal (a.u.) in function of height from top surface (cm) of the repair system, and its evolution during hydration time is shown in Figure 4.4 (a). Global water content within different parts is presented in Figure 4.4 (b) by the integration of SPI profiles. The lost points (from 10 to 16 hours) were created due to a problem of air compress system of MRI apparatus during monitoring, but this vacancy does not affect the review of general evolution.

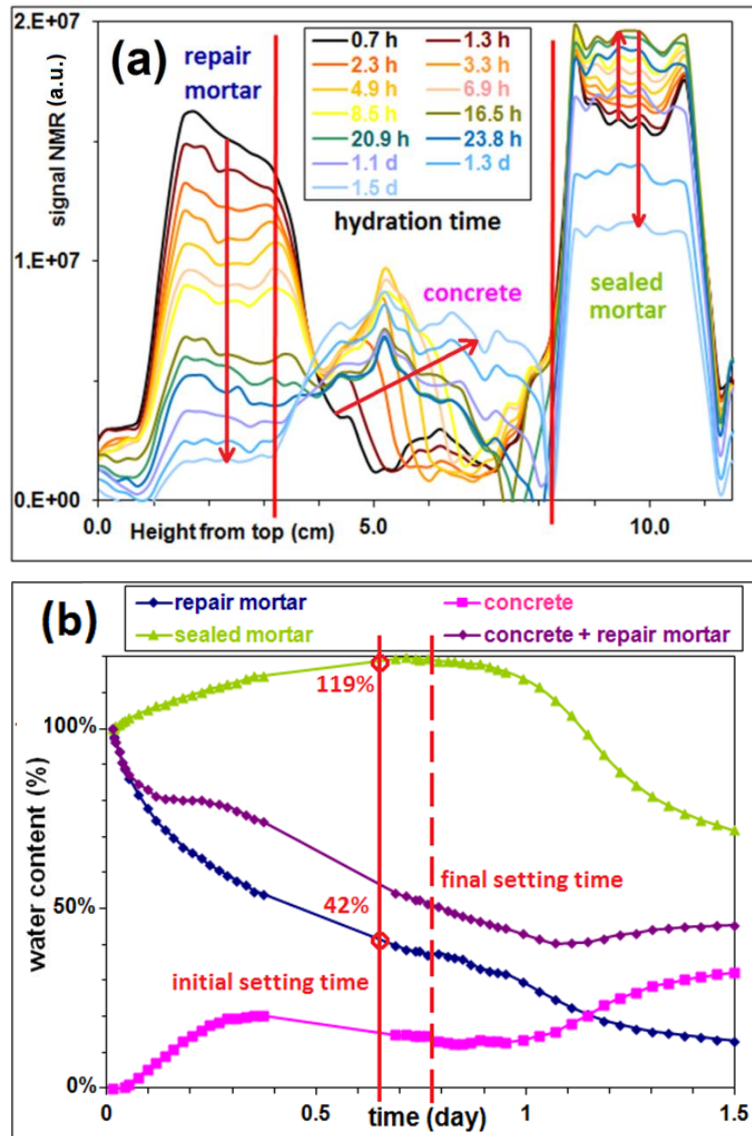


**Figure 4.4: Repair mortar containing SAP on initially-dried concrete (a) SPI Profiles (b) Integration of accumulated intensities.**

By considering the right part in Figure 4.4 (a) which corresponds to the sealed mortar, an increase in free water content during the first hours is emphasized. Concerning the water content at initial setting time, it exists 119% in sealed mortar by comparing to signal at placing. It can be illustrated by the evolution of pH value in pore solution within the cement matrix, which influences the absorption capacity of SAP gel. Pre-absorbed water (during the period before casting, when dry SAP powders were pre-mixed with liquid phase [85]) is released, when the pH value of pore solution within cement matrix increases during the first stages of hydration as reported by Friedemann *et al.* [23]. After final setting time at 18 hours, the signal intensity starts to decrease due to water depletion by hydration reactions. This

phenomenon in sealed SAP-modified mortar corresponds to the same X-ray tomographic results shown by Lura *et al.* [86], where exist also an increasing in signal intensities.

It can be illustrated that, water within SAP gel is partially detected by SPI since casting.

According to Equation 2.3,  $S = \rho \exp\left(-\frac{t_p}{T_2^*}\right) * \left[\frac{1 - \exp\left(-\frac{TR}{T_1}\right)}{1 - \cos\theta \exp\left(-\frac{TR}{T_1}\right)}\right] * \sin\theta$ , thus SPI signal is proportional to  $\frac{1 - \exp\left(-\frac{TR}{T_1}\right)}{1 - \cos\theta \exp\left(-\frac{TR}{T_1}\right)}$ . In this thesis, TR is set to 100 ms and  $\theta$  is  $\pi/8$  [33]., initial  $T_1$  is 17 ms and 2400 ms for detectable water within cement matrix (less flexible) and SAP gel (more flexible). Thus more than 99.9% of signal is obtained within cement matrix, and only 35.9% within SAP gel.

It is worth comparing the simultaneous moisture transfer in Figures 4.2 (a) and 4.4 (a). Due to water retention properties by SAP, this transfer is slightly less evident than that in reference repair mortar. It is also worth mentioning that the simultaneous moisture transfer towards concrete in Figure 4.4 (a), before initial setting time at 15 h, is similar as illustrated in Figures 4.1 (b) for the reference repair mortar. Due to water retention properties by SAP, this transfer is slightly less evident. Actually, free water content within concrete is stabilized since the end of induction period (6 - 7 h) until a few hours after final setting time at 18 hours according to Figure 4.4 (b). This phenomenon can be explained that initial effective w/c in mortar with SAP (0.25) is much lower than that in reference mortar (0.3). Thus the available free water for moisture transfer towards substrate is reduced, and a finer microstructure is obtained; while hydration reactions are active and cement grains chemically fix water with a rapid kinetic. After final setting time at 18 hours, SAP also plays an interesting role on water dispersion: free water content should be reduced due to the kinetics of water depletion within repair system isolated from environment; but SAP gel progressively and continuously releases pre-absorbed water (purple curve) into poorly-hydrated repair mortar and diffuses towards concrete. It provides an available water source into cement matrix during on-going hydration and is also available for anhydrates. If the quantity of SAP is increased within formula, this phenomenon will be more evident.

On the whole, this study reveals that SAP can be used to control the interactions between water depletion, setting process and moisture transfer within the repair system. This internal post-curing material has more advantages than external post-curing methods (such as: humidification by spraying water, protection by other curing compounds or various cover



materials, etc.) since SAP represents a homogeneous curing after setting, provides a continuous cement hydration, and reduces the effect of immediate moisture transfer from the fresh mortar to the old concrete. It reduces the initial w/c to obtain a finer microstructure, thus the self-desiccation, autogenous shrinkage and micro-crackings are prevented.

#### **4.1.1.4 Conclusion**

MRI allows an investigation of hydration process where exists moisture transfer within the aforementioned repair systems. This method can be applied in the investigation of other composite systems, where exist complex couplings of water depletion, moisture transfer and water diffusion, in an efficient and simple way. Moisture transfer at the interface between the repair mortar and the old concrete is delicately observed thanks to the integration of SPI profiles, which present the global amount of free water content in each part and at different heights with an accuracy of 2 mm (FoV = 26 cm with 128 points).

The water absorption properties of a commercial SAP within a repair mortar on an initially-dried concrete was investigated. The internal post-curing effect of SAP helps to balance moisture transfer and ions diffusion kinetics towards degraded concrete during and after a repair procedure. These phenomena were presented by comparing two repair mortars: one as reference without SAP, and the other one with SAP. This material can be applied in controlling immediate moisture transfer during first stages of hydration and providing continuous free water as a source after setting [75]. Furthermore, it assures a more homogeneous microstructure which will be verified in chapter 4.2.

#### **4.1.2 Application of characterized methodology on UHPFRC materials**

Most applications of high performance materials are assigned to prestressed concrete design and composite UHPFRC-concrete structures, in order to withstand high levels of tensile deformation combined with aggressive environment for extended service lifetime. For example: a beam or a slab for which deteriorated concrete is replaced by UHPFRC [87].

The investigation of moisture transfer properties is required in aforementioned systems for research purposes. The interactions between UHPFRC and concrete are expected to be significant and can modify the properties of the whole structure over hydration time. These mechanisms are still partially-known and difficult to be investigated by traditional methods.

As already proved in section 4.1.1, MRI techniques can be applied in composite systems, where exist moisture transfer interacting with hydration process, and present either water absorption or desorption properties within concrete bulks. This method of characterization is

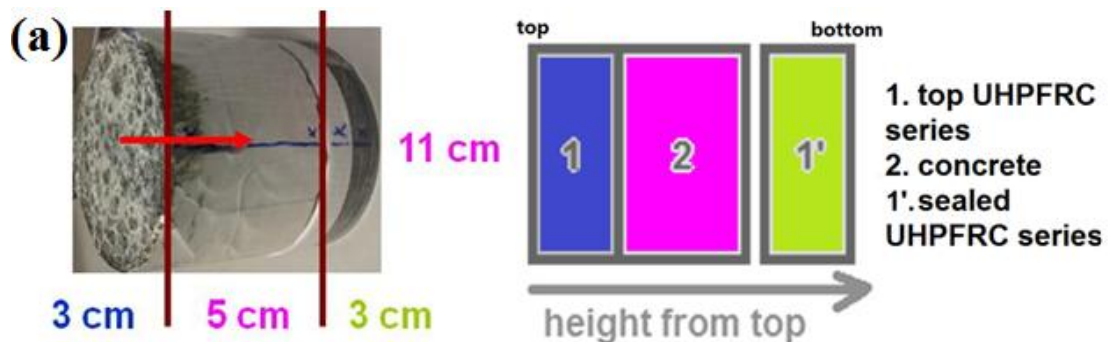
thus applicable to investigate “UHPFRC on M25” systems. These composite systems are frequently applied in construction field, as on bridge and road pavement surface [27]. For simplifying proposes, the same substrate is chosen to compare with the results of repair systems obtained in section 4.1.1.

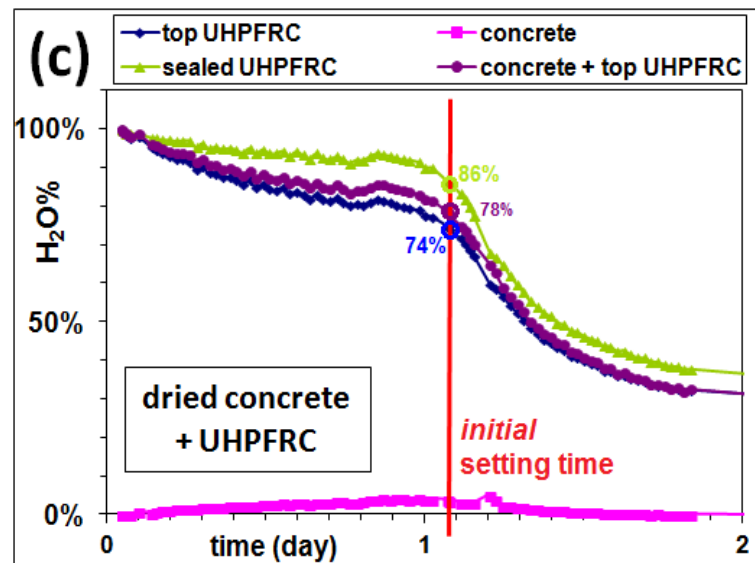
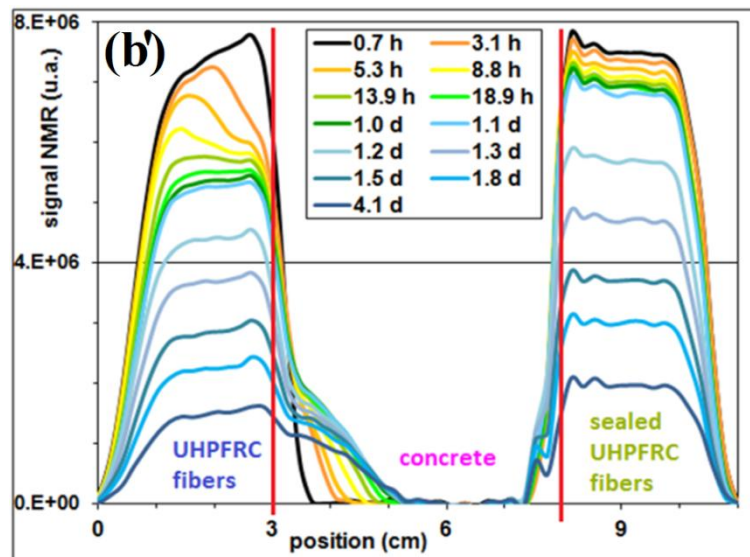
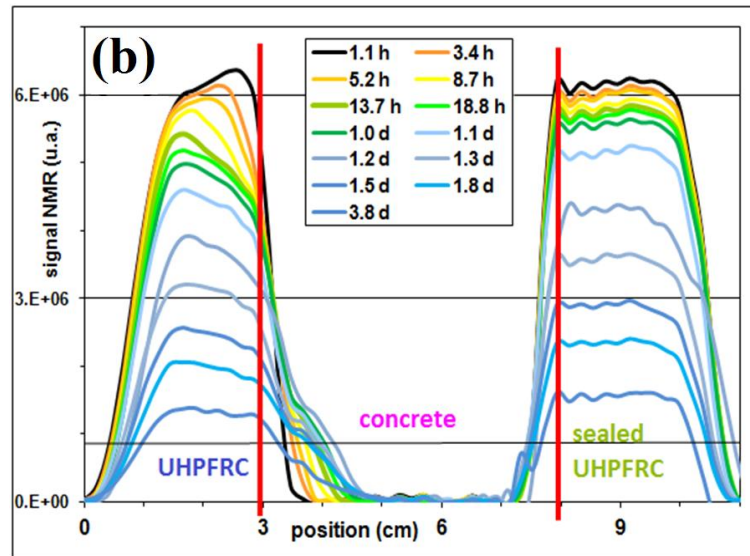
Two UHPFRC materials (UHPFRC matrix and with aramid fibers ( $\varnothing = 0.8$  mm,  $L = 20$  mm)) have been selected. The steel fibers commonly used in commercial formula, are replaced by aramid fibers, for the reason that metal parts are forbidden in MRI apparatus. By comparing to steel fibers, aramid fibers absorb extra water, but provide excellent mechanical performance and chemical resistance [22]. The application of aramid fibers with similar size as standard steel fibers, maintains similar microstructure and PSD within these UHPFRC materials [27].

In order to investigate aforementioned systems, TR is set to 40 ms according to specimens' nature ( $TR > 5T_1$ ). The initial  $T_1$  values are 5.9 ms for UHPFRC matrix and 5.2 ms for UHPFRC with fibers, measured at casting time according to feasibility test. SN is set to 32,  $t_p$  is set to 130  $\mu$ s, and Rg is set to 16, to obtain accurate SPI profiles and under suitable experimental duration. The time to perform one measurement is about 10 minutes.

#### **4.1.2.1 UHPFRC matrix and with fibers on initially-dried M25**

UHPFRC matrix and with fibers of w/c = 0.16 are applied on initially-dried M25. These configurations are shown in Figure 4.5 (a), identical as for investigated repair systems. NMR signal (a.u.) in function of height from top surface (cm) in composite system, and its evolution during hydration time is shown in Figures 4.5 (b) and (b'). Identical color is applied for the profiles corresponding to the same time for both UHPFRC materials. The normalization by setting equal value of the maximum signal intensities since casting is also performed. Accumulated intensities of SPI profiles within each part are respectively investigated in Figures 4.5 (c) and (c'). The microstructure of sealed UHPFRC materials at different positions after 3 days of hydration is investigated by MIP tests, as presented in Figure 4.5 (d).





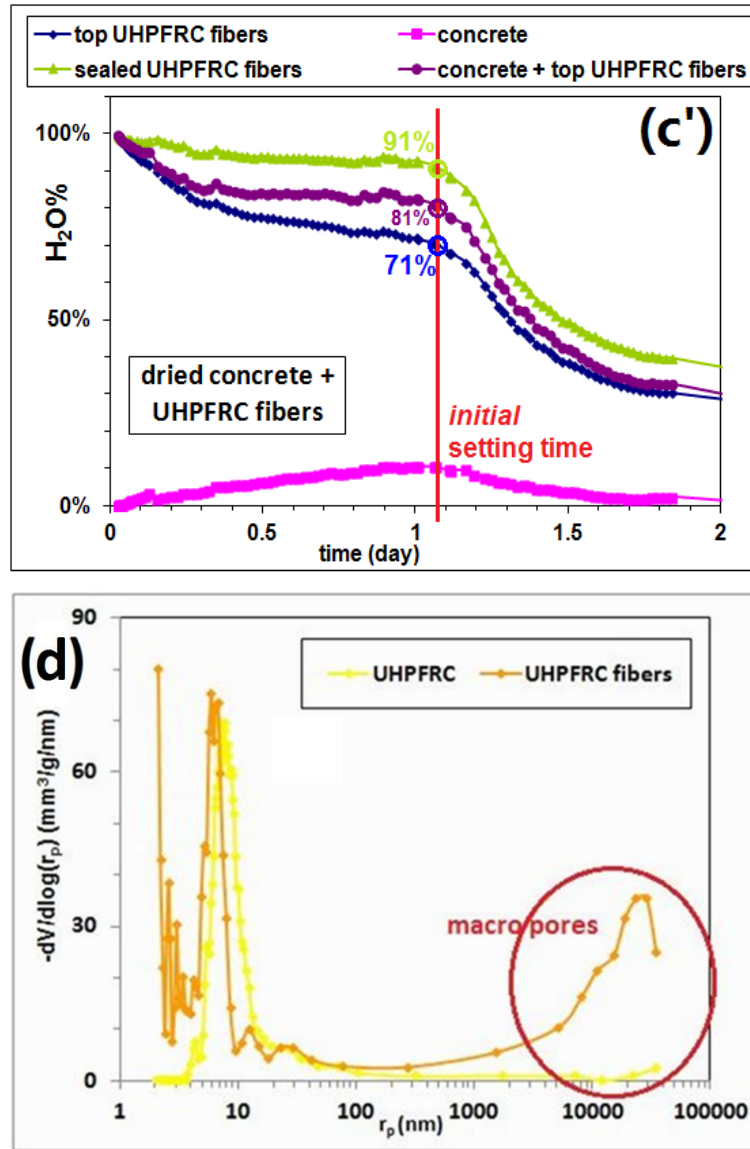


**Figure 4.5: UHPFRC matrix and with fibers on initially-dried concretes (a) Configuration of composite system; (b) (b') SPI Profiles; (c) (c') Integration of accumulated intensities; (d) PSD within UHPFRC materials by MIP after 3 days of hydration.**

By comparing these results for UHPFRC materials in Figures 4.5 to those of reference mortar on initially-dried concrete in Figures 4.2, immediate moisture transfer is hindered. There exists an evident water retention effect within top UHPFRC before initial setting time as shown in Figure 4.5 (b) and (b').

It is also interesting to observe that, UHPFRC materials trend to maintain excess water close to the interface between top UHPFRC and concrete as setting starts. Due to self-desiccation of UHPFRC, strong internal  $p_c$  dominates and slows down the moisture transfer towards substrate, and also leads to a finer microstructure. Some free water which was transferred to the substrate before setting, tends to find its way return to the interface after setting. This

phenomenon can be observed by comparing the moisture profiles at 1.1 d and 1.8 d, for the substrate between positions 3 cm (interface) and 4 cm (within concrete), and for the UHPFRC materials between positions 2 cm (within top UHPFRC) and 3 cm (interface) [84].

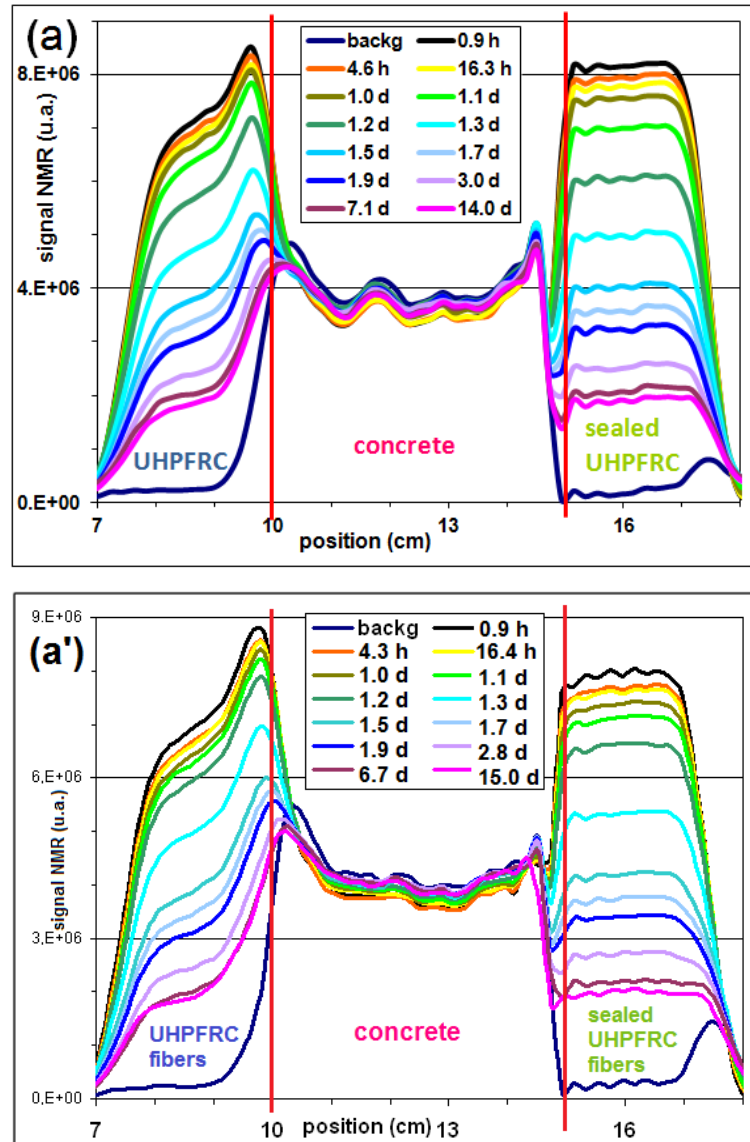
According to Figures 4.5 (c) and (c'), moisture transfer is quantified: at initial setting time of 26 hours for both materials, it remains 86 % to initial water content in sealed UHPFRC matrix vs. 74 % in top UHPFRC matrix, while 91 % in sealed UHPFRC with fibers vs. 71 % in top UHPFRC with fibers. During mixing process, dry aramid fibers absorb redundant water [88]. Within both UHPFRC materials, initial water content is set to both 100% since hydration begins. But in fact there exists less free water in UHPFRC with fibers than in UHPFRC matrix since casting, thus available water seems more important before setting within UHPFRC with fibers. At casting time, the water within aramid fibers is partially detected by SPI sequence. As described in section 4.1.1.3, SPI signal is proportional to  $\frac{1 - \exp\left(-\frac{TR}{T_1}\right)}{1 - \cos\theta \exp\left(-\frac{TR}{T_1}\right)}$  [33]. As in this thesis, TR is set to 40 ms and  $\theta$  is  $\pi/8$ , initial  $T_1$  is 5.2 ms for UHPFRC with fibers and 84 ms for saturated fibers. Thus almost 100% of signal is obtained for free water UHPFRC with fibers, and only 88.9% of signal is acquired for water within saturated fibers which is more flexible.

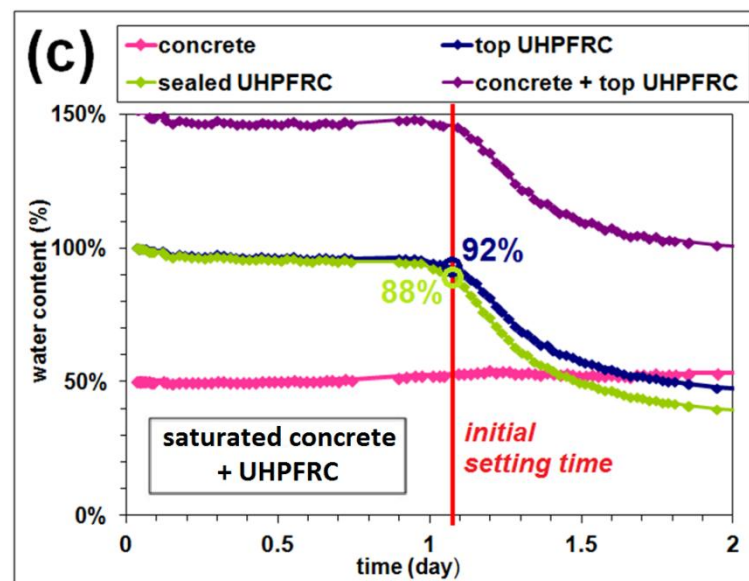
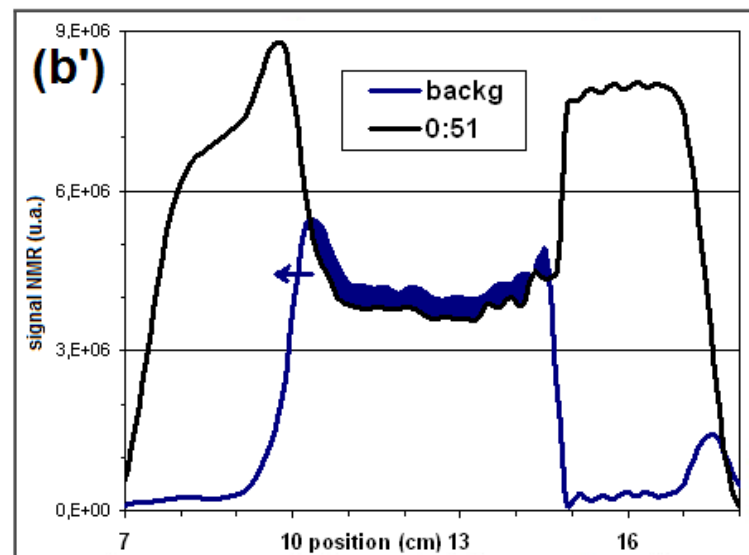
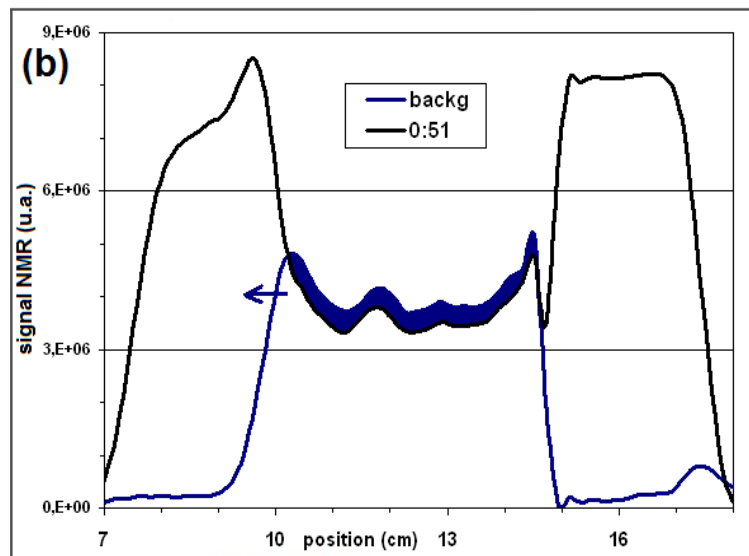
Although the content of absorbed water within aramid fibers is difficult to be quantified during different periods of hydration, due to complex couplings of chemical reactions and absorption properties within pore solution. It is still worth to mention that, the phenomenon of back-flow is more evident within UHPFRC with fibers (about 10% of water is transferred towards substrate at initial setting time, and this part of water comes back to UHPFRC after setting) than within UHPFRC matrix (while only 4% of water is transferred towards substrate around setting).

As shown in Figure 4.5 (d), both materials present a fine microstructure at 3 days of hydration (below 10 nm). UHPFRC matrix presents a homogenous microstructure and contains no macro pores. UHPFRC with fibers presents a heterogeneous microstructure, both macro and micro pores are more evident. The average size of macro pores created by aramid fibers is at the order of  $10^4$  to  $10^5$  nm [22], much rougher than the average size of micro-pores at the order of 1 to 10 nm. Due to created passage at the interface by fibers and micro-capillary effects, this observation of evident back-flow is explained [89].

#### 4.1.2.2 UHPFRC matrix and with fibers on initially-saturated M25

Normalized NMR signal (a.u.) in function of height from top surface (cm) of composite systems, and their evolutions during hydration time of UHPFRC materials are shown in Figure 4.6 (a). Immediate moisture transfer from saturated concrete to UHPFRC materials since placing is presented in Figure 4.6 (b). Accumulated local water contents (SPI profiles) within each part are respectively presented in Figures 4.6 (c) and (c').





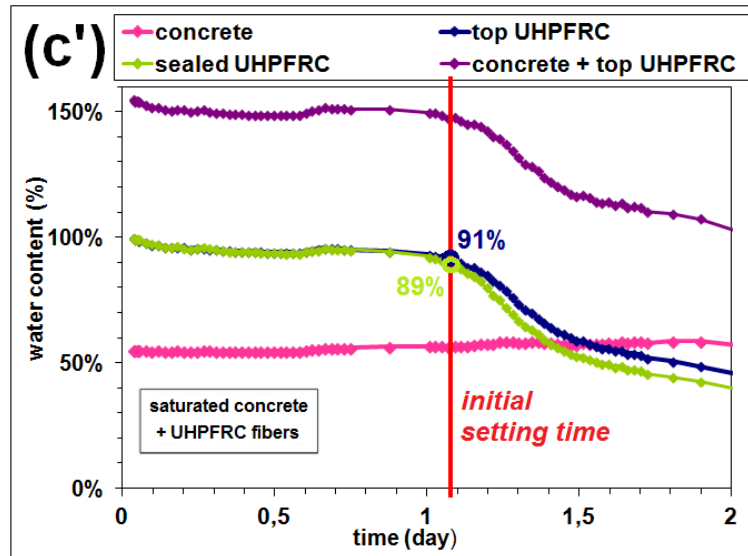


**Figure 4.6: UHPFRC materials on initially-saturated concretes: (a) (a') SPI profiles; (b) (b') Immediate moisture transfer after placing; (c) (c') Integration of accumulated intensities.**

By comparing the results in Figures 4.6 (a) and (a') to those in sections 4.1.2.1 and 4.1.1.2, although there exist excess water within composite system of UHPFRC materials and initially-saturated concrete, moisture transfer is evidently reduced.

It is worth mentioning that, the immediate moisture transfer after placing starts from saturated concrete to UHPFRC materials as shown in Figures 4.6 (b) and (b'). But this part of free water only stays within UHPFRC materials and close to the interface until setting. It can be explained due to self-desiccation of UHPFRC as aforementioned, strong internal  $p_c$  dominates and also slows down the moisture transfer from substrate [27].

Except for this part of free water close to the interface within fresh UHPFRC materials, bulk water is homogenous after setting according to Figures 4.6 (c) and (c'). A water retention phenomenon within top UHPFRC materials on initially-saturated concrete maintains identical water content within top UHPFRC materials as within sealed UHPFRC materials. The micro-capillary effect for prevention of moisture transfer where exists excess water is verified.

M25 with a w/c ratio of 0.84 is porous, and leads to coarser microstructure under laboratory conditions than other concrete structures under site conditions. This formula is neither commercial nor ideal, but it helps to emphasize the moisture transfer and to validate the methodology. For the purposes to combine moisture transfer and influence in microstructure during hydration, other composite systems of UHPFRC and concrete (rehabilitation of concrete structures in pavement, barrier wall, bridge pier, industrial floor, etc. [90]) can also



be investigated with the same methodology. Capillary effect and hydration process of UHPFRC can be thus verified in various cases.

Absorption measurements on conventional concrete generally show curves with two slopes. The absorption rate is high at first and then decreases. Absorption of water in conventional concrete generally shows a rapid kinetic at the beginning and a subsequent constant flow rate. For UHPFRC specimens, one can observe a linear curve of constant absorption from the beginning of the experiment: 22 minutes water absorption  $0.013 \text{ L/m}^2$ , 2.89 days water absorption  $0.18 \text{ L/m}^2$ . This difference is related to the limited amount of capillary pores in UHPFRC [91]. On the whole, the hydrostatic force has probably played a significant role in fluid transport mechanism in UHPFRC and may explain the greater absorption rate for a higher range of residual deformation. Moreover, the wider fracture process zone of the UHPFRC compared to concrete, which is favorable to absorption, may also explain the trend of the results. The interaction is favored by the presence of cracks and their opening. The mechanism of continued hydration in areas where the material is undamaged can also decrease water transport over time. UHPFRC has the characteristics for presenting significant self-healing capability since its matrix is very dense and a large amount of residual clinker is available to hydrate and seal cracks.

#### **4.1.2.3 Fresh UHPFRC matrix ( $w/c = 0.16$ ) on fresh concrete M25 ( $w/c = 0.84$ )**

In this section, the effect of “fresh on fresh” is investigated by casting UHPFRC matrix on freshly casted concrete, in order to observe the respective hydration within each part during first ages of hydration. This study is applied to monitor the actual case in road construction field. After the installation of road basement and the casting of conventional concrete, a thin pavement of UHPFRC is applied directly on the concrete. SPI profiles and immediate moisture transfer after placing are shown in Figures 4.7 (a) and (b).

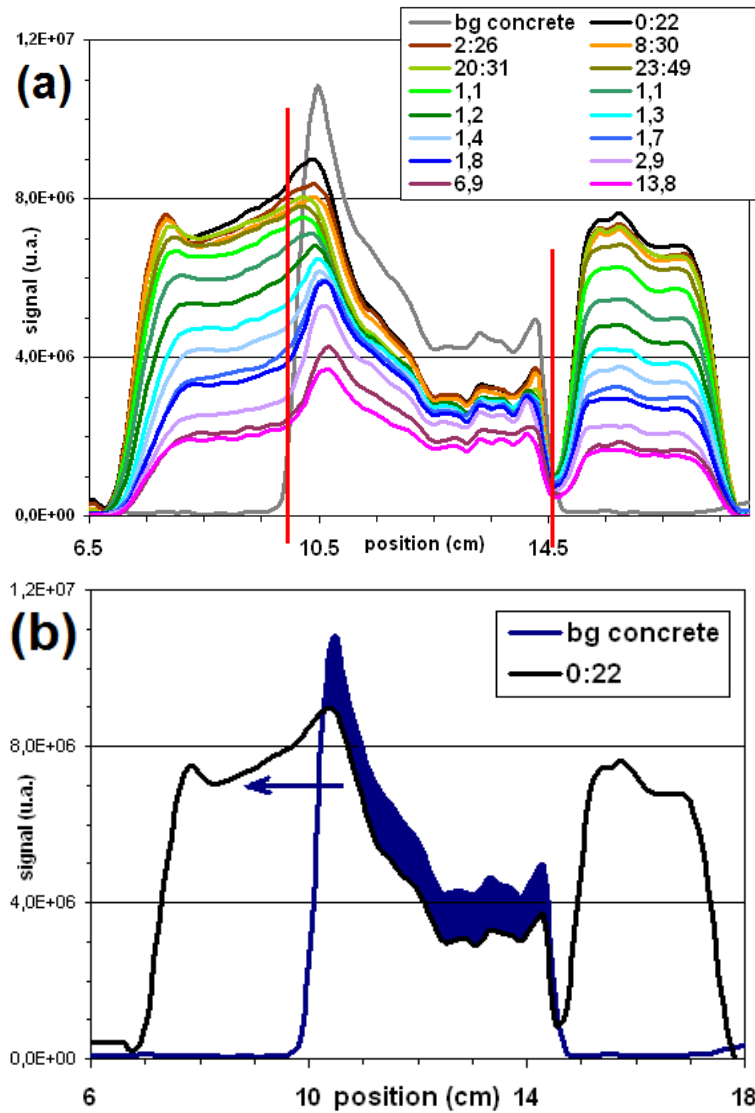


**Figure 4.7: Fresh UHPFRC without fibers on fresh concrete M25 (a) SPI profiles (b) Immediate moisture transfer after placing (bg concrete = background, initial profile of concrete)**

As shown in Figures 4.7 (a), it remains slightly more water content within top UHPFRC matrix, by comparing to sealed UHPFRC matrix. At the very beginning since casting, due to immediate moisture transfer from fresh substrate in Figure 4.7 (b), this surplus part of water stays within concrete and close to interface. This phenomenon of water retention is similar as observed in Figures 4.6, but extra water remains in concrete rather than UHPFRC. This part never comes into UHPFRC without fibers even after setting. Because the evident difference in w/c ratio (0.84 in concrete vs. 0.16 in UHPFRC without fibers), M25 always contains a very high water content, when isolated from atmosphere.

This phenomenon is possibly harmful to the formation of microstructure within concrete and the adhesion properties at interface during early age. Actually, during the procedure of road

and bridge pavement construction, conventional concrete with lower w/c is applied. And the whole composite system is exposed to environment, thus this part of water is avoided by evaporation. Even there exists excess of water in “fresh UHPFRC on fresh concrete” systems, especially at the interface. But moisture transfer are evidently reduced by comparing to “repair mortar on concrete” systems. Generally there exists no evident effect on hydration process of this composite system.

Aforementioned research results in section 4.1.2 are mainly investigated to reveal water retention properties and capillary effects of UHPFRC materials. These phenomena are observed for UHPFRC materials on initially-dried, initially-saturated and fresh concretes.

#### **4.1.3 Relations between SPI integration and FID - global free water content and chemical setting times**

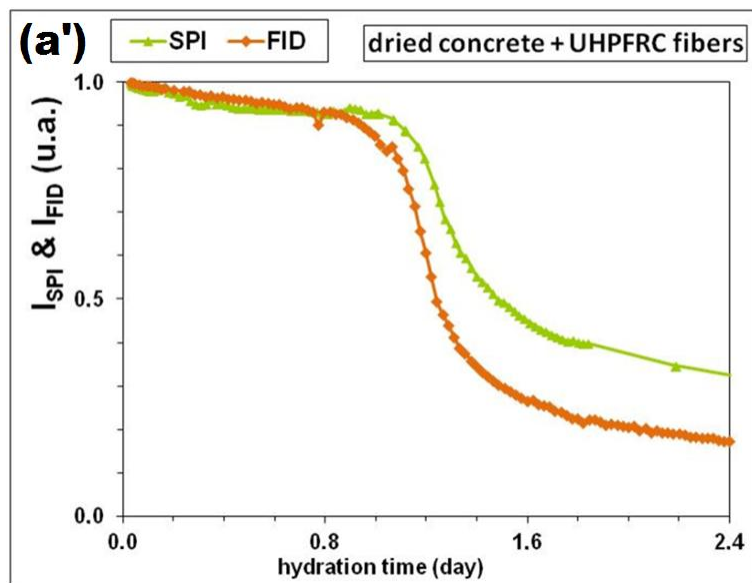
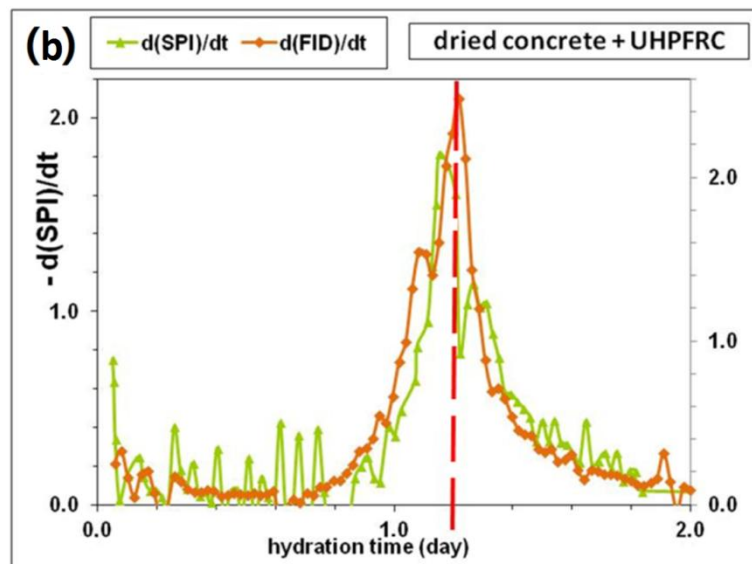
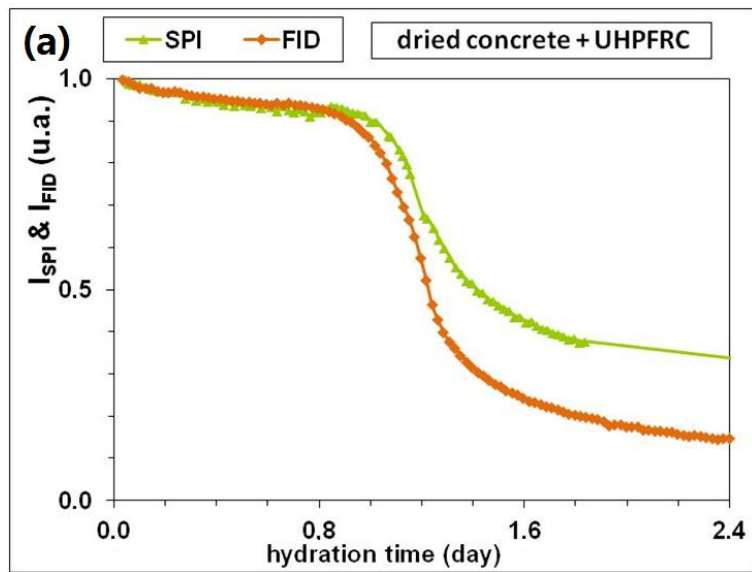
According to the principles of SPI as described in section 2.3.2.1, the profiles are corresponding to local free water content within repair system at a scale of 2 mm in height. Thus the integration of SPI profiles by averaging signal intensities accumulates the free water content within each part.

Considering the FID sequence as shown in section 2.3.1.1, the intensity is related to global free water content of the whole specimen. FID technique is not convenient for repair and composite systems, as they contain different parts of materials. Global signal of the whole system is impossible to distinguish the water content within each part.

The relations between SPI integration and FID intensity thus are important and interesting to be investigated, in order to compare these two characterization methods of free water content.

The accumulation of SPI profiles in sealed UHPFRC materials can be compared with the evolution of FID in only UHPFRC materials as shown in Figures 4.7 (a) and (a'). The time derivative of FID signal enables to determine the *chemical* setting time and can be compared to the derivative of SPI accumulation in Figures 4.7 (b) and (b').

This SPI accumulation corresponds to the integration of “up” part of sealed UHPFRC materials to avoid the effect of sedimentation, and there exist no evident difference if the integration is made from “whole”, “middle” or “down” parts of sealed UHPFRC materials.



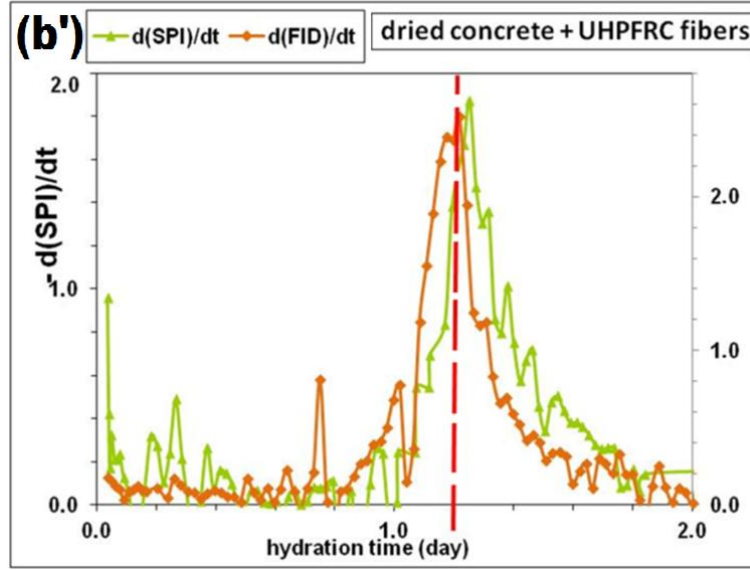


**Figure 4.8: For sealed UHPFRC without fibers: (a) Evolution of SPI accumulation & FID intensity; (b) Derivative of SPI accumulation & FID intensity corresponding to *chemical* setting. For sealed UHPFRC with fibers: (a') Evolution of SPI accumulation & FID intensity; (b') Derivative of SPI accumulation & FID intensity corresponding to *chemical* setting.**

By comparing Figure 4.7 (a) and (b), (a') and (b'), SPI accumulation and FID signal intensity are both corresponding to the global free water content. Except the difference as shown in Figures 4.7 (a) and (a'), it can be explained by different experimental principles and parameters of these two sequences. For SPI,  $t_p$  is set to 130  $\mu s$  for phase encoding; for FID,  $\pi/2$  pulse duration is set to 110  $\mu s$ , and then it recovers as damped sinusoid and is recorded during dead time of 40  $\mu s$ . Furthermore by considering data treatment process, first 6 points are eliminated from 1024 points (Reduced signal intensity was explained in section 3.2.1.4). Thus SPI integration contains more signal intensity than FID, but FID is more sensible than SPI as the acquisition time is much shorter.

The *chemical* setting time (corresponding to the portion of the peak of  $dI_{FID}/dt$ ) is related to the time corresponding to the maximum of  $d(SPI)/dt$  as shown in Figures 4.7 (b) and (b'). This phenomenon explains the intrinsic relations between these two analyses, which are both characteristic methods of *chemical* setting through the depletion of water within UHPFRC. It is worth mentioning that, the maximum of  $dI_{FID}/dt$  occurs a bit earlier because of the water absorption by aramid fibers since casting.

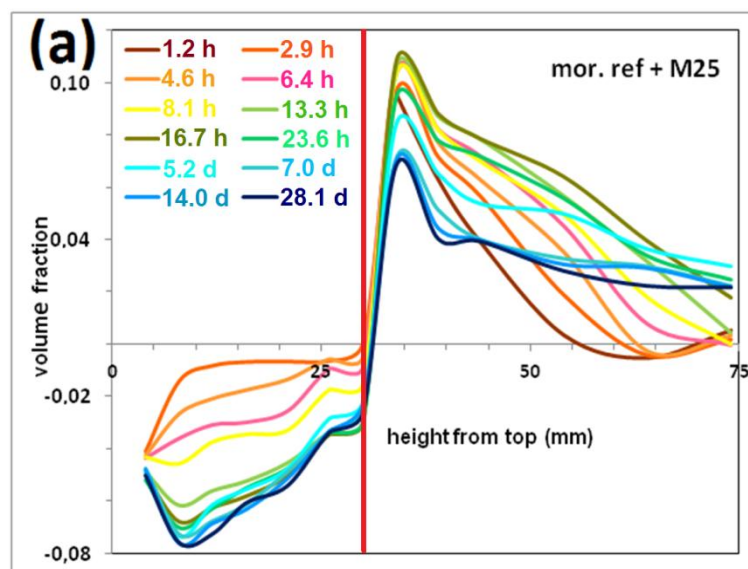
#### 4.1.4 Investigation of moisture transfer within old concrete by density profiles

As described in section 2.3.2.1, during repair procedure, moisture transfer can also be monitored by density profiles through GRA. It is comparable with moisture profiles through SPI, and corresponds to density gap but not an absolute value.

The same repair systems are prepared as investigated by SPI profiles through MRI, and coated with self-adhesive aluminum paper instead of thin polymer layer. The monitoring begins since placing specimens within GRA apparatus. Each measurement lasts 6 to 10 minutes at different layers; the global curve is not obtained at the same but similar hydration time. The average time during one cycle of measurements is applied to demonstrate results.

##### 4.1.4.1 Reference repair mortar on initially-dried M25

Reference repair mortar of  $w/c = 0.3$  and  $s/c = 2.0$  is applied on initially-dried M25. The density profiles during hydration in function of height from top surface (mm) of repair system are shown in Figures 4.9 (a) and (b). In both cases, the evolution within old concrete is compared to initial state before casting. However the evolution within repair mortar is compared to the first measurement at 1.2 hours in Figure 4.9 (a), and to stable state measured at 28.2 days of hydration in Figure 4.9 (b). After hardening since several days, global homogeneity is concerned. Density profiles are almost constant within repair mortar.



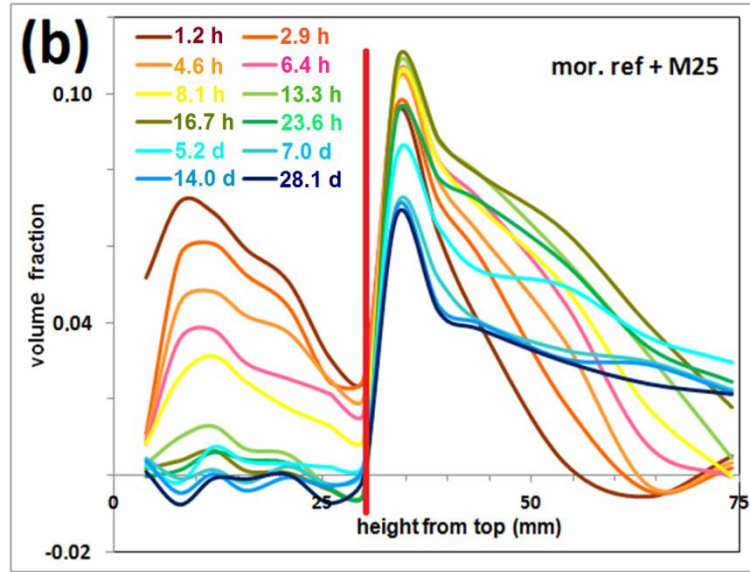


**Figure 4.9:** Density profiles (0 - 28 days) of “repair mortar ref. + initially-dried M25” by comparing to initial state before casting in M25, to (a) 1.2h after casting (b) 28 days in repair mortar.

Generally, density profiles are correlated principally to moisture profiles within different parts of the repair system. It reveals a general decreasing during setting process. But it is difficult to investigate the fresh repair mortar only by GRA results to distinguish the contributions by moisture transfer to substrate and by hydration reactions which form new hydrate compounds.

In conclusion, GRA technique can be applied to visualize moisture transfer within old concrete. Furthermore, it provides more information within the whole repair system by comparing to SPI profiles. These results will be detailed in following section.

#### **4.1.4.2 Comparison with SPI profiles**

Global water content within different parts is respectively presented in Figure 4.10 (a) for profiles within concrete, and in Figure 4.10 (b) for those within repair mortar. Identical color is applied for SPI profiles and density profiles by GRA corresponding to the same hydration time. The height from top is normalized in the same figure for different profiles; signal intensity and volume fraction are adjusted to correlate results.



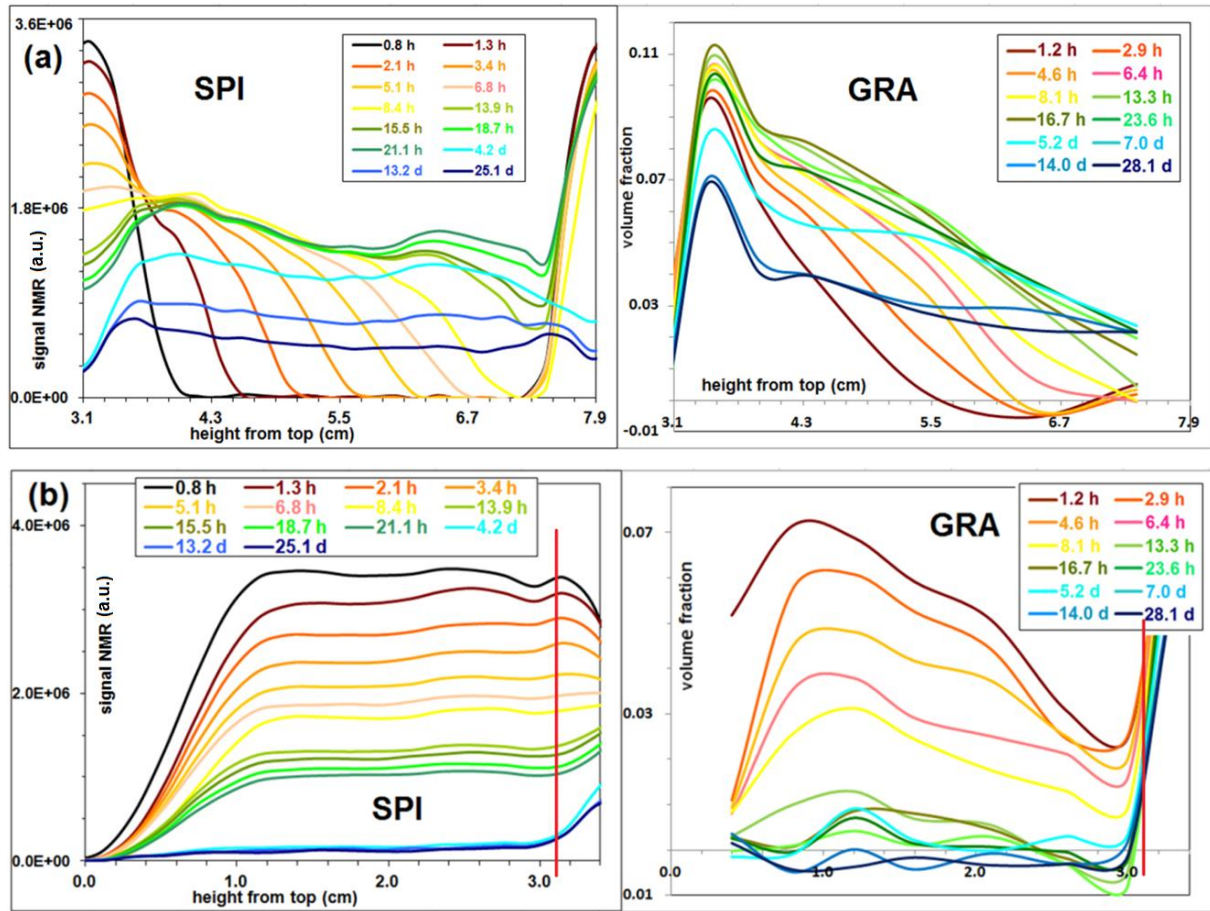


**Figure 4.10: SPI profiles by MRI and density profiles by GRA (0 - 28 days) of “repair mortar ref. + initially-dried M25”: (a) within concrete both by comparing to initial state (b) within repair mortar by comparing to initial state by SPI and to stable state by GRA.**

By comparing the profiles obtained by SPI and GRA, general evolutions are similar and homogenous diffusion of water content is observed in both cases, especially within concrete bulk. Before setting, immediate moisture transfer towards concrete is evident; during and after setting, this part of water cannot come back to mortar because of capillary effects. This phenomenon is opposite to the case of reference repair mortar on initially-saturated concrete.

It is interesting to mention that, phenomena at the interface are different for the profiles obtained by both techniques. By considering the profiles at the same time, for example, brown curves at 1.3 h for SPI and 1.2 h for GRA, the investigations are presented as follows:

- For concrete as shown in Figure 4.10 (a), moisture transfer diffuse much deeper according to density profiles. It can be explained by the effect of time deviation during one GRA measurement. For example, 1.2 h is both the average time for a cycle of measurements, and exact moment for the measurement at 30 mm from the top (according to preset parameters,



this height corresponds to the halfway measure, 7<sup>th</sup> of 13 measurements at different heights). Each measurement lasts about 8 minutes. Thus at 54 mm of height from top surface, it corresponds to the result at 1.7 h. It is also interesting to mention that, by comparing the curves from 3.1 cm (interface) to 4 cm (concrete) since casting until setting, moisture profiles decrease faster than density profiles. It can be explained by re-hydration of non-hydrated compounds (re-alkalization) within old concrete which increases the density after setting [6]. Homogenous diffusion of water content is observed in both profiles. This evolution remains similar after time normalization excluding the effect of time deviation. It is also important to investigate repair efficiency, moderate moisture transfer thus contributes.

- For mortar as shown in Figure 4.10 (b), due to the same reason of time deviation during one GRA measurement, the water content close to interface is much lower. After setting, the moisture transfer is almost finished, thus the density profiles are globally constant.

In conclusion, moisture profiles by SPI and density profiles by GRA are comparable. Both techniques are consistent and informative to investigate repair procedure. Re-hydration within concrete occurs close to interface, this phenomenon is positive in repair efficiency, due to moisture and ions transfer.

## **4.2 After 90-day repair procedure**

### **4.2.1 Total porosity determined by GRA**

As described in section 2.3.2.2, by comparing different repair systems at dried and saturated states, the total porosity can be obtained by GRA. This method permits a non-destructive characterization of water content in capillary and macro-pores.

In this section, total porosities in function of height from top surface (mm) within repair and sealed mortars are presented for three systems, which were investigated by both MRI and GRA techniques since early ages:

1. Reference repair mortar on initially-dried concrete
2. Reference repair mortar on initially-saturated concrete
3. Repair mortar with SAP on initially-dried concrete

These results are shown respectively in Figures 4.11 (a), (b) and (c). Concerning the height at about 30 mm, it corresponds to the interface between the repair mortar and the concrete within repair system, or the bottom side of sealed mortar. These results were obtained by different states of materials dried at 45 °C and of materials saturated in distilled water. And

due to segregation effect, the porosities at the bottom side are generally much finer than those at top side within mortars.

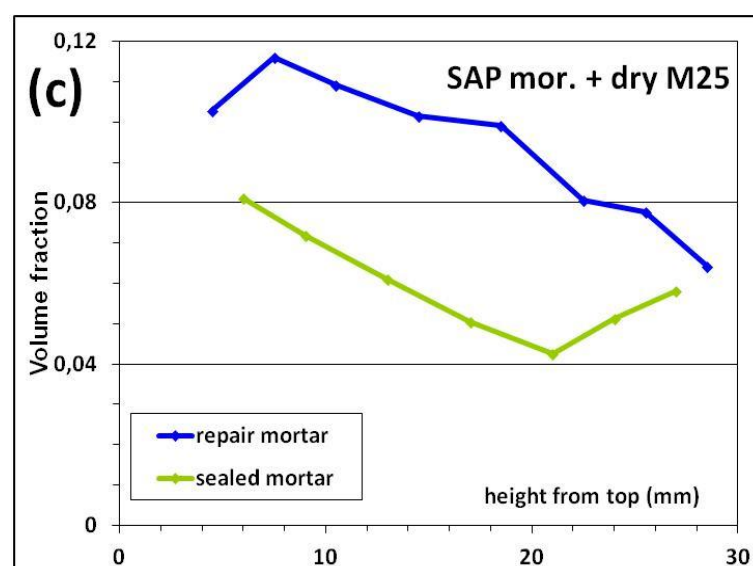
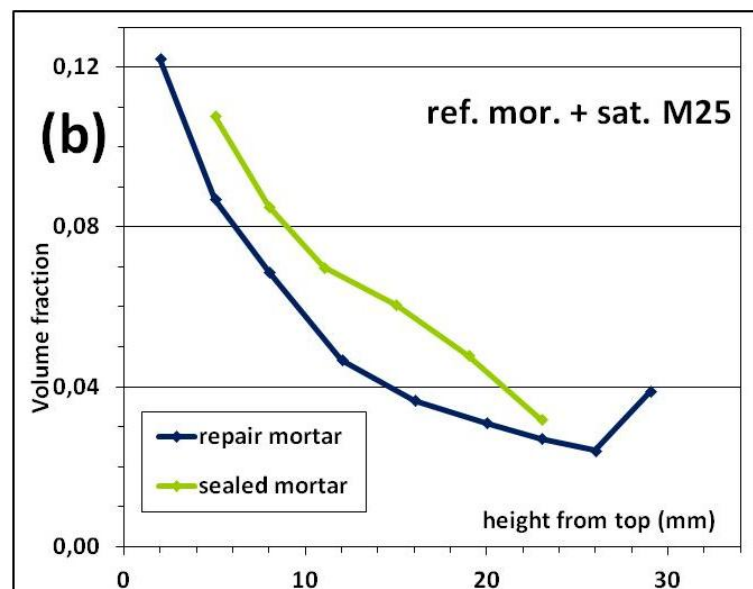
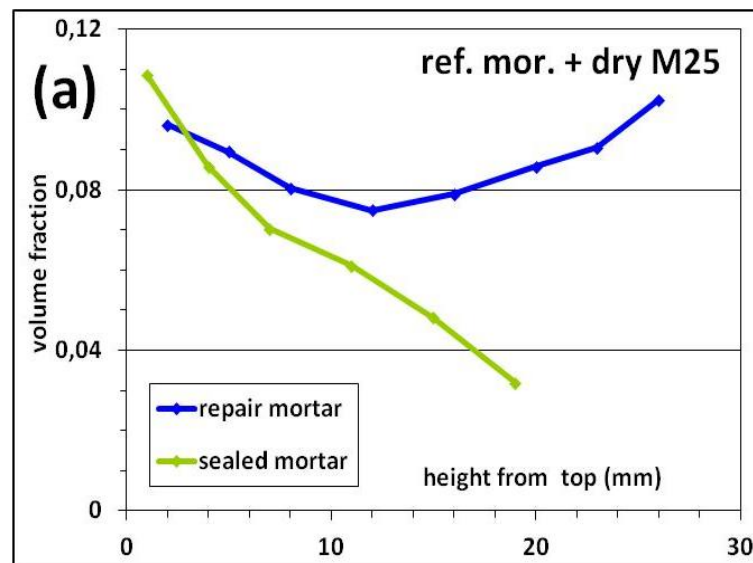


**Figure 4.11: Total porosity determined by GRA in repair mortar and sealed mortar for: reference mortar on (a) initially-dried M25; (b) initially-saturated M25; (c) SAP mortar on initially-dried M25**

In Figure 4.11 (a), the total porosity within the repair mortar is more important than that within sealed mortar. Evident moisture transfer hinders hydration process of repair mortar. There exist non-hydrated cement grains and macro-pores within cement matrix are not fulfilled during hydration. This phenomenon is intensified at the interface where the porosity weakens the mechanical compatibility between mortar and concrete.

In Figure 4.11 (b), the total porosities in both mortars are similar, while it is a bit promoted at the repair mortar - concrete interface. It proves that excess water within repair mortar did not evidently influence total porosity and microstructure. According to on-site condition of repair works, the humidification of degraded concrete is necessary before repair procedure. As described in section 4.1.1.2, macro pores are observed close to top surface of the repair mortar. It is thus required to apply a convenient saturation level to improve repair efficiency.

In Figure 4.11 (c), total porosity is more important within repair mortar with SAP than within sealed one. Thanks to released water by SAP gel since casting until setting, close to interface within repair mortar, total porosity is similar as within sealed mortar. It is possible to predict that, if more SAP is added in mortar formula, water retention capacity will be more evident. Furthermore, by comparing Figures 4.11 (a) and (c), mortar containing SAP presents a generally higher porosity than reference mortar. It can be explained that, during drying at 45 °C, SAP desorbs certain water as temperature increases [92], and re-absorbs water during saturation procedure. Thus the calculated porosity is more important than the actual porosity. But this phenomenon is not quantitative because of the limitations in experimental condition as shown in section 2.3.2.2.

It is worth mentioning that, this drying procedure at 45 °C of free water evaporation is neither complete as conventional condition at 105 °C (destructive), nor the saturation with distilled water in vacuum. Obtained results are much lower than reality but still approaching, it is not accurate to determine absolute total porosity but still informative to observe the difference within each part between repair and sealed mortars.

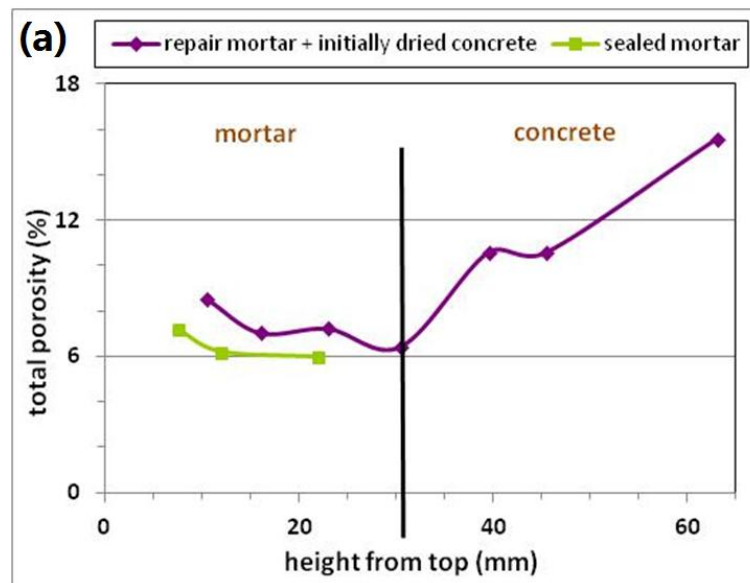
And these results will be compared to total porosity obtained by MIP in section 4.2.2. The advantages of GRA techniques in detecting porosity are non-destructive, easy to be operated,

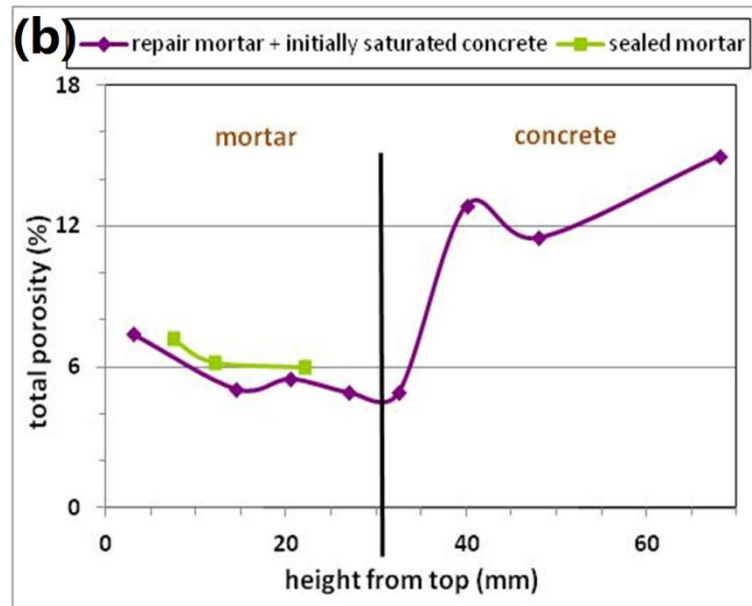
with more precision in sampling (3 - 10 mm according to different positions within repair system, while MIP needs to saw specimens and it is hard to control the exact height of each layer, the results are also affected by local sampling), global measurement to avoid the effects of aggregates (while MIP results are affected by samples from different positions). In general, GRA is more convenient, but the preparation needs to be improved; MIP is more informative, but the cutting needs to be well controlled, and it is suggested to progress parallel testing.

#### 4.2.2 Total porosity and porous distribution determined by MIP

As explained in section 2.3.2.2, after the repair procedure, specimens (mass = 1 to 2 grams according to porosity) were taken from different layers of the repair system and pre-dried by cryo-sublimation. They are then tested by MIP to review the accumulate porosity and PSD. To avoid the heterogeneity and boundary effect of the repair system, the samples were taken from the middle and within cement matrix by removing aggregates phase.

Results for reference repair mortar on initially-dried and initially-saturated concretes are respectively shown in Figures 4.12 (a) and (b).

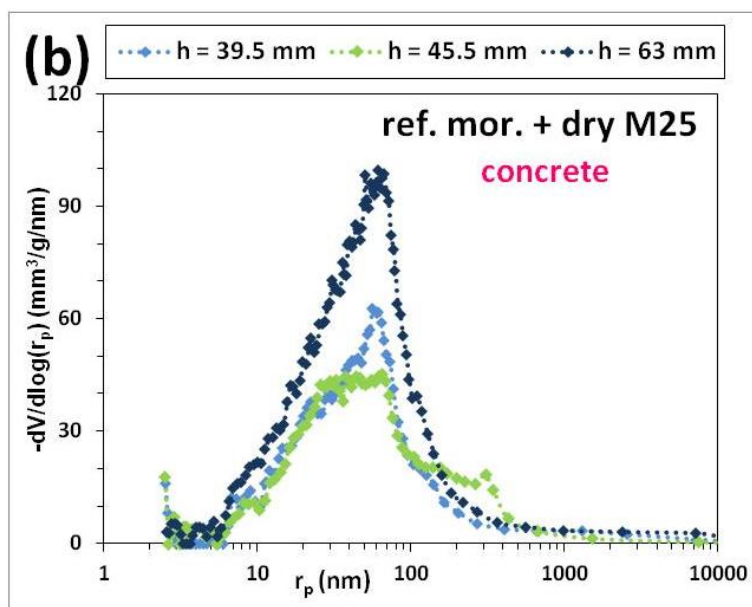
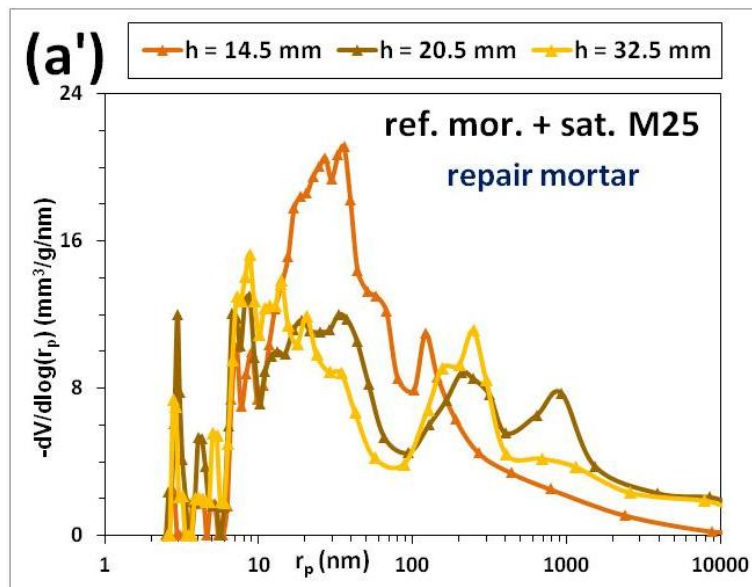
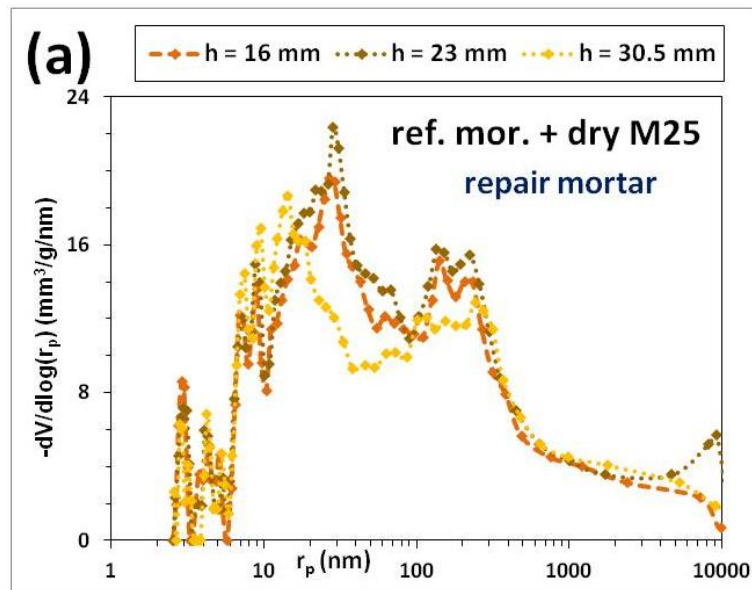




**Figure 4.12: Total porosity by MIP for: sealed mortars + reference repair mortars on (a) initially-dried M25, (b) initially-saturated M25.**

Similar as detected by GRA, there exists more important porosity within repair mortar than within sealed mortar as shown in Figures 4.11 (a) and 4.12 (a), while it is less important in Figures 4.11 (b) and 4.12 (b). As excess water from substrate into mortar provides sufficient water for hydration, except macro-pores on the top surface, an almost-complete hydration process is obtained within the mortar bulk.

The difference of total porosity within concrete is hard to be explained, i.e., if it is caused by heterogeneity effect or phenomenon of re-hydration. Thus it is also important to investigate PSD at different heights of the repair system, as shown in Figures 4.13 (a), (a'), (b), (b') and (c), in order to investigate at different positions within the same system, or the same material part in different systems. The height hereby is related to the distance from the top surface. The value is higher, when it is closer to bottom side within concretes or related to the interface within repair mortars.



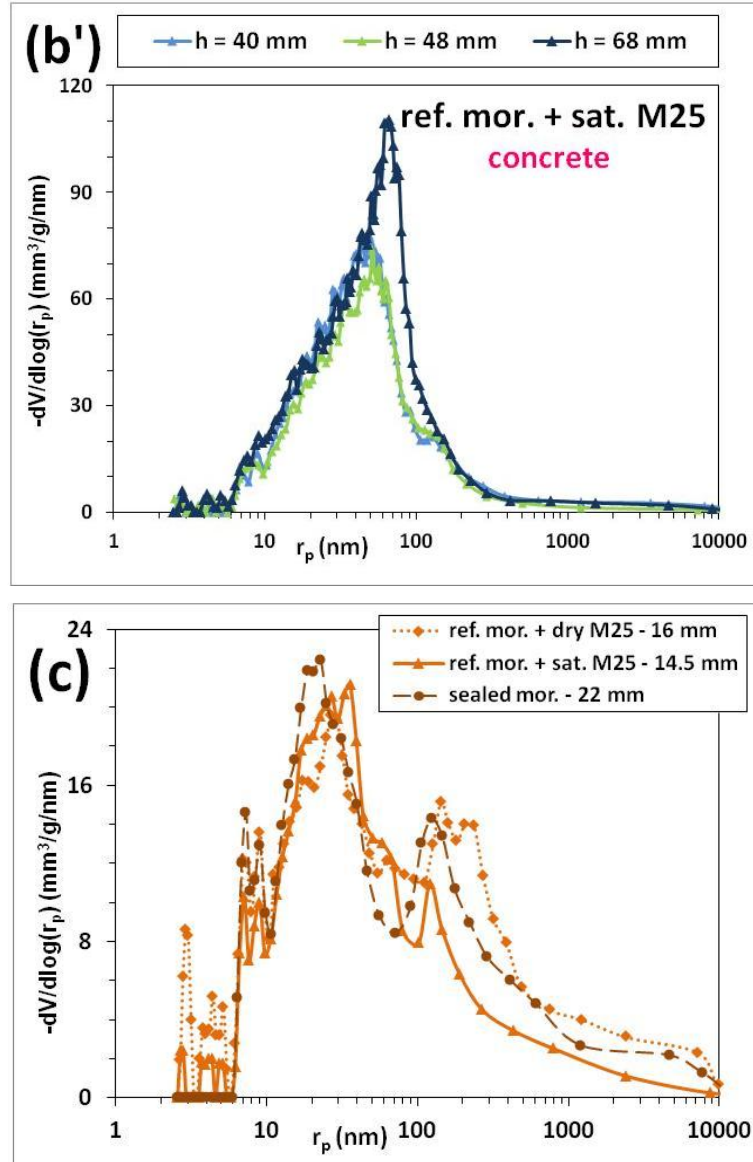


**Figure 4.13:** Porous distribution for: (a) repair mortar, (b) M25, in “ref. mor. + ini. dried M25”; (a’) repair mortar, (b’) M25, in “ref. mor. + ini. sat. M25”; (c) repair and sealed mortars in both systems

Concerning Figure 4.13 (a), it is evident that repair mortar on initially-dried concrete is more porous close to interface ( $h = 23$  mm) than to bulk ( $h = 16$  mm) within mortar, due to moisture transfer towards concrete. While as shown in Figure 4.12 (a’) for repair mortar on initially-saturated concrete, the porosity close to interface within repair mortar ( $h = 20.5$  mm) is improved, less porous than to bulk ( $h = 14.5$  mm) within mortar.

In Figures 4.13 (b) and (b’), both concretes are much finer close to interface ( $h = 39.5$  and  $40$  mm). And this phenomenon is more evident within initially-dried substrate. Thus the explication is related to the re-hydration of substrate during saturation process.

By comparing repair mortars to sealed mortar as shown in Figure 4.13 (c), the differences are not evident. But the effect of a coarser microstructure (pore size  $> 100$  nm) due to moisture transfer is observed by comparing the repair mortar in “ref. mor. + dry M25” system and the sealed mortar. These three curves are obtained in the middle of mortars in order to avoid sedimentation effect.

But due to limited cutting conditions, the heights of specimens are not exactly the same. This problem makes the analysis more difficult to distinguish the differences between different systems. As described in section 4.2.1, MIP is a destructive technique with complex procedure of specimen preparation by comparing to GRA but still informative. According to aforementioned results, it is thus suggested to use both techniques for characterization, in order to obtain an overall investigation.

### **4.2.3 Repair efficiency and preview of durability**

#### **4.2.3.1 Profiles of water immersion by GRA (wetting properties)**

As described in section 1.3.1, many degradation mechanisms are related to humid environment. The penetration of aggressive agents such as carbonate, chloride, sulfate, and other ions, etc., is promoted in high RH or solution. Thus the wetting properties (water immersion profiles) are important to be firstly understood before the investigation of other durability indicators.

Experimental procedure was detailed in section 2.3.2.3, distilled water was added onto the top surface of a pre-dried repair system. By GRA, the density profiles are obtained at different durations in contact with water. Three systems are thus investigated after the repair procedure: reference repair mortar and with SAP on initially-dried concretes, reference repair mortar on initially-saturated concrete.

#### ***Reference repair mortar and with SAP on initially-dried M25***

Different curves of immersion are presented in Figure 4.14 (a) for reference repair mortar and in Figure 4.14 (b) for mortar with SAP both on initially-dried substrates M25. The volume fraction in function to height from top surface is shown according to immersion time since 1 hour until about 4 to 5 days.



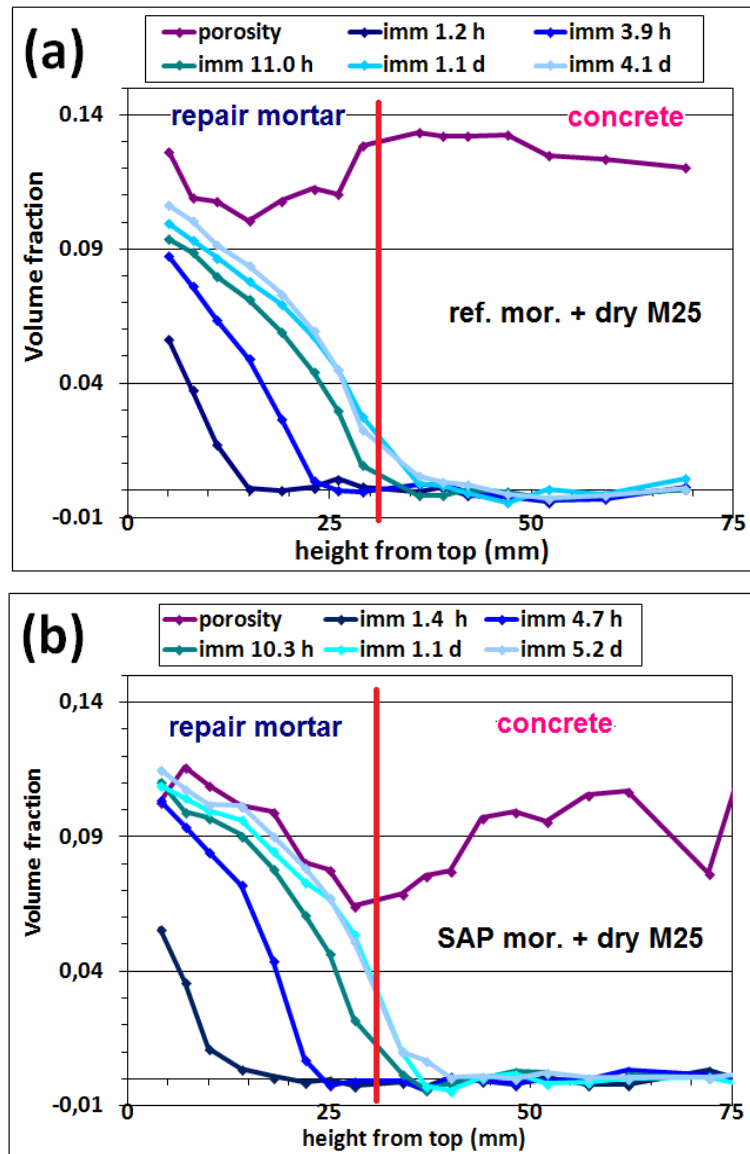


**Figure 4.14: Water immersion properties and total porosity after repair procedure for: reference mortar on (a) initially-dried M25 at 100 days (since casting) (b) initially-saturated M25 at 70 days.**

For a M25 of 5 cm in height, after 4 days of immersion with distilled water, moisture content will penetrate the whole specimen and reach bottom side. This phenomenon was observed by Wang [23] in his thesis. But for both cases in this thesis, moisture transfer hinders at the mortar - concrete interface. It is difficult to continue penetrating into the old concrete and water profiles are prevented.

And by comparing to total porosity (related to same investigation as shown in section 4.2.1 by comparing GRA profiles between systems dried at 45 °C and saturated in vacuum), it is far than enough to reach a full saturation by immersion. The prevention for penetration of aggressive agents in liquid phase is thus predicted in this repair system.

By comparing Figures 4.14 (a) and (b), the moisture profiles for mortar containing SAP are almost the same as those for reference mortar, and the porosities at 0 - 20 mm from top surface are also similar. But there exists a lower porosity at the SAP mortar - concrete interface. As described in section 4.2.1, this phenomenon can be explained as the improvement of microstructure by the SAP gel performing as water resource after setting, unhydrated cement starts to hydrate and ions transfers towards concrete leads to a re-hydration. Repair efficiency and mortar hydration are both assured.

#### ***Reference repair mortar on initially-saturated M25***

Different curves of immersion are presented in Figure 4.15 for reference repair mortar on initially-saturated concrete. The volume fraction in function to height from top surface is shown according to immersion time since 1 hour until about 3 days.

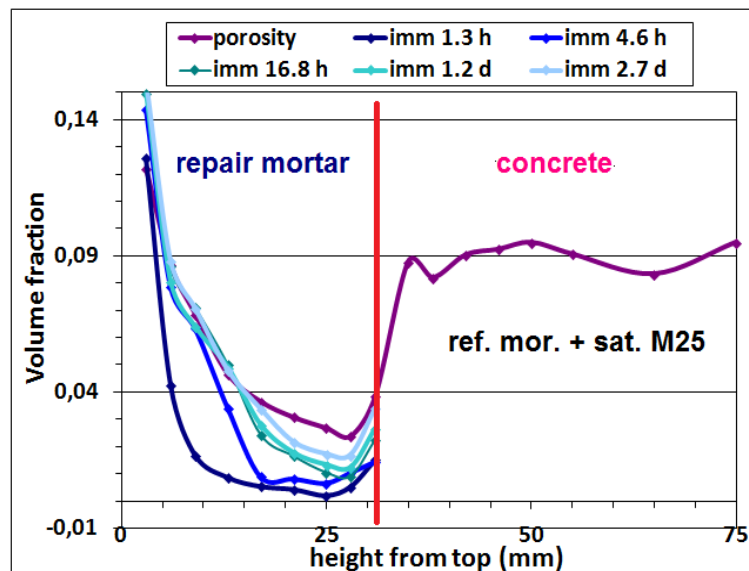


**Figure 4.15: Water immersion properties and total porosity after repair procedure for reference repair mortar on initially-saturated M25 at 70 days since casting**

In this case, the junction between mortar and concrete was not applied with water-proof silicone. There exists moisture side-flow into concrete bulk, through small interval and crackings at the interface. Thus immersion profiles are removed within concrete part, but it is still interesting to view evolution within the repair mortar and total porosity of repair system.

This repair mortar (with lower porosity than mortars in Figures 4.14) contains sufficient water for hydration reactions, as the initially-saturated concrete provided excess free water. But the

porosity at top surface is extremely high due to created macro-pores by water bubbles. This result is related to SPI profiles and observations in Figures 4.2.

In conclusion, reference repair mortar and with SAP on initially-dried concretes, reference repair mortar on initially-saturated concrete, all systems present the prevention of moisture transfer into concrete. The microstructure is improved at the interface as porosity decrease. The liquid phase 1D diffusion is supposed to be hindered, thus the penetration of aggressive agents, such as chloride ions in solution are limited within repair systems. Porosity is generally decreased at the interface.

#### **4.2.3.2 Carbonation profiles and penetration depth**

As detailed in section 2.3.2.3, to compare their resistances to carbonation penetration, different systems such as reference mortar on M25, SAP-modified mortar on M25, and only M25 are prepared. Before repair procedure, substrates are initially-dried at 105 °C for all these systems. Reference repair mortar and with SAP were respectively applied on M25 during 1 month in sealed condition from environment (repair procedure), and then dried at 45 °C for another 1 month (non-destructive drying). Only M25 substrates were also prepared with the same method. Before carbonation procedure, all these specimens were pre-dried at 105 °C during 48 hours and coated. They were then conserved in carbonation container of 10% CO<sub>2</sub> under RH = 53 % and temperature = 20 °C for optimal accelerated carbonation. Each specimen is monitored respectively at 0 (reference without carbonation) and several days after carbonation by GRA to obtain carbonation profiles in function of duration (non-destructive and continuous tests). Phenolphthalein indicator is applied on each specimen after final carbonation procedure to determine penetration depth (destructive).

These specimens were named as (a) M25+ref, (b) M25+SAP, (c) M25. At 3, 28 and 43 days since initial carbonation time, penetration states are measured. These results are shown respectively in Figures 4.16 (a), (b) and (c).

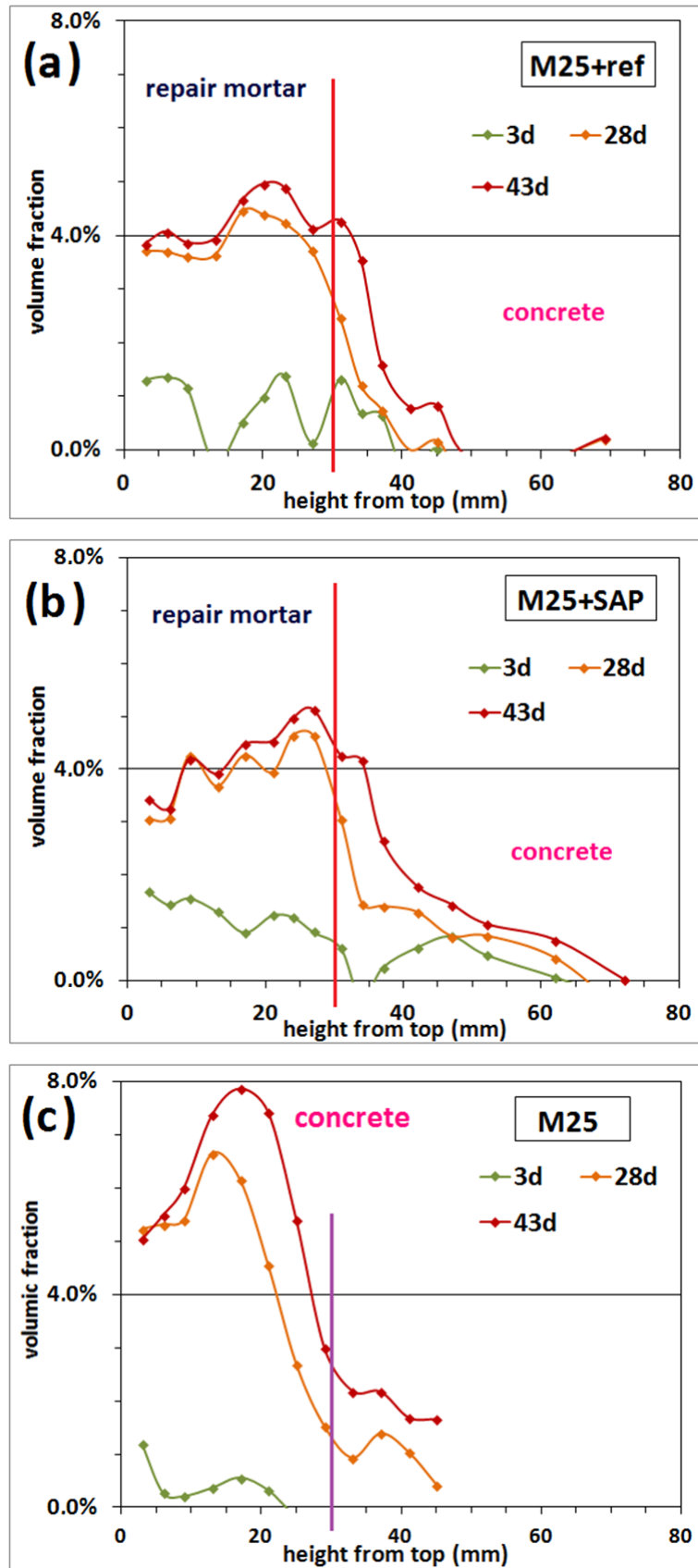


Figure 4.16: Density profiles by GRA to investigate carbonation profiles for (a) reference mortar + M25; (b) mortar with SAP + M25; (c) only M25 concrete.

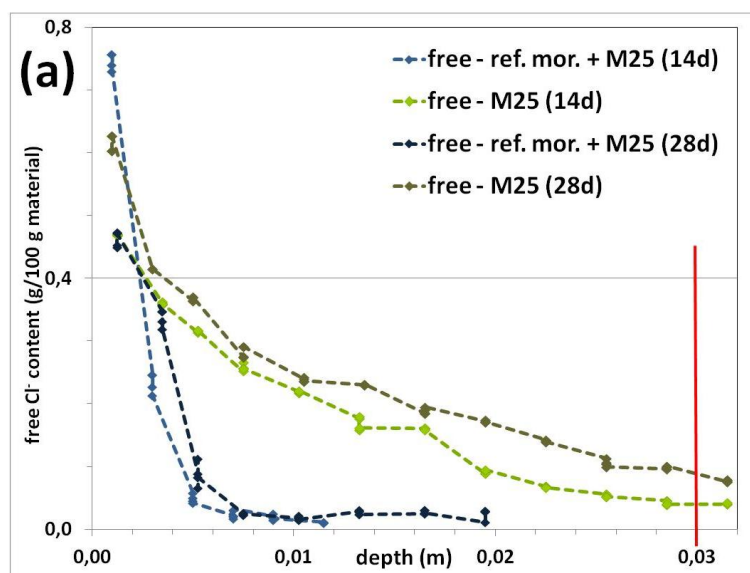
By considering carbonation procedure, there are no evident differences between reference repair mortar and with SAP in preventing carbonation process.

But by comparing reference repair mortar + M25 to only M25 concrete, the carbonation is hindered by the application of a repair mortar. The carbonation rate is retarded during penetration throughout mortar matrix. It is also interesting to prospectively investigate other repair materials by this method.

#### **4.2.3.3 Accelerated $Cl^-$ diffusion profiles**

Reference mortar on initially-dried M25 and only M25 are prepared to compare their resistances to accelerated chloride ions diffusion at 14, 28 and 150 days at different layers. In Figures 4.17 (a), the prevention of chloride penetration is observed for repair systems. The contents of free chloride ions within M25 and repair system at 14 and 28 days are presented. In Figure 4.17 (b), the relation between free and total chloride ions contents is revealed for M25 at 14 days. The penetration within M25 (free chloride ions content) according to diffusion duration is also presented in the same figure.

Because of experimental problems, the results for mortar with SAP on initially-dried M25 were disturbed. It will be also interesting to compare various repair systems with different repair materials.



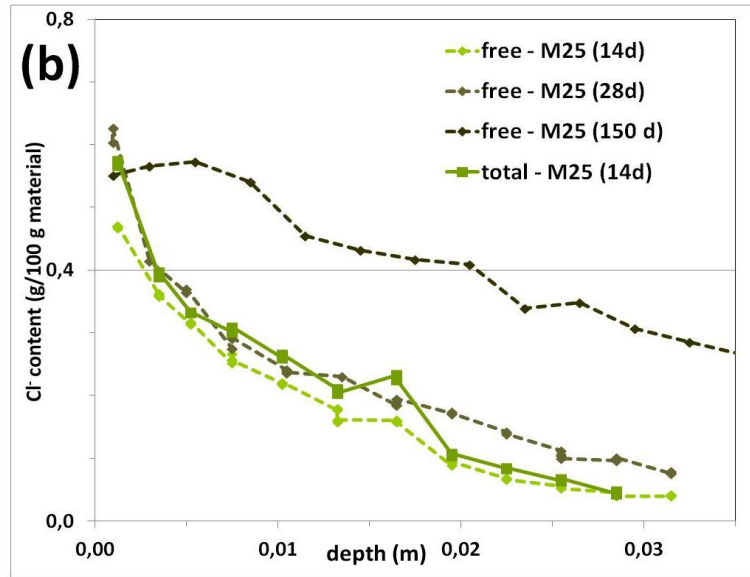


**Figure 4.17: (a) Free chloride ions content in M25 and repair system at 14 and 28 days; (b) Free and total chloride ions content for only M25 at different ages.**

As shown in Figure 4.17 (a), the penetration into repair system is both hindered at 14 and 28 days. The red bond line is corresponding to the mortar - concrete interface within repair system. After 28 days of chloride ions diffusion, it is observed that the penetration is still so slow and remains within repair mortar. The prevention of chloride ions penetration is observed as predicted in section 4.2.3.1, as the moisture transfer are hindered according to water immersion tests.

The free and total contents of chloride ions are coherent and their evolutions are similar as shown in Figure 4.17 (b). Thus further discussions and comparisons are carried out only for free content of chloride ions in order to simplify the investigation. For only M25 substrate, the penetration rate of chloride ions evolves regularly.

### **4.3 Global overview**

In this chapter, SPI sequences are applied to obtain the profiles of moisture transfer, in order to investigate the repair procedure in a non-destructive way. Reference repair mortars on initially-dried and initially-saturated concretes, mortar with SAP on initially-dried concrete, are respectively monitored. By comparing to immediate transfer from reference mortar to old concrete, SAP presents an optimal phenomenon of water retention properties during hydration. Saturated concrete provides excess water within repair mortar, but according to theoretical analysis and experimental results, the saturation level of old concrete before repair work needs to be verified to get an efficient performance.

This methodology can be also used for other composite systems, such as UHPFRC materials on initially-dried and initially-saturated old concretes, also on fresh concrete. UHPFRC without and with fibers both present the capacities to prevent moisture transfer. The hydration procedure of UHPFRC materials is not affected by the substrate states.

Furthermore, by comparing SPI integration with FID intensity, both sequences are related to free water content within the whole system. SPI integration is more informative and accurate, since SPI profiles allow monitoring local water content at each layer with a sensitive accuracy at 2 mm. But FID intensity is more sensitive and its acquisition time is shorter.

GRA is also a non-destructive technique by indirect manner to follow hydration during repair procedure. It is interesting to compare density profiles by GRA to moisture profiles by SPI. Both profiles are coherent to moisture evolution within concrete and a rehydration is observed close to the interface.

After a repair procedure, total porosity is measured by GRA and MIP, PSD at certain layers within repair system is obtained by MIP. These two techniques have both disadvantages and advantages. GRA is more convenient, but the procedure of drying and saturating needs to be improved to get a complete result (at 105 °C but microstructure was destroyed). MIP is more informative, but the cut specimens needs to be well operated to control its height and position within repair systems, and it is suggested to progress several parallel tests to avoid the heterogeneous effects of aggregates. The rehydration and microstructural improvement within concrete are observed subsequently.

Initially-wetted substrate is thus preferentially used for repair work, as it prevents harmful moisture transfer from repair mortar and thus there remains sufficient water for hydration.

Systems after repair procedure are investigated for monitoring their prolonged durability in long term. The moisture immersion, carbonation and chloride ions penetration are hindered, by using the reference repair mortar and with SAP on M25 with different saturation levels at initial state (0 % and 100 %). The repair mortar forms a protection layer to restrain the aggressive agents in liquid phase (water, chloride solution) or gas phase ( $\text{CO}_2$ ). Thus the aggressive attack is thus hindered. By this methodology, durability at longer duration for penetration of aggressive agents can be estimated by measured values at shorter duration.

According to aforementioned techniques and results, repair works can be evaluated by this methodology, since casting until hardening. By combining destructive and non-destructive techniques, experimental repair techniques are theoretically verified for their performances. And it can also be applied in various composite systems where exist **moisture transfer** and **microstructural evolution during hydration procedure**.

Thus procedure is also practice and easy to be applied in site condition. After surface preparation and mortar casting, specimens are taken for non-destructive MRI and GRA experiments, and then prepared for MIP experiments after one month. Not only as penetration of chloride ions, carbonation, and also as sulfate attack, freeze-thaw cycle, etc., all these **durability indicators** are useful to investigate and estimate further service lifetime after repair procedure. Other degradation mechanisms are thus can be further studied by this method. There will be abundant prospects for the investigation of durability properties during a repair procedure. By considering the selection of convenient repair products and conditions, this methodology will be useful for investigation.

It is possible to establish data base of durability performance for various commercial repair products on typical substrates, by repetitive experiments and modeling. Theoretical support is thus applied on empirical repair works and construction works will be more efficient.





## 5. *Conclusions and perspectives*

NMR sequences allow investigating **hydration process** within cement-based materials. The evolution of the optimum  $T_1$  values was used to monitor the hydration mechanisms since casting time until hardening, and corresponds well to the evolution of mechanical properties provided by Vicat needle test. The evolution of FID intensity was measured to follow the global free water depletion, and represents a relevant chemical indicator of hydration such as temperature monitoring. Thus **mechanical** and **chemical setting times** are defined, which are corresponding respectively to the maximum of derivatives of optimum  $T_1$  value ( $dT_1/dt$ ) and the initial setting time ( $t_{s, ini}$ ), to the maximum of both derivatives of FID intensity ( $dI_{FID}/dt$ ) and temperature evolution ( $dT/dt$ ). These parameters can be easily applied to compare the performance of different materials during hydration in one diagram of setting times.

The NMR methods also allow determining the **duration of hydration periods** such as acceleration (nucleation-growth) and deceleration (diffusion-control) around the setting times. These results can be compared to percolation properties of solid phase, which are determined by Vicat needle test.

Furthermore, the effects of other additions, such as standard sands, silica fume, super-plasticizer, were also investigated. The modified setting processes are complex, but they can be investigated by both defined setting times and peak information of  $dT_1/dt$  and  $I_{FID}$ , etc., thus the analysis becomes quantified in a convenient way.

A numerical modeling is also validated by comparing experimental results in this thesis and data in reference for cement pastes.

MRI sequences allow investigating **moisture transfer** at the interface between the repair mortar and the old concrete, during the complex hydration procedure at early ages of repair mortar. The moisture profiles were observed from rapid SPI profiles which present the local content of free water.

The **water retention** properties of a commercial **SAP** during a repair work on an initially-dried concrete was also investigated. The moisture properties have been presented by comparing two mortars: reference without SAP and one with 0.3% SAP/c in mass. This composition performs as water resource during setting process and improves the microstructural properties to finer porosity within repair system, especially at the interface. Immediate moisture transfer occur since placing the mortar on initially-dried M25, and SAP

absorbs partial water back as the hydration procedure is progressing. This phenomenon will be more evident if SAP quantity will increase.

The substrate states are also important for repair works, initially-dried or initially-saturated concretes have various influences on moisture transfer. The boundary conditions are set to further studies with various saturation rates.

The application of aforementioned methodology is possible for other composite systems where simultaneously exist moisture transfer and hydration process.

**UHPFRC materials** are frequently applied in construction fields for protection or reinforcement. The installation of fresh UHPFRC is similar as the condition of repair mortar on existed structures. UHPFRC without and with aramid fibers on initially-dried and initially-saturated concretes were thus investigated.

The water retention properties of UHPFRC materials are evident at the interface. As the w/c ratio is only 0.18 in this matrix, fine microstructure is related to capillary effects of water absorption. By comparing to repair mortars, the application is thus extensive and independent from initial states of substrates.

By applying various techniques, such as GRA and MIP, and comparing those results to NMR/MRI results. Density evolution, total porosity, porous distribution, etc., at different positions are thus investigated within repair systems.

During the investigation, the non-simultaneity of density (GRA) and moisture (SPI) profiles is observed within concrete and close to the interface. This phenomenon can be explained by the rehydration of non-hydrates in old concrete.

By comparing total porosity by GRA and MIP, both advantages and disadvantages are considered in these two techniques. GRA is relatively fast and convenient in specimen preparation, accurate in height locating at a scale of mm. MIP is accurate in pre-dried state by cryo-sublimation, and more informative in the investigation of porosity and PSD within cement matrix, but the preparation procedure is destructive and complex.

Finally, the performance of repaired systems is followed by accelerated carbonation and chloride diffusion, and the long-term durability is previewed. Extended service lifetime is thus possible to be predicted by the investigation at short duration. Generally, within repair systems, water immersion rate and the penetration of other aggressive agents are hindered or prevented by the application of repair mortar on concrete.

In this thesis, due to the limited duration of thesis mission (fixed-term contract for 3 years in IFSTTAR), also to considerate the numerous spent time on bibliography (multivariate analysis), the validation of methodology with strenuous experiments and various techniques, several aspects were not investigated but important to be performed by further studies.

Perspectives of this thesis are thus to measure mechanical behaviors (such as deformation, cracking, adhesion of interface, etc.), to apply experimental data base of the hydration process and moisture transfer on the establishment of numerical modeling to study transfers and interface. Furthermore, the microstructure and durability properties need to be investigated for longer term. Various states of concrete (with different saturation rates, carbonated, cracked, etc.) are also required to be prepared for reinforce the influence by substrates.



## ***Bibliography***

---

- [1] P.E. Grattan-Bellew. Microstructural investigation of deteriorated Portland cement concretes. *Construction and Building Materials*, Feb. 1996, Volume 10, Issue 1, Pages 3 - 16.
- [2] L.C. Hollaway, P.R. Head. *Advanced Polymer Composites and Polymers in the Civil Infrastructure: Chapter 1 - Introduction*. 2001, Pages 1 - 4.
- [3] Technical guidebook of IFSTTAR (ex LCPC). (Fr) Choix et application des produits de réparation et de protection des ouvrages en béton. Aug. 1996. Pages 30 - 36, 8, 16 - 26 / 75.
- [4] P. Faure, S. Caré, C. Po, S. Rodts. An MRI-SPI and NMR relaxation study of drying-hydration coupling effect on microstructure of cement-based materials at early age. 2005, *Magnetic Resonance Imaging*, Vol. 23, Pages 311 - 314.
- [5] Guangling Song, Ahmad Shayan. Corrosion of steel in concrete: causes, detection and prediction. State-of-the-art Review Report 4, ARRB Transport Research. July 1998, Pages 4 - 5/77.
- [6] Technical guidebook of IFSTTAR (ex-LCPC). (Fr) Protection des bétons par application de produits à la surface du parement. Dec. 2002. Pages 24, 23 - 30 / 99.
- [7] K.L. Scrivener, A. Nonat. Hydration of cementitious materials, present and future. 2011, *Cement and Concrete Research*, Vol. 41, Pages 651–665.
- [8] T.C. Hansen. Physical structure of hardened cement paste, a classical approach. 1986, *Mat. Struct.*, Vol. 19, Pages 423 – 436.
- [9] M. Pigeon. Composition et hydratation du ciment Portland = Composition and hydration of Portland Cement. Sep. 1981, séminaire progrès dans le domaine du béton, Québec, Pages 36 - 72
- [10] Thesis of V éronique Baroghel-Bouny. Caract érisation des pâtes de ciment et des bétons - Méthodes, analyse, interpr étations. June 1994. Pages 84 - 87 / 487.

- 
- [11] T. C. Powers. Physical properties of cement paste. 1960, Research and Development Laboratories of the Portland Cement Association, 4th international Symposium of the Chemistry of Cement, Washington DC, Vol. 1 (54), Pages 577-609.
- [12] P.J. McDonald, A. Valori, V. Rodin. NMR Relaxometry of Cement Pastes. Proceedings of MRPM 10, Leipzig, 2010.
- [13] M.H.Decter, C. Keeley. Durable concrete repair importance of compatibility and low shrinkage. Construction & Building Materials, 1997, Vol. 11, Pages 267-273.
- [14] N. Verma, R. Balasubramaniam. Corrosion of Steel Reinforcements in Concrete. Term Paper of Indian Institute of Technology Kanpur. 2007, Pages 3-6.
- [15] Thesis of Mickaël Thiery. (Fr) Modélisation de la carbonatation atmosphérique des matériaux cimentaires. 2005. Pages 9 - 15, 39 - 45, 50 - 51 / 331.
- [16] Thesis of Xiaomeng Wang. (Fr) Modélisation du transport multi-espaces dans les matériaux cimentaires saturés ou non saturés et éventuellement carbonatés. April 2012, Pages 9 - 12, 65 - 66, 131 - 136 / 210.
- [17] VS. Ramachandran, R.C. Seeley, G.M. Polomark. Free and combined chloride in hydrating cement and cement compounds. Materials and Structures. 1984, Vol. 19, Pages 285-289.
- [18] A. Neville. Chloride attack of reinforced concrete: An overview. Materials and Structures, 1995, Vol. 28(2), Pages 63-70.
- [19] K. Audenaert, G. De Schutter. Study of chloride penetration in self-compacting concrete by simulation of tidal zone. Concrete Repair, Rehabilitation and Retrofitting II – Alexander *et al.* © 2009 Taylor & Francis Group, London, ISBN 978-0-415-46850-3.
- [20] V. Baroghel-Bouny, A. Ammouche, H. Hornain, J. Gawsewitch. Vieillessement des bétons en milieu naturel - Une expérimentation pour le XXI<sup>e</sup> siècle II – Caractérisation microstructurale sur éprouvettes de bétons de résistance 25 a 120 MPa. Technical book 228, Sep. 2000, Pages 71 - 86.

---

[21] Teijin Aramid, Technora® - High Tenacity Aramid Fiber. Sales brochure.

[22] Degradation of Technora aramid fibres in alkaline and neutral environments. Guillaume Derombise, Laëtitia Vouyovitch Van Schoors, Peter Davies. *Polymer Degradation and Stability* Volume 94, Issue 10, October 2009, Pages 1615–1620.

[23] K. Friedemann, F. Stallmach, J. Kärger. NMR diffusion and relaxation studies during cement hydration - A non-destructive approach for clarification of the mechanism of internal post curing of cementitious materials. May 2006, *Cem. Concr. Research*, Vol 36 (5), Pages 817–826.

[24] O. M. Jensen, P. F. Hansen. Water-entrained cement-based materials. I. Principles and theoretical background. 2001, *Cement and Concrete Research*, Vol. 31, Pages 647-654.

[25] A. Kamen, E. Denarié, H. Sadouki, E. Brühwiler. Thermo-mechanical response of UHPFRC at early age - Experimental study and numerical simulation. June 2008, *Cem. Concr. Res.*, Vol. 38(6), Pages 822-831.

[26] E. Denarié. Full scale application of UHPFRC for the rehabilitation of bridges – from the lab to the field. Competitive and Sustainable Growth (GROWTH) Programme report, Dec. 2005.

[27] H. Kazemi-kamyab, E. Denarié, E. Brühwiler, B. Wang, M. Thiéry, P. Faure, V. Baroghel-Bouny. Characterization of moisture transfer in UHPFRC-concrete composite systems at early age. *Proceeding of Second International Conference on Microstructural-related Durability of Cementitious Composites*, 11-13 April 2012, Amsterdam, Netherlands.

[28] D. Canet, J.C. Boubel, and E. Canet-Soulas. *La RMN concepts, méthodes et applications*. Dunod 2ème édition, 2002. 235 pages.

[29] P.T. Callaghan. *Principles of nuclear magnetic resonance microscopy*. Oxford science publications, 1991. 516 pages.

[30] N. Huang, G. Ovarlez, F. Bertrand, S. Rodts, P. Coussot, D. Bonn. Flow of wet granular materials. 2005, *Physical Review Letters*, Vol. 94(2).



---

[31] P.Coussot, F.Bertrand, B. Herzhaft. Rheological Behavior of drilling muds, characterization using MRI visualization. 2004, Oil & Gas Science and Technology - Revue de l'IFP, Vol. 59 (1), Pages 23 – 29.

[32] P. Faure, P. Coussot. Drying of a model soil. Sep. 2010, Physical Review E: Statistical, Nonlinear, and Soft Matter Physics, American Physical Society, Vol. 82 (3), Pages 036303.

[33] P. Faure, S. Rodts. Proton NMR relaxation as a probe for setting cement pastes. 2008, Magn. Reson. Imaging, Vol. 26 (8), Pages 1183-1196.

[34] P. Faure, S. Car é J. Magat, T. Chaussadent. Drying effect on cement paste porosity at early age observed by NMR methods. April 2012, Construction & Building Materials. Vol. 29, Pages 496 - 503.

[35] S.W. Provencher. A constrained regularization method for inverting data represented by linear algebraic or integral equations. 1982, Comput. Phys. Commun., Vol. 27, Pages 213 - 227.

[36] K.P. Whittall, A.L. MacKay. Quantitative interpretation of NMR relaxation data. 1989, J. Magn. Reson., Vol. 84(1), Pages 134-152.

[37] Teddy Fen-Chong, Antonin Fabbri, Aza Azouni. Transient freezing–thawing phenomena in water-filled cohesive porous materials. Oct. 2006, Cold Regions Science and Technology, Vol. 46(1), Pages 12-26.

[38] P. Livesey, A. Donnelly, C. Tomlinson. Measurement of the heat of hydration of cement. 1991, Cem. Concr. Composites, Vol. 13 (3), Pages 177-185.

[39] R. Ylmén, U. Jäglid, B.-M. Steenari, I. Panas. Early hydration and setting of Portland cement monitored by IR, SEM and Vicat techniques. May 2009, Cem. Concr. Res., Vol. 39 (5), Pages 433–439.

[40] P. Mounanga, V. Baroghel-Bouny, A. Loukili, A. Khelidj. Autogenous deformations of cement pastes: Part I. Temperature effects at early age and micro–macro correlations. January 2006, Cem. Concr. Res., Vol. 36 (1), Pages 110-122.

- 
- [41] B. Lothenbach, F. Winnefeld. Thermodynamic modelling of the hydration of Portland cement. 2006, *Cem. Concr. Res.*, Vol. 36 (2), Pages 209–226.
- [42] O. Bernard, F.-J. Ulm, E. Lemarchand. A multiscale micromechanics - hydration model for the early-age elastic properties of cement-based materials. 2003, *Cem. Concr. Res.*, Vol. 33 (9), Pages 1293-1309.
- [43] S. Arrhenius, *Quantitative Laws in Biological Chemistry*, G. Bell and Sons, London, 1915.
- [44] Nguyen, M.D. Modelling of coupling between hydration and drying of cement-based materials after stripping. - Studying of transfer properties degradation. (fr) Modélisation des couplages entre hydratation et dessiccation des matériaux cimentaires à l'issue du décoffrage. IFSTTAR (ex-LCPC) and Ecole des Ponts Paristech. Dec. 2009. Thesis.
- [45] D.P. Bentz, P.E. Stutzman. Curing, hydration, and microstructure of cement paste. Sep.-Oct. 2006, *ACI Materials Journal*, Vol. 103 (5), Pages 348-356.
- [46] O.M. Jensen, P.F. Hansen. Water-entrained cement-based materials: I. Principles and theoretical background. April 2001, *Cem. Concr. Res.*, Vol. 31 (4), Pages 647-654.
- [47] S. Emid and J.H.N. Creydon. High resolution NMR imaging in solids. 1985, *Physica B*, Vol. 128, Pages 81–83.
- [48] B.J. Balcom, J.C. Barrita, C. Choi, S.D. Beyea, D.J. Goodyear, T.W. Bremner. Single-point magnetic resonance imaging (MRI) of cement based materials. 2003, *Materials and structures*, Vol. 36, Pages 166–182.
- [49] P.J. Prado, B.J. Balcom, S.D. Beyea, R.L. Armstrong, T.W. Bremner, P.E. Grattan-Bellew. Concrete/mortar water phase transition studied by single-point MRI methods. 1998, *Magn. Reson. Imaging*, Vol. 16 (5/6), Pages 521-523.

- 
- [50] Michelle Y. Troutman, Igor V. Mastikhin, Bruce J. Balcom, Thomas M. Eads, Gregory R. Ziegler. Moisture migration in soft-panned confections during engrossing and aging as observed by magnetic resonance imaging. 2001, Journal of Food Engineering, Vol. 48, Pages 257-267.
- [51] B.J. Balcom, R.P. MacGregor, S.D. Beyea, D.P. Green, R.L. Armstrong, T.W. Bremner. Single Point ramped imaging with  $T_1$  enhancement (SPRITE). Nov. 1996, Journal of Magnetic Resonance, Vol. 123 (1), Pages 131-4.
- [52] S.D. Beyea, B.J. Balcom, T.W. Bremner, P.J. Prado, D.P. Green, R.L. Armstrong, P.E. Grattam-Bellew. Magnetic resonance imaging and moisture content profiles of drying concrete. Cement and Concrete Research, 28 :453–463, 1998.
- [53] P.J. Prado, B.J. Balcom, S.D. Beyea, R.L. Armstrong, T.W. Bremner. Concrete thawing studied by single-point ramped imaging. 1997, Solid State Nuclear Magnetic Resonance, Vol.10:1-8.
- [ 54 ] G. Villain, P. Roussel. (fr) Mode opératoire et consignes: essais sur le banc de gammadensimétrie = (en) Procedure and instructions: essays on gamma-ray attenuation. Technical guidebook, IFSTTAR (ex-LCPC), 2002.
- [55] M. Relis, I. Soroka. Variation in density of portland cement hydration products. Nov. 1977, Cement and Concrete Research, Vol. 7, Issue 6, Pages 673 - 680.
- [56] G. Arliguie, H. Hornain. GranDuB é - Grandeurs associées à la Durabilité des Bétons. 2007, Presses de l'école nationale des ponts et chaussées.
- [57] V. Baroghel-Bouny, T. Chaussadent. Mesures de surface spécifique (par adsorption d'azote) et de porosité (par porosimétrie au mercure) de pâtes de ciment durcies. Sep. 1992, Synthesis report L.C.P.C./L.E.R.M, Research report L.C.P.C., 26 pages.
- [58] Caractéristiques microstructurales et propriétés relatives à la durabilité des bétons. Méthode d'essai n°58.4: Porosimétrie des bétons durcis par intrusion de mercure.

---

[59] Caractéristiques microstructurales et propriétés relatives à la durabilité des bétons. Méthode n°58.13 Evaluation de la résistance à la carbonatation à partir d'un test accéléré – stations d'essai disponibles dans le réseau des LPC.

[60] G. Villain, M. Thiery, G. Platret. Measurement methods of carbonation profiles in concrete : Thermogravimetry, chemical analysis and gammadensimetry. *Cement and Concrete Research* 37 (2007) 1182–1192.

[61] Caractéristiques microstructurales et propriétés relatives à la durabilité des bétons. Méthode d'essai n°58.9 Détermination des profils de concentration en chlorures et du coefficient de diffusion des chlorures dans les bétons durcis en régime non stationnaire à partir d'un essai de diffusion.

[62] J.-P. Korb, L. Monteilhet, P.J. McDonald, J. Mitchell. Microstructure and texture of hydrated cement-based materials: A proton field cycling relaxometry approach. 2007, *Cem. Concr. Res.*, Vol. 37, Pages 295–302.

[63] N. Nestle. A simple semi-empiric model for NMR relaxometry data of hydrating cement pastes. March 2004, *Cem. Concr. Res.*, Vol. 34 (3), Pages 447-454.

[64] J. Hansen, T. Sharpe, E.E. Bittar. Phosphate metabolites in single barnacle muscle fibers investigated by phosphorus-31 nuclear magnetic resonance. 1986, *Comparative Biochemistry and Physiology Part B: Comparative Biochemistry*, Vol. 83 (4), Pages 875-879.

[65] L. Pel, K. Kopinga, H. Brocken. Determination of moisture profiles in porous building materials by NMR. 1996, *Magn. Reson. Imaging*, Vol. 14 (7-8), Pages 931-932.

[66] N. Nestle, C. Zimmermann, M. Dakkouri, J. Kärger. Transient high concentrations of chain anions in hydrating cement - indications from spin relaxation measurements. 2002, *J Phys D Appl Phys*, Vol 35 (2), Pages 166–171.

[67] J.-P. Korb, P.J. McDonald, L. Monteilhet, A.G. Kalinichev, R.J. Kirkpatrick. Comparison of proton field-cycling relaxometry and molecular dynamics simulations for proton-water surface dynamics in cement-based materials. 2007, *Cem. Concr. Res.*, Vol. 37, Pages 348-350.

- 
- [68] A. Plassais, M.-P. Pomiès, N. Lequeux, P. Boch, J.-P. Korb. Micropore size analysis in hydrated cement paste by NMR. April–May 2001, *Magn. Reson. Imaging*, Vol 19 (3–4), Pages 493-495.
- [69] M. Gussoni, F. Greco, F. Bonazzi, A. Vezzoli, D. Botta, G. Dotelli, I. Natali Sora, R. Pelosato, L. Zetta. <sup>1</sup>H-NMR spin-spin relaxation and imaging in porous systems: an application to the morphological study of white portland cement during hydration in the presence of organics. July 2004, *Magn. Reson. Imaging*, Vol. 22 (6), Pages 877–889.
- [70] H. Minard, S. Garrault, L. Regnaud, A. Nonat. Mechanisms and parameters controlling the tricalciumaluminate reactivity in the presence of gypsum. 2007, *Cem. Concr. Res.*, Vol. 37 (10), Pages 1418–1426.
- [71] J.-P. Gorce, N.B. Milestone. Probing the microstructure and water phases in composite cement blends. March 2007, *Cement & Concrete Research*, Vol. 37 (3), Pages 310-318.
- [72] W.P. Halperin, J.-Y. Jehng, Y.-Q. Song. Application of spin-spin relaxation to measurement of surface area and pore size distributions in a hydrating cement paste. 1994, *Magn. Reson. Imaging*, Vol. 12 (2), Pages 169-173.
- [73] Thesis of J. Magat. (fr) Apport de l'Imagerie par Résonance Magnétique dans l'étude des mécanismes de structuration des matériaux cimentaires: Application au suivi des modifications engendrées par le séchage. (en) Contribution of magnetic resonance imaging in the study of structuring mechanisms of cementitious materials: Application in following the modifications caused by drying. University of Paris-Est, octobre 2008.
- [74] V. Baroghel-Bouny. Water vapour sorption experiments on hardened cementitious materials: Part I: Essential tool for analysis of hygral behaviour and its relation to pore structure. March 2007, *Cem. Concr. Res.*, Vol. 37 (3), Pages 414–437.
- [75] K. Friedemann, F. Stallmach, J. Kärger. Carboxylates and sulfates of polysaccharides for controlled internal water release during cement hydration. April 2009, *Cement & Concrete Composites*, Vol. 31 (4), Pages 244-249.

- 
- [76] P. Halamickova, R. J. Detwiler, D. P. Bentz, E. J. Garboczi. Water permeability and chloride ion diffusion in portland cement mortars: Relationship to sand content and critical pore diameter. May 1995, *Cem. Concr. Res.*, Vol. 25 (4), Pages 790-802
- [77] Tazawa, E.I., Miyazawa, S. Influence of cement and admixture on autogenous shrinkage of cement paste. 1995, *Cem. Concr. Res.*, Vol. 25 (2), Pages 281-287.
- [78] J. Strupi Suput, D. Dimic, T. Apih. Study on the influence of HRWR admixtures on the hydration processes of different types of Portland cements by means of NMR spectroscopy.
- [79] B.W. Langana, K. Wengb, M.A. Warda. Effect of silica fume and fly ash on heat of hydration of Portland cement. 2002, *Cem. Concr. Res.*, Vol. 32, Pages 1045–1051.
- [80] M.W. Grutzeck, S.D. Atkinson, D.M. Roy. Mechanism of hydration of CSF in calcium hydroxide solutions. Proceedings of the First International Conference on the Use of Fly Ash, Silica fume, Slag and Natural Pozzolans in Concrete. 1983, Vol. 2, SP-79, American Concrete Institute, Pages 643–664.
- [81] Katrin Habel, Marco Viviani, Emmanuel Denarié, Eugen Brühwiler. Development of the mechanical properties of an Ultra-High Performance Fiber Reinforced Concrete (UHPFRC). July 2006, *Cem. Concr. Res.*, Vol. 36 (7), Pages 1362-1370.
- [82] L. Li, H. Han, B.J. Balcom. Spin echo SPI methods for quantitative analysis of fluids in porous media. June 2009, *Journal of Magnetic Resonance*, Vol. 198 (2), Pages 252-260.
- [83] D.P. Bentz. Influence of water-to-cement ratio on hydration kinetics: Simple models based on spatial considerations. Feb 2006, Vol. 36(2), *Cem. Concr. Res.*, Pages 238–244.
- [84] L. Courard, J.-F. Lenaers, F. Michel, A. Garbacz. Saturation level of the superficial zone of concrete and adhesion of repair systems. May 2011, *Construction and Building Materials*, Vol. 25 (5), Pages 2488–2494.

---

[85] Lu í Pedro Esteves. Superabsorbent polymers: On their interaction with water and pore fluid. August 2011, Cement and Concrete Composites, Vol. 33 (7), Pages 717–724.

[86] P. Lura, K. Friedemann, F. Stallmach, S. Mönnig, M. Wyrzykowski, L.P. Esteves. 4. Kinetics of water migration in cementbased systems containing super absorbent polymers. Application of Super Absorbent Polymers (SAP) in Concrete Construction. RILEM State of the Art Reports, 2012, Volume 2, 21-37, DOI: 10.1007/978-94-007-2733-5\_4

[87] E. Denarié, Structural rehabilitations with ultra-high performance fibre reinforced concretes (UHPFRC), in: M. Alexander, H.-D. Beushausen, F. Dehn, P. Moyo (Eds.), International Conference on Concrete repair, rehabilitation and retrofitting, Taylor & Francis, London, 2005.

[88] Steven E. Keinath, Roger J. Morgan. Moisture content of aramid and polybenzimidazole fibers. 15 Sep. 1990, Thermochimica Acta, Vol. 166, Pages 17-26.

[ 89 ] R.D. Toledo Filho, E.A.B. Koenders, S. Formagini, E.M.R. Fairbairn. Performance assessment of Ultra High Performance Fiber Reinforced Cementitious Composites in view of sustainability. April 2012, Materials & Design, Vol. 36, Pages 880-888.

[90] Eugen Brühwiler, Emmanuel Denarié Rehabilitation of concrete structures using Ultra-High Performance Fibre Reinforced Concrete. UHPC-2008: The Second International Symposium on Ultra High Performance Concrete. March 05 - 07, 2008, Kassel, Germany

[91] J.-P. Charron, E. Denarié, E. Brühwiler. Transport properties of water and glycol in an ultra high performance fiber reinforced concrete (UHPFRC) under high tensile deformation. 2008, Cem. Concr. Research, Vol. 38, pp. 689–698.

[92] Zhao-Fen Jin, Yutaka Asako, Yoshiyuki Yamaguchi, Hirohisa Yoshida. Thermal and water storage characteristics of super-absorbent polymer gel which absorbed aqueous solution of calcium chloride. 2000, International Journal of Heat and Mass Transfer, Vol. 43, Pages 3407-3415.